2014-06-11

Characterization and Optimization of Thermal Protective Fabrics Designed to Protect Against Splash Hazards

Jeremy Osguthorpe
Brigham Young University - Provo

BYU ScholarsArchive Citation

Osguthorpe, Jeremy, "Characterization and Optimization of Thermal Protective Fabrics Designed to Protect Against Splash Hazards" (2014). *All Theses and Dissertations*. 4096.
https://scholarsarchive.byu.edu/etd/4096

Characterization and Optimization of Thermal Protective Fabrics Designed to Protect Against Splash Hazards

Jeremy Osguthorpe

A thesis submitted to the faculty of
Brigham Young University
in partial fulfillment of the requirements for the degree of

Master of Science

Matthew R. Jones, Chair
W. Jerry Bowman
Brian D. Iverson

Department of Mechanical Engineering

Brigham Young University

June 2014

ABSTRACT

Characterization and Optimization of Thermal Protective Fabrics Designed to Protect Against Splash Hazards

Jeremy Osguthorpe
Department of Mechanical Engineering, BYU
Master of Science

Thermal textiles used in Personal Protective Equipment (PPE) are used to protect individuals from the hazards of thermal energy. An analytical model of the diffusion of thermal energy within the fabric was developed to simulate the transfer of thermal energy due to a hot liquid splash. Based on the model results, it was determined that that the use of an orthotropic material in which the thermal conductivities in the radial and axial directions are different can be used to decrease the amount of heat transferred through the fabric and thereby increase amount of protection in PPE. An orthotropic material particularly performs well under situations where splashes are small in size and short in time duration. The increased level of protection may be enough to prevent a second-degree burn as determined by the Stoll criterion for materials in which the radial thermal conductivity is much larger than the axial thermal conductivity. , However, situations with larger splashes over longer duration, the benefits are minimal and at best may reduce the amount of energy transferred over part of the splash site thereby minimizing potential size of burn areas. A semi empirical test method in which analytical results are matched to experimental results by iteratively changing the radial thermal conductivity was presented as a way to extract information about the extent that a fabric is orthotropic. Preliminary results as compared to numerical CFD experimentation show that with a calibrated model, the method has potential of giving good results. Further physical experimentation is recommended to further validate that this method could be of use in determining the extent that a fabric is orthotropic.

Keywords: heat transfer, thermal textiles, personal protective equipment, orthotropic, radial thermal conductivity

ACKNOWLEDGEMENTS

I would like to express my appreciation to my committee, especially Dr. Jones, for their time and guidance that they have provided me. In addition, I would like to express my appreciation to Chapman Innovations for providing funding related to this research. Finally, I would like to express my appreciation to my family for their love and support for me.

TABLE OF CONTENTS

LIST OF TABLES

LIST OF FIGURES

NOMENCLATURE

Variable	Description
A	Mean Component of Sinusoidal Term (W)
B	Alternating Component of Sinusoidal Term (W)
Bi_0	Biot Number at Upper Surface
Bi_w	Biot Number at Lower Surface
c_p	Heat Capacity (J/kg)
d	Density (kg/m^3)
f	Frequency (Hz)
h	Convective Heat Transfer Coefficient (W/m^2*K)
H()	Heaviside Function
$J_0()$	Bessel Function of First Kind
k_r	Radial Thermal Conductivity (W/m*K)
k_z	Axial Thermal Conductivity (W/m*K)
Q_0	Energy Released (J)
r	Radial Position (m)
r_0	Radius of Splash Size (m)
T	Temperature (K)
t	Time (s)
T_∞	Ambient Temperature (K)
t_0	Time Duration of Splash (s)
U	Overall Heat Transfer Coefficient (W/m^2*K)
w	Thickness of Fabric (m)
z	Axial Position (m)
α	Thermal Diffusivity (m^2/s)
β_n	Distinct Eigenvalues
$\delta()$	Delta Dirac Function
ε	Non-Dimensional Ratio of Thermal Conductivity
ζ	Non-Dimensional Axial Position
θ	Non-Dimensional Temperature
λ	Continuous Eigenvalues
ρ	Non-Dimensional Radial Position
τ	Non-Dimensional Time
$\varphi()$	Eigen-function

1 INTRODUCTION

The ultimate goal of this research is to analyze and improve a thermal protective system's ability to protect an individual from hot liquid splashes. Thermal protective systems are combinations of different layers of thermal protective fabrics designed to protect an individual from thermal energy. Often, various types of materials are layered to optimize the system for thermal performance, as well as comfort to the individual wearing them. Typically, thermal protective systems are put in the broad category of personal protective equipment (PPE).

1.1 Thermal Protective Systems

It is common for people to be required to work in environments in which they are exposed to various hazards that can be dangerous, and even potentially fatal. Depending on the type of industry, these hazards can range from being electrical, chemical, thermal, or mechanical in nature. In particular, protection from thermal energy has been of elevated interest more recently as more scenarios are arising in which people are exposed to thermal hazards. Situations where protection from thermal energy is needed is common in metal manufacturing, cutting and welding operations, firefighting, mechanic work, and is even becoming more common in other markets such as motor racing. To mitigate hazards associated with work in those environments, various forms of personal protective equipment (PPE) are used, and when used properly for the intent in which they were designed, they can ensure some level of safety to workers.

PPE is designed to protect an individual with a specific application in mind. For example, fabrics developed to provide high levels of protection for an individual from thermal radiation may not adequately protect an individual from a hot liquid splash. There has been a lot of engineering work that has gone into manufacturing materials that are flame resistant, have low thermal conductivities, high specific heat, etc. Despite all the work that has gone into developing technology for these fabrics, there is yet room for improvement, as will be shown.

1.2 **Motivation**

In 2009 alone, The Aluminum Association received 60 reports [1] of incidents where molten aluminum was spilled or splashed onto an individual during the manufacturing processes of Aluminum. The causes of these incidents vary, ranging from explosions to spills in various phases of production. Out of those 60 incident reports, there were 26 reported injuries; most of them minor in nature, but a few were severe including one fatality. In most of the cases, it was reported that the individual was wearing PPE, and that the PPE either prevented an injury or prevented an injury from being much more severe.

The previous statistics, referring only to Aluminum production, are but one field in which PPE is used to protect against hot environments and materials. In other industries that have risk for thermal burns, there is potential for similar statistics. Just about anybody that has been involved in molten metal or hot liquid manufacturing and processing long enough probably has seen firsthand the value of wearing thermal protective clothing. In general, if the proper PPE is used, most injuries can be prevented. Yet despite all the advances in technology in developing materials that can protect an individual, there are still accidents that happen every year. It is estimated that 20-25% of all treated burn injuries are workplace injuries [2]. It is these industrial workplace accidents that efforts should be made to minimize, as they are usually the preventable ones.

A news article [3] from 2011 summarizes an accident at a steel production factory where there were several injuries and fatalities. The article references an OSHA accident report in saying that the workers lacked the proper PPE, and that better PPE may have saved the lives of those who died. In most molten metal manufacturing environments, the majority of workers wear standard flame resistant cotton clothing, unless directly handling hazardous material in which they wear additional clothing; often a long aluminized coat, gloves, and face shield. The standard cotton clothing is used in large part because they are comfortable to wear for the workers when they are in positions that they are less likely to be injured, such as people observing or passing by. In this accident, as well as many others, the workers that were injured were just wearing the standard cotton flame resistant clothing. This cotton clothing has been described to "burn like paper" when exposed to the heat of liquid steel, and offers minimal protection against temperatures that high. The basic consensus was that if the workers were wearing better protective clothing, those injuries and deaths might have been prevented.

In our modern world, in just about every work place that has hazards present to its workers, companies go to great lengths and promote safety within the workplace. This is for both concern for the workers, reputation, and financial reliabilities. However, one of the biggest issues faced is compliance to safety regulations within the workplace. It's not so much as issue of not having clothing that offers adequate protection; it's more an issue of getting individuals to wear the proper clothing. There is great resistance by many workers to wear clothing that is neither comfortable nor convenient if they don't have to. It can be incredibly uncomfortable to wear full PPE in hot environments, as they neither breathe well nor offer any sort of cooling. In addition, they are often cumbersome to wear and make performing their job even more difficult. It can be inconvenient to properly don and doff the necessary protective clothing, and many times workers won't put them on if a job seems relatively short and simple. It is when workers have this mentality to find reasons to not wear better PPE that a large amount of accidents occur.

There is a need for new improvements in fabric technology that will allow for better protection against the hazards of hot liquid and molten metal splashes. There are many ways that the level of protection in PPE can be improved. For example, fabrics can always be made thicker to provide more resistance to heat transfer, but this comprises the comfort of the individual wearing the clothing. It can be a miserable experience working in an environment in which you have to wear clothing that is extremely uncomfortable. In addition to being uncomfortable to wear, if the fabrics were made thicker, they become even more cumbersome and would make workers' jobs even more difficult. New developments in fabric technology that allow for light, supple materials that workers would be willing to wear, yet still provide adequate protection against the specific hazards that are present.

1.3 **Objectives**

The object of this research is to develop a simplified analytical model of heat transfer through thermal protective clothing, and using that model determine how improvements can be made to the design of the fabric for optimized performance. Secondary objectives will be to numerically verify the model and perform experimental validation. This will involve creating Finite Element Method (FEM) model for the numerical verification, and creating an experimental test setup that could be applied for testing materials of this nature.

1.4 **Thesis Overview**

Chapter 2 of this thesis will first give background of skin structure and burns and how this relates to the industry standard acceptable level of heat transfer, known as the Stoll curve. Experimental methods used to assess the performance of thermal textiles will be covered, followed by an overview to previous related analytical modeling.

Chapter 3 will describe the development and solution of the analytical model. The results of the analytical model will be presented as well as how it compares to the idealized thermal protective system.

Chapters 4 will discuss numerical verification. Fluent will be used for FEA analysis, and these results will be compared to the results analytical model.

Chapter 5 will discuss simulated experimental work that was done. The theory will be discussed, as well as presenting the preliminary results using simulated CFD data.

Chapter 6 will include a summary of the results and conclusions and recommendation of areas for further research.

2 BACKGROUND AND LITERATURE REVIEW

2.1 Skin Structure and Burns

Thermal protective fabrics are used to prevent burns to the skin and other tissue. A brief overview of skin structure and burn classifications, and how they are formed is presented here for background information. Skin is comprised of two primary layers, the epidermis and Dermis, and another secondary layer, the hypodermis. The epidermis is the outer-most layer, and provides the body's first line of defense in keeping foreign material out and provides waterproofing for the body. The next layer, the dermis, is where most of what we could consider the living parts of our skin are located, such as nerve ending which give our sense of heat and touch, as well as hair follicles and sweat glands. The hypodermis, which is not technically a layer of the skin, but is often included when referring to skin structure, attaches the skin to underlying layers of muscle and bone and supplying nerves and blood vessels to the Dermis and Epidermis.

A burn is defined as thermal damage to the skin when the skin reaches a temperature of 44 degrees Celsius or higher for an extended length of time. The severity of a burn, or the amount of damage that occurs from thermal energy, is a function of both the temperature that the skin reaches and the amount of time that the skin is exposed to the increase to that elevated temperature. Tissue that is raised to the same an elevated temperature for different lengths of time may receive varying severity of damage. Depending on the depth and severity of the burn, different classifications of burns exist, commonly referred to as first, second, or third degree burns.

First-degree burns are defined as tissue located within the Epidermis is raised to an elevated temperature and minor damage occurs. They are characterized by pain and reddening of the tissue, which may last for a few days. Tissue will regenerate from these types of burns, and other than temporary discomfort, there are usually no other immediate complications.

Second-degree burns occur when the next layer of skin, the Dermis, which is located approximately 80 μm below the surface of the skin, is subjected to elevated temperatures and more severe tissue damage occurs. These types of burns can vary to some extent in severity to how deep within the Dermis that thermal damage occurs. Second-degree burns are characterized by pain and blistering and mark the threshold point of tissue regeneration. Tissue will regenerate from 2nd degree burns, but if any more damage were to occur, then the tissue would not regenerate and necrosis, or death of the cells, would occur. Potential complications such as infection may also result and lead to further complications.

Third degree burns occur when tissue through the entire Dermis and even into the Hypodermis is damaged, and marks the point that the thermal damage is so great that the cells experience necrosis. At this point, no pain is felt directly by the tissue experiencing a third degree burn, as tissue is no longer considered living. However, pain may be felt in nearby tissue that experiences less thermal damage. Numerous complications can arise from third degree burns, including infection and shock. Removal of the damaged tissue is usually required, and often skin grafts and/or amputation may be necessary, depending on the location and extent of the burn.

2.2 **Stoll Curve**

Industrial standards have been developed that specify whether or not a fabric provides sufficient thermal protection and serves as a baseline performance metric. The standard that has been set is that a fabric must provide sufficient thermal protection in its intended application so that the severity of a burn that may be received will be less than a second-degree burn. This standard comes from what is referred to as the Stoll Curve, and this will be discussed in more detail.

The first efforts in determining how much energy it takes before burns occur were experimental in nature and involved measuring the amount of heat absorbed by a person before they would experience a second-degree burn. Despite the questionable ethics of using human test subjects to determine burn thresholds, the information is useful and establishes a good baseline that can relate the amount of energy per unit surface area a person can absorb before they will be burned. An empirical correlation of that data, named the Stoll Curve [4], describes the amount of energy that a person can receive as a function of time before they would receive a second-degree burn. A curve fit of the data results in an equation in units of J/m^2 for the Stoll Curve shown below in Eq. 2.1 and plotted in Figure 2-1.

$$Q''_{absorbed} = 50204 \cdot t^{0.2901} \text{ J/m}^2 \tag{2.1}$$

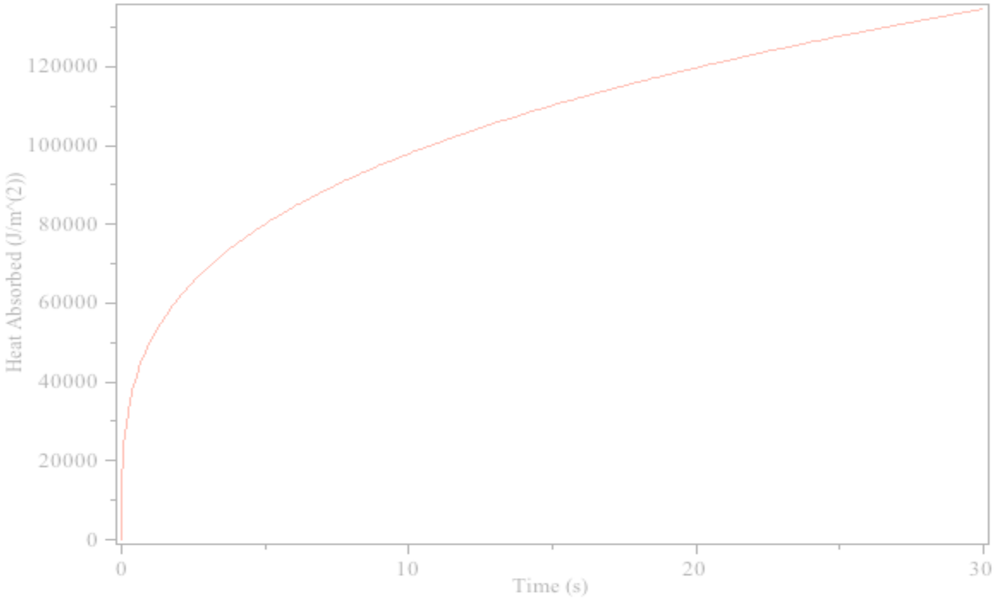

Figure 2-1: Stoll curve plotted as total absorbed energy as a function of time

As Eq. 2.1 gives the total amount of absorbed energy per unit surface area as a function of time, which is useful for comparing experimental data. However, in terms of mathematical modeling, the analysis is often in terms of heat flux. To be able to compare the results from analytical models, the results must be integrated over time, and then can be compared directly to the Stoll Curve.

2.3 Experimental Evaluation of Protective Systems

With a baseline standard in place for determining if a fabric provides adequate protection for a particular situation, testing protocols have been developed to obtain data for the comparison. There are numerous tests out there, each specifically designed for a particular application. In the realm of hot liquid splashes, the ASTM F955-07 [5] test is used for assessing a fabric's ability to protect against molten metal splashes. The ASTM F2701–08 [6] test is used to assess a fabric's ability to protect against hot liquid splashes. The basic methodology is the same for both tests; a sample of fabric is exposed to a splash of either molten metal or other hot liquid, and the heat flux is measured through the fabric. Once the data is obtained, it is compared to the Stoll curve to determine if it provides a sufficient level of protection.

Either test is conducted by placing a swatch of fabric over a board with low thermal conductivity in which copper calorimeter heat flux sensors are embedded. Once the liquid splashes on the fabric, thermocouple measurements are used to determine the rise in temperature of the copper disks, and based on a simple energy balance on the copper disks, the heat flux can be related to the temperature rise using the heat capacity, density, and geometry of the copper.

Once the data is gathered, the total energy absorbed by the copper disk is plotted against the Stoll Curve. The performance of a fabric has been simply described by the experimentally measured heat flux, and its relation to the Stoll curve. Specifically, developers of these fabrics have been interested to know whether or not the data lies above or below the curve, as if it was a simple "pass" or "fail" test. If at any point, the data crosses the Stoll curve line, then it is assumed that a person would receive a second-degree burn and the fabric is considered inadequate in its ability to protect an individual. An example of experimental data that was gathered by the author in accordance to the ASTM 955 standard is shown in Figure 2.2. In this figure the Stoll curve is compared against the energy transferred through two different types of fabrics. In the testing of a fabric designated by "Fabric 2", after about 12 seconds of exposure, it can be assumed that the individual would receive a second-degree burn. In the tests for "Fabric 1", the data never crosses the Stoll curve, so it is assumed that this fabric would provide sufficient protection to prevent a second-degree burn and would be accepted in the industrial world as being good enough. In the next section, the experimental method for obtaining the data will be presented.

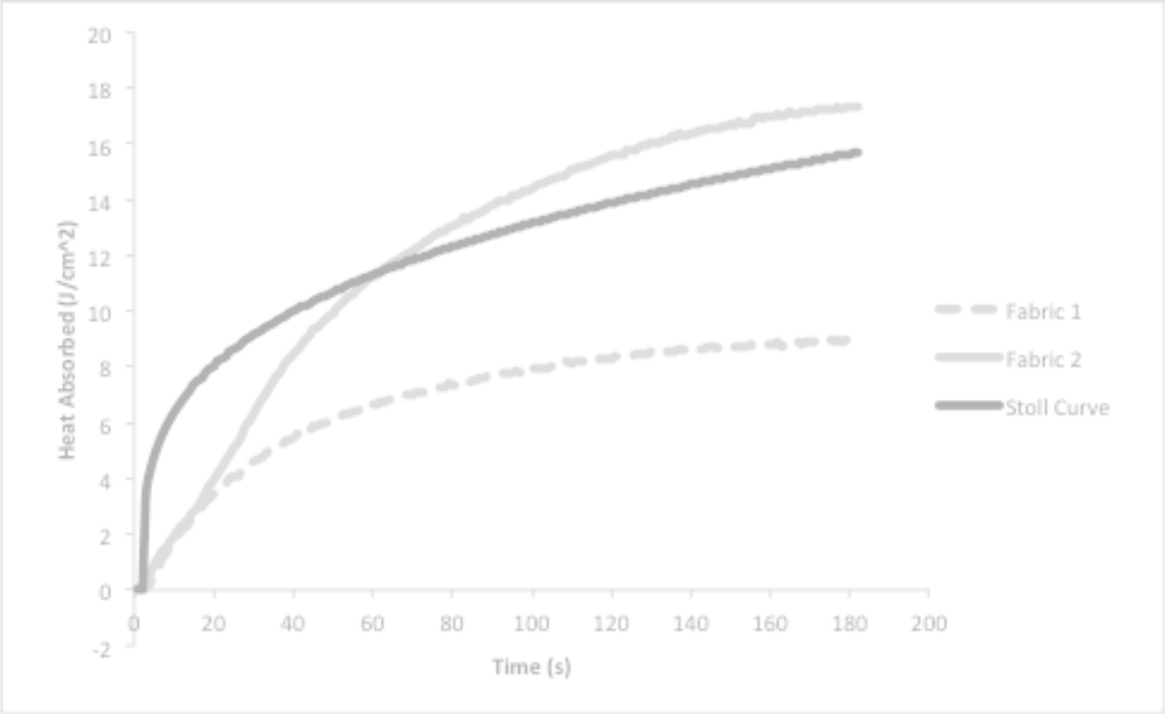

Figure 2-2: Example of the Stoll curve as compared to experimental data taken with two different fabrics

2.4 Current Test Methods

For materials subject to hot liquid splashes, the ASTM 955 test has been the standardized test in the industry for assessing a fabric's ability to protect an individual from thermal burns. The basic concept entails placing a sample of fabric over a board embedded with copper slug calorimeters that have thermocouples attached to them that measure the temperature change when a hot liquid is poured over the fabric. That information is used to determine the energy transfer as a function of time by thermodynamic relationships, which is then compared to the Stoll curve to determine the pass/fail criteria of the fabric.

In more specific details, that test setup entails using embedded copper slug calorimeters into a material with an extremely low thermal conductivity; often a form of ceramic such as

Alumina is used because of its low thermal conductivity and ability to withstand high temperatures. 40 mm diameter, 1.6 mm thick copper slug calorimeters are used with the outer surface coated with high emissivity high temperature black paint. 30-gauge type J thermocouple are attached to the back of the copper slug calorimeters, and are used due to the low thermal mass of the thermocouple so the response time can be as high as possible. A test swatch of fabric is then placed over the surface board containing the copper disks and then approximately one kilogram of hot liquid is then poured over the fabric at a predetermined angle of 70 degrees to simulate what has been designated as conditions characteristic of a typical splash and shedding of a hot liquid on an individual. A data acquisition system is used to simultaneous take temperature measurements over a period of 45 seconds at a rate of 4 samples per second for each sensor. A picture of a test setup that has been used to obtain data for this method is shown in Figure 2.3

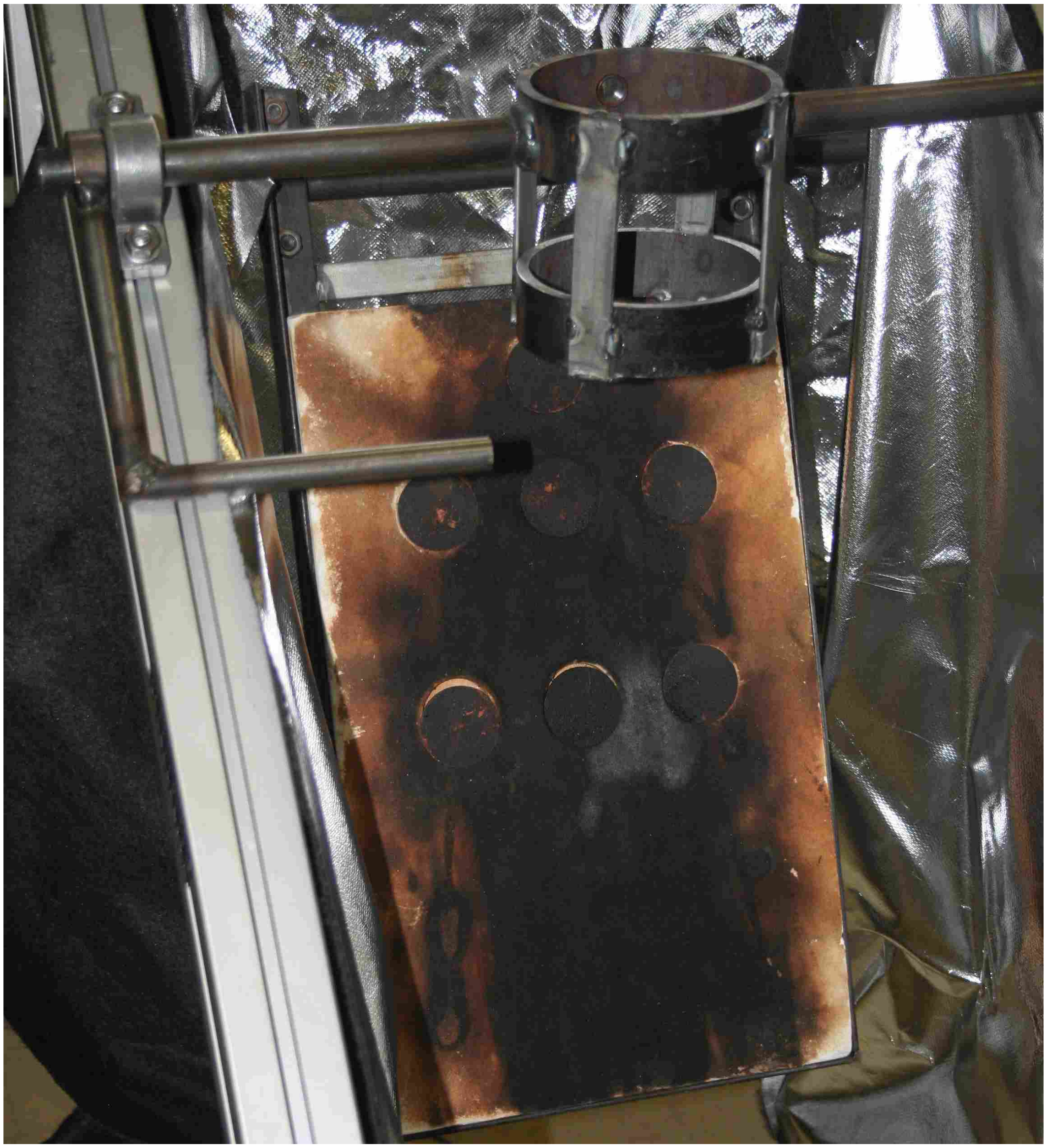

Figure 2-3: Test apparatus used for obtaining data in accordance to ASTM 955 test for assessing the performance of fabrics subject to hot liquid splashes.

Once the temperature measurements are obtained, they are analyzed to translate temperature measurements on the backside of the copper slug calorimeters into more useful information of the total absorbed energy. Using a control volume approach in which the volume of copper is taken as a system, it is assumed that over the period of time that the test would occur, the dominant form of heat transfer is the energy transferred from the hot liquid to the copper calorimeter. All other forms of heat transfer are negligible over that period of time due to the low thermal conductivity of the surrounding ceramic board and semi-enclosed air cavity on the back of the copper disk which behaves as a layer of insulation. Using thermodynamic relationships of the single heat interaction and the change in internal energy of the copper, the change in temperature can be related to the total heat absorbed averaged over the calorimeter, in units of J/cm^2 as a function of time as shown in Eq. 2.2.

$$Q'' = dwc_p(t)\Delta T \tag{2.2}$$

Each time step during the test has an associated change in temperature, or ΔT that is dependent upon how the heat capacity, or c_p(T) changes as a function of temperature, so the change in the heat capacity needs to be known as a function of temperature for the most accurate results. In reality the change in the heat capacity is relatively small for the range of temperature changes that would be expected, so although it could be a reasonable approximation to model the heat capacity as constant, the standard practice is to include the temperature dependence.

It is not necessarily the amount of energy that is transferred through the fabric, but it is a combination of how much and how quickly the energy is transferred that is important in terms of making the information useful in relating a fabric's ability to protect an individual. If the energy transfer happens slowly enough, then the body will either dissipate the energy away from the contact site through conduction to the surrounding tissue or transfer the energy away into the blood stream by means of internal convection. Hence the energy absorbed per unit area needs to be determined as a function of time, such as was shown in Figure 2.2.

This test method does indicate how well a particular fabric works for a particular hot liquid and is ultimately the most important data used to determine how well a fabric works in the real world to protect people from the dangers of hot liquids. However, in being able to improve the fabric design, relying on this experimental method can only give more generalized information about a fabric's overall performance and not specific information about individual properties. While tests of this nature can be used to some extent to determine how changing one property affects the overall performance of the material, the specific information about each property is indiscernible in the data. For example, in comparing one fabric to another fabric, you can only tell how the overall system works; specific information about which fabric has a higher thermal conductivity or heat capacity is indiscernible in the results. Other tests exist that are commonly used to determine specific properties such as heat capacity, thermal conductivity, but none of them take into account the potential for a fabric to be orthotropic in regards to the thermal conductivity. It is for this reason that another method is necessary to provide more detailed information about the radial thermal conductivity. In any experimental test, the first thing that needs to be done is the development of an analytical model, which will be discussed next in order to develop the foundation for more advanced tests that could be developed.

2.5 **Analytical Modeling of Thermal Protective Systems**

The use of experimental methods is the most important method to determine how well a fabric can protect an individual. However, they are of limited usefulness in the design stage terms of being developing optimum fabrics for a particular application. Developing analytical models can help to identity the parameters that the system is dependent upon, and how changing these parameters can ultimately affect the end performance of the fabric. They are especially useful in the design or development phase of these fabrics, and proper use allows saving money and time that would be required in unnecessary experimental testing.

There have been several analytical models developed for modeling the heat transfer processes through fabrics for various situations. A brief summary and overview of some of the models and their applications will be discussed.

Many general models [7-12] have been developed that model heat transfer through fabrics in the general sense, particularly modeling heat transfer from the body to the environment. Models such as these are useful in modeling the day-to-day conditions that most people encounter such as heat and mass transfer through typical fabrics, but have limited usefulness when considering protection from a highly concentrated source thermal energy.

Other more specialized models [13-15] have been developed that model heat transfer from radiant heat sources. These models are predominately related to firefighting applications, in which the incident energy is thermal irradiation from hot gases. This has been the primary area of interest in terms of modeling heat transfer through PPE, and little modeling has been done outside of this realm. Articles by Song, et al develop an a

These models are based on the assumption of uniform irradiation on the surface of the fabric, such as would occur in situations such as radiation from a fire that could be approximated as uniform over the exposed surface. When considering a liquid splash, the energy transfer is localized to a small area, often as small as a single point, and hence the energy transfer is multidimensional in nature. The energy source for liquid splashes is not dominated by thermal radiation; conduction and convection from hot liquids are the dominant forms of energy transfer because of direct contact. Hence, the models previously mentioned, are inadequate for these applications and a new model needs to be developed that will model heat transfer through thermal textiles when subject to hot liquid splashes.

3 ANALYTICAL MODELING

The physical mechanisms of thermal energy transfer that occur during a hot liquid splash will be first discussed. Based on the physical processes that occur, a mathematical model will be presented and the general solution method outlined. A step-by-step mathematical development to the solution of the model is not shown here, but is shown in Appendix A. The results and a discussion of the results of more specific cases then will be presented.

3.1 Development of Analytical Model

When a hot liquid splash impinges upon a surface, thermal energy or heat is transferred via multiple modes from the hot liquid to fabric. The heat transfer process is complicated, but includes a combination of conduction, convection, and thermal radiation from the hot liquid to the fabric. The dominant form of energy transfer is highly dependent upon the specific splash and a general assumption can't be made about one form on energy transfer being more dominant than the others. For example, during some splashes, the liquid adheres to the surface of the fabric and in those situations; conduction may be the primary mode of heat transfer. In other splash scenarios, the liquid may have little or no adherence and flow over the surface of the fabric with convection being the dominant mode of heat transfer.

Regardless of the mode of transfer of the energy from the hot liquid to the fabric, once the energy is transferred to the fabric, it will then be stored or diffused within the fabric via conduction. As fabrics are weave-based in their construction, the weave properties may create a preferred path of travel if there is less thermal resistance in certain directions, such as along the length of the fibers rather than across them. It will be assumed that the thermal energy will take one of two paths either through the fabric in an axial direction, or across the fabric outward radially. At some point, all the energy transferred to the fabric will either diffuse outward and be lost by free convection and thermal radiation at the surface, or will diffuse through the thickness of the fabric and be transferred to the next system. The energy that is diffused through the thickness of the fabric will either be in contact with another solid, such as skin or other fabric layers, or be exposed to small layer of air, often stagnant. The worst case scenario, which would happen when the greatest amount of energy is transferred through the fabric, would occur when there is contact with either the skin or other fabric layers, so that is the primary focus of this analysis.

All of these physical processes may be modeled mathematically by the heat diffusion equation with the appropriate boundary and initial conditions. The model will begin with the two-dimensional heat diffusion equation in cylindrical coordinates for an orthotropic medium with an arbitrary heat generation source, shown below in Eq. 3.1

$$k_r \frac{1}{r}\frac{\partial}{\partial r}\left(r\frac{\partial T(r,z,t)}{\partial r}\right) + k_z \frac{\partial^2 T(r,z,t)}{\partial z^2} + \dot{q} = dc_p \frac{\partial T(r,z,t)}{\partial t}. \tag{3.1}$$

An orthotropic material is assumed here to allow for the thermal conductivity to vary in different directions. Because of weave patterns and the non-continuum nature of textiles, this assumption will account for any variation that may exist due to different thermal conductivities for each direction. It should be noted that because the fabric is a weave and a non-continuum, the thermal conductivities used in the model are essentially effective thermal conductivities for each direction. The thermal conductivity of the pure fiber is typically higher, but due to air within the weave of the fabric, the effective thermal conductivity is lower than that of the pure fiber. It is assumed that conduction along the azimuthal direction is negligible and is not considered in this model.

Although no heat generation physically occurs when a hot liquid splashes on fabric, the model will include a source term that approximates a hot liquid splash. It would be very complicated to try and model a splash directly and would require advanced tools such as CFD to make any sort of reasonable prediction. This research is focused on how the fabric transfers energy internally and is not concerned so much with the effects of how the energy was transferred from the liquid to the fabric. Hence a localized heat generation source will simulate a spike in temperature at the surface of the fabric, such as one that would occur from a liquid splash. Although in reality a liquid splash is not a source of heat generation internal to the fabric, modeling the liquid splash as a heat generation source term as a small point will allow boundary conditions that are uniform, and thereby allow for an analytical solution to the model which would otherwise not be possible.

A schematic showing the boundary and initial conditions in mathematical terms is shown in Figure 3.1. The upper surface is exposed to free convection to an ambient air temperature of T_∞ and will be modeled using an average free convection heat transfer coefficient h. Thermal radiation at the upper surface will be neglected largely for the sake of mathematical simplicity. Although there can be thermal radiation from other sources besides a liquid splash, they are not considered important in this analysis where most applications consider contact with hot liquid splashes that would be on the order of 1500 degrees Celsius or more. The lower surface will be modeled as being in contact with another solid, such as skin or other fabric layers at a temperature of T_∞. An overall heat transfer coefficient or contact conductance of U will be used to model the transfer of thermal energy by conduction and account for any contact resistance. It is assumed that the fabric is axisymmetric and semi-infinite in the radial direction, implying the fabric will be unaffected by a splash at larger radial distances. Finally it is assumed that initially the fabric is uniformly at the ambient temperature of T_∞.

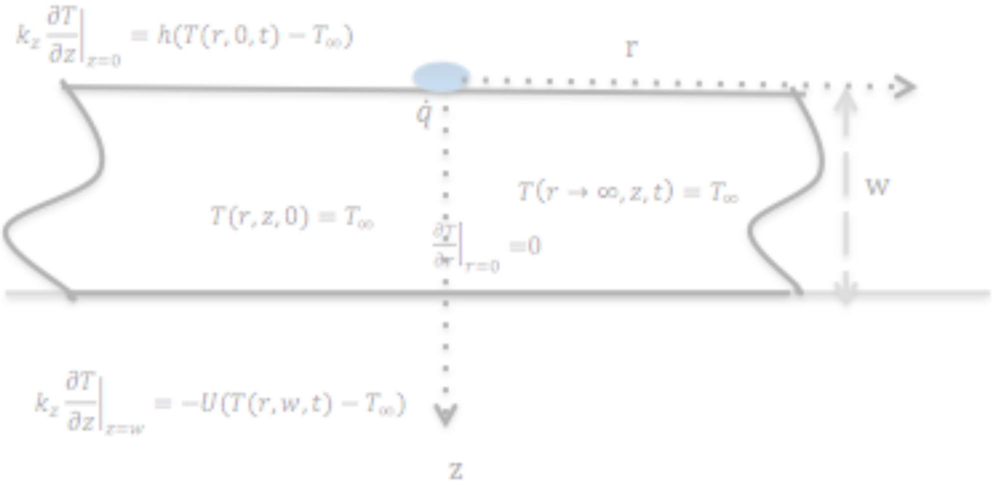

Figure 3-1: Schematic of boundary/initial conditions

3.1.1 Analytical Solution

In order to facilitate a general solution, non-dimensional parameters are used to obtain a non-dimensional solution. This will reduce the number of parameters that the solution is dependent on, and will also make the solution easier to obtain by transforming non-homogenous boundary conditions to homogenous ones. Applying the non-dimensional parameters defined in the nomenclature yields the governing non-dimensional equation in Eq. 3.2.

$$\frac{1}{\epsilon^2}\frac{1}{\rho}\frac{\partial}{\partial \rho}\left(\rho\frac{\partial \theta}{\partial \rho}\right) + \frac{\partial^2 \theta}{\partial \zeta^2} + \frac{\dot{q}\alpha}{k_z r_{ref} T_{ref}} = \frac{\partial \theta}{\partial \tau} \tag{3.2}$$

In Eq. 3.2, this equation is in much simpler form than in Eq. 3.1. The mathematical definition for each of the non-dimensional parameters can be found in Appendix A, but a brief description will be provided here. The parameter ε is defined as a ratio of thermal conductivity and is the parameter that will be the focus of this research. The variable ρ is the non-dimensional radial position, and ζ is the non-dimensional height, θ is the non-dimensional temperature variable, and finally τ is the non-dimensional time. The collective term that includes the heat generation source could be referred to as the non-dimensional source term. It will be left in this format temporarily to avoid confusion as the solution will involves using some mathematical transformations, and a new source term will be redefined later.

Applying the non-dimensional parameters defined in the nomenclature to the boundary and initial conditions yields the non-dimensional boundary and initial conditions shown in Table 3-1. Effectively the boundary conditions are the same as they were previously, but in non-dimensional form, they are now homogenous and allows for a relatively simple mathematical solution. It should be noted that with all the boundary and initial condition being homogenous, the driving source of the solution then would be the heat generation source term.

Table 3-1: Summary of non-dimensional initial and boundary conditions

Upper Boundary	$\left.\frac{\partial\theta}{\partial\zeta}\right\|_{\zeta=0} = \frac{hw}{k_z}\left(\theta(\rho,0,\tau)\right) = Bi_0\theta(\rho,0,\tau)$
Lower Boundary	$\left.\frac{\partial\theta}{\partial\zeta}\right\|_{\zeta=1} = \frac{Uw}{k_z}\left(\theta(\rho,1,\tau)\right) = -Bi_w\theta(\rho,1,\tau)$
Radial Boundary	$\theta(\rho\to\infty,\zeta,\tau) = 0$
Radial Boundary	$\left.\frac{\partial\theta}{\partial\rho}\right\|_{\rho=0} = 0$
Initial Condition	$\theta(\rho,\zeta,0) = 0$

The solution to the governing equation is found by using the integral transform method. A Finite Fourier Transform is applied, followed by a Hankel Transform to yield a first order differential equation that is only a function of non-dimensional time. The time dependent differential equation is then solved using an integrating factor by applying the transformed initial condition. Using the inverse Hankel Transform and Inverse Finite Fourier Transform, the solution is transformed back in terms of the non-dimensional radial and axial position.

As the specific solution is dependent upon the specific heat generation source used, a generalized solution will be presented. To obtain specific case results, Hankel and Fourier Transforms have to be applied to the source term to obtain a transformed source term, which is then used for the specific case solution. The generalized solution is shown below in Eq. 3.3

$$\theta(\rho,\xi,\tau) = \sum_{n=1}^{\infty}\frac{\phi(\beta_n,\zeta)}{N(\beta_n)}\int_0^{\infty}\lambda J_0(\lambda\rho)e^{\left\{-\left(\frac{\lambda^2}{\epsilon^2}+\beta_n{}^2\right)\tau\right\}}\int_0^{\tau}e^{\left\{\left(\frac{\lambda^2}{\epsilon^2}+\beta_n{}^2\right)\tau'\right\}}\bar{\bar{Q}}d\tau'\;d\lambda. \qquad (3.3)$$

The transformed heat generation term is found from applying the Hankel and Fourier Transform to the initial heat generation term, shown in Eq. 3.4 below

$$\bar{\bar{Q}} = \frac{\alpha_2}{k_2 w r_{ref}} \int_0^\infty \int_0^1 \phi(\beta_n, \zeta)\rho J_0(\lambda\rho)\dot{q}\ d\zeta d\lambda. \tag{3.4}$$

The Eigen-function, which is found from the corresponding Sturm-Louisville problem, is found for specific cases in literature [16], and is shown below in Eq. 3.5

$$\phi(\beta_n, \zeta) = \beta_n \cos(\beta_n \zeta) + Bi_0 \sin(\beta_n \zeta). \tag{3.5}$$

The Eigen-values are found from the roots to the transcendental equation obtained from evaluating the boundary conditions in the corresponding Sturm-Louisville problem. For this specific case, the transcendental equation is found in literature [16] and is given in Eq. 3.6

$$tan(\beta_n) = \frac{\beta_n(Bi_0 + Bi_w)}{{\beta_n}^2 - Bi_0 Bi_w}. \tag{3.6}$$

The Eigen-values obtained from the transcendental equation are a function of the non-dimensional parameters Bi_0 and Bi_w, which are the non-dimensional parameters that show up in boundary conditions at the upper and lower surface. These non-dimensional parameters are defined in Eq. 3.7 and Eq. 3.8 below.

$$Bi_0 = \frac{hw}{k_z} \tag{3.7}$$

$$Bi_w = \frac{Uw}{k_z} \tag{3.8}$$

The normalization constant, which is found based on the principle of orthogonality is given in literature [16] for this specific case and is shown in Eq. 3.9 below

$$N(\beta_n) = \frac{1}{2}\left(({\beta_n}^2 + {Bi_0}^2)\left(1 + \frac{Bi_w}{({\beta_n}^2 + {Bi_0}^2)} + Bi_0\right)\right). \tag{3.9}$$

The solution to the governing equation gives the non-dimensional temperature profile within the fabric. The non-dimensional temperature profile is of limited usefulness. The purpose of thermal protective fabrics is to minimize heat transfer through the fabric. Hence, the non-dimensional heat flux at the lower surface will be what is examined in this analysis. The non-dimensional heat flux can be found either by differentiating with respect to zeta, or by using the boundary condition at the lower surface as is shown in Eq. 3.10.

$$q''_{non-dimensional} = \mathrm{Bi}_w \cdot \theta(\rho, \zeta = 1, \tau) \tag{3.10}$$

For the sake of simplicity in comparison, the heat flux will be kept in non-dimensional format, and using the definition of the non-dimensional parameters, the dimensional heat flux can be obtained if desired.

The solution given in Eq. 3.5 – Eq. 3.9 is a function of only three parameters. Regardless of the source term, the solution is dependent upon the ratio of thermal conductivities indicated by ε, and the non-dimensional parameters Bi_0 and Bi_w from the boundary conditions. Minimizing the amount of heat transferred through the fabric can be achieved by using an optimal set of these three parameters. The non-dimensional boundary conditions are a function of the axial thermal conductivity, the thickness of the material, and either the convective or overall heat transfer coefficient for the upper or lower surface respectively. As each non-dimensional parameter is a defined as a combination of other properties and parameters of the system, the individual properties will be examined to determine best how to minimize the heat transfer through the fabric thickness.

The average free convection heat transfer coefficient, which is part of the upper non-dimensional boundary condition shown in Eq. 3.7, governs how much energy is transferred by convection. The values of the free convection coefficient vary depending on many factors, including air temperature, surface temperature of the fabric, incline angle, etc. Values for the free-convection heat transfer coefficient may be estimated for specific cases of interest using correlations that can be found in any reference on the subject matter or heat transfer textbook. Typical values for free-convective heat transfer coefficients will range from 2-10 W/m*K. To minimize heat transfer through the fabric, a large free convection coefficient is desirable. Practical limitations prohibit controlling this parameter, as this is a property that depends on the surroundings, and not of the fabric itself.

The overall heat transfer coefficient on the lower surface governs how much energy is transferred at the lower surface. This system property is part of the non-dimensional boundary condition used at the lower surface, indicated in Eq. 3.8. The overall heat transfer coefficient can be somewhat difficult to predict, as it depends on the fabric material, the material in which it is in contact with, as well as other considerations, such as moisture content. Typically, fabrics are worn loosely and poor thermal contact is a result between the fabric and other layers or skin. Many common materials that are used, such as fleece or other fabrics that we would consider "fuzzy" would result in a especially poor thermal contact. This poor thermal contact is a result of the surfaces non-smooth nature and the air gaps between the two surfaces. To determine the exact value, experimental estimates could be made for an overall heat transfer coefficient, but this would be valid only for very specific conditions in which testing occurred. Related research [16] involving contact in which an analytical model was presented for different conditions, estimate of the value for the contact resistance ranges from 200-400 W/m*K during experimental testing. To minimize heat transfer, a small value for the overall heat transfer coefficient is desirable. Similar to the free convection coefficient, the overall heat transfer coefficient is difficult to control in the design stage of material development.

Fabric thickness is a property of the system that both the upper and lower non-dimensional boundary conditions are dependent on, and to minimize the amount of energy transferred, thickness should be made as large as possible to make the non-dimensional boundary conditions large. Practical limitations govern how thick materials can be made. It is well understood that basically any level of protection that is desired could be achieved by making the fabric thick enough. However, the limiting constraint is if fabric systems can be made comfortable enough that people will wear them or not. The necessity for clothing systems that are cool and breathe well, and allow enough freedom of movement and dexterity, limits the material thickness to something on the order of millimeters in thickness, depending on the materials used.

The axial conductivity is a material property that both non-dimensional boundary conditions are dependent upon, as well as the ratio of thermal conductivities. As noted earlier, this is an effective thermal conductivity, and is a function of both the properties of the material used and the manner in which it is constructed. To minimize the non-dimensional boundary conditions, it is desirable to have this value as small as possible and is only limited based upon which materials are available. Fabrics used in these applications have a thermal conductivity for in the range in the range of 0.03-0.08 W/m*K.

An orthotropic material that has a ratio of thermal conductivities less than one can minimize heat transfer regardless of the environment in which the fabric is used and without having to make fabrics thicker sacrificing comfort for protection. As the parameter ε is defined as the axial thermal conductivity normalized by the radial thermal conductivity, it is desirable to have ε range from 0 to 1, indicating that the radial thermal conductivity is larger than the axial thermal conductivity. The radial thermal conductivity can be made so that it will be greater than one, but this would make the process even more one-dimensional in nature and would adversely affects how energy is transferred.

The ratio of thermal conductivities, or ε, is the parameter that will be the focus of the remainder of this research, particularly how changing this ratio affects the amount of energy transferred through the material. For the other parameters, the values that are chosen are of less consequence as the effect of each of those parameters is well understood. The worst-case scenario, which would correspond to the case that will allow the maximum magnitude of energy transfer, of h=2 W/m^2*K and U=400 W/m^2*K, and typical values of k_z=0.03 W/m*k and w=1 mm will be used in this analysis as a baseline to compare how changing the ratio of thermal conductivity affects the energy transfer through the material. These values correspond to the non-dimensional boundary conditions of Bi_w=13.3 and Bi_0=0.067.

3.1.2 Point Source Solution and Results

The first scenario that will be analyzed is when the energy being released can be modeled using a point source, in which all the energy is released at a single point in space over a single point in time. This will be modeled using delta functions and is shown in Eq. 3.11 below

$$\dot{q} = \frac{Q_0 \delta(r)\delta(t)\delta(z)}{2\pi r}. \tag{3.11}$$

In this scenario, an amount of thermal energy, Q_0, is released over a short instance in time indicated by δ(t), and over the infinitesimal volume defined by δ(r) and δ(z). The use of delta functions for both spatial dimensions and the one temporal dimensions limits the energy generation to a single point. Although somewhat physically unrealistic to have such a large amount of energy released over an infinitesimally small amount of time in an infinitesimally small volume, its simplicity is useful in analyzing how energy is transferred within the material. As all the energy is localized, any real splash can be compared to this idealized scenario. The value of Q_0 is not important for this model. To use this model to replicate an actual splash, it would be necessary to know this term, but that is not the focus of this research. Ultimately the solution will be non-dimensionalized to analyze how the energy is transferred within the fabric via conduction, and the non-dimensional solution that will be used for the analysis is not dependent upon Q_0..

Transforming the source term in Eq. 3.11 into non-dimensional format yields the non-dimensional source term in Eq. 3.1.12

$$\dot{q} = \delta(\rho)\delta(\zeta)\delta(\tau). \tag{3.12}$$

The general solution may be applied and a case-specific solution may be obtained by substituting the source term of Eq. 3.1.12 into Eq. 3.1.4 and evaluating to yield the transformed non-dimensional source term. Substituting the transformed source term into Eq. 3.3 yields the non-dimensional solution, given below in Eq. 3.13 through 3.17.

$$\theta(\rho,\xi,\tau) = \sum_{n=1}^{\infty} \frac{\phi(\beta_n,\zeta)}{N(\beta_n)} \int_0^{\infty} \lambda J_0(\lambda\rho) \frac{\beta_n}{8} e^{\left\{-\left(\frac{\lambda^2}{\epsilon^2}+{\beta_n}^2\right)\tau\right\}} d\lambda. \tag{3.13}$$

$$\bar{\bar{\bar{Q}}} = \frac{\beta_n}{8} \tag{3.14}$$

$$\phi(\beta_n,\zeta) = \beta_n \cos(\beta_n\zeta) + Bi_0 \sin(\beta_n\zeta) \tag{3.15}$$

$$N(\beta_n) = \frac{1}{2}(({\beta_n}^2 + {Bi_0}^2)(1 + \frac{Bi_w}{({\beta_n}^2+{Bi_0}^2)} + Bi_0)) \tag{3.16}$$

$$tan(\beta_n) = \frac{\beta_n(Bi_0+Bi_w)}{{\beta_n}^2 - Bi_0 Bi_w} \tag{3.17}$$

Using the solution to the non-dimensional temperature profile, and then applying the definition of the non-dimensional parameters to obtain the temperature in dimensionalized form again, the instantaneous heat flux through the fabric can be determined for Fourier's law of conduction determined. Then the total heat transferred through the fabric can be found for a hypothetical situation in which an arbitrary amount of energy is released, specified by Q_0. By integrating the heat flux with respect to time, the solution can be compared to the Stoll curve as is shown in Figure 3.2 for various ratios of k_z/k_r. In the isotropic case, when $k_z/k_r=1$, the curve representing the amount the total energy transferred through the fabric touches the Stoll Curve, indicating that an individual would receive a second-degree burn. If an orthotropic material were used where the radial thermal conductivity is greater than the axial thermal conductivity, an individual would not receive a second-degree burn, indicated by the curves representing the total energy absorbed being well below the Stoll Curve. This establishes the foundation of this research that the use of an orthotropic material in which the radial and axial thermal conductivities are different can be used to improve a fabric's ability to protect an individual, even to the extent that a material with all other properties being identical could prevent a second degree burn if it were made in such a way that it could have orthotropic properties in regards to the thermal conductivity.

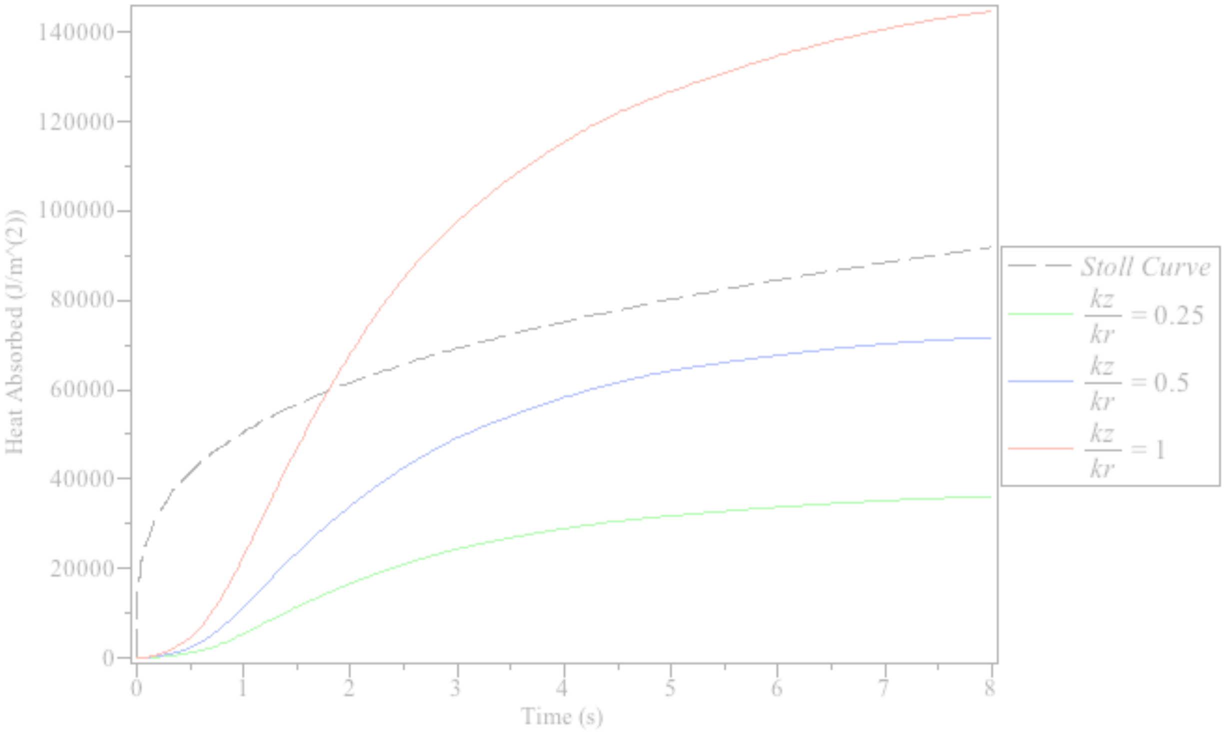

Figure 3-2: Total heat absorbed for various ratios of thermal conductivities as compared to Stoll curve

From Figure 3.2, we can determine that for at least for the specific hypothetical case analyzed, that a second-degree burn would be prevented locally at that point through use of an orthotropic material with the radial thermal conductivity being larger than the axial thermal conductivity under those conditions. There are a few things to consider though from these results; as mentioned this was for a hypothetical situation in which an arbitrary amount of energy was released of sufficient magnitude to be on the same order as the Stoll curve. In real life, it is almost impossible to correlate a splash to an exact amount of energy that needs to be input in the model without significant experimentation. The goal of this research is not to directly model the transfer of energy from a splash through a fabric, but to model the behavior of energy transfer internal to the fabric. So ultimately, comparing the results to the Stoll curve is not the ideal way to analyze the results of the model. Figure 3-2 is no more than a proof of concept to show that the results could mean that the information could be useful in the real world.

Leaving the solution in non-dimensional form is not dependent directly upon the value of the source term, as the value does not need to be known for a non-dimensional solution, it is merely a scaling number. To transform the non-dimensional solution back into a dimensional format, then the value of Q_0 would have to be known. Instead, the non-dimensional heat flux through the fabric will be analyzed so that greater insight can be gained on the behavior of energy transfer by conduction within the fabric when the radial and axial thermal conductivity are different. This is found simply by taking the gradient, or derivative of the solution in the non-dimensional axial direction.

The non-dimensional heat flux through the fabric as a function of non-dimensional time is shown at the center, or $\rho=0$, where the maximum heat flux occurs in Figure 3.3. The source term was released at this non-dimensional radial position, hence the maximum heat flux occurs at this non-dimensional radial location. The magnitude of the maximum heat transfer is drastically reduced by use of an orthotropic material. A thing to note is that although the source defined by the delta dirac function reaches a maximum value at τ=0, the heat flux through the fabric will not occur at that time. There will be a delay because energy has to both be transferred across the fabric, and some of that energy will be stored by the fabric, which is not an instantaneous process.

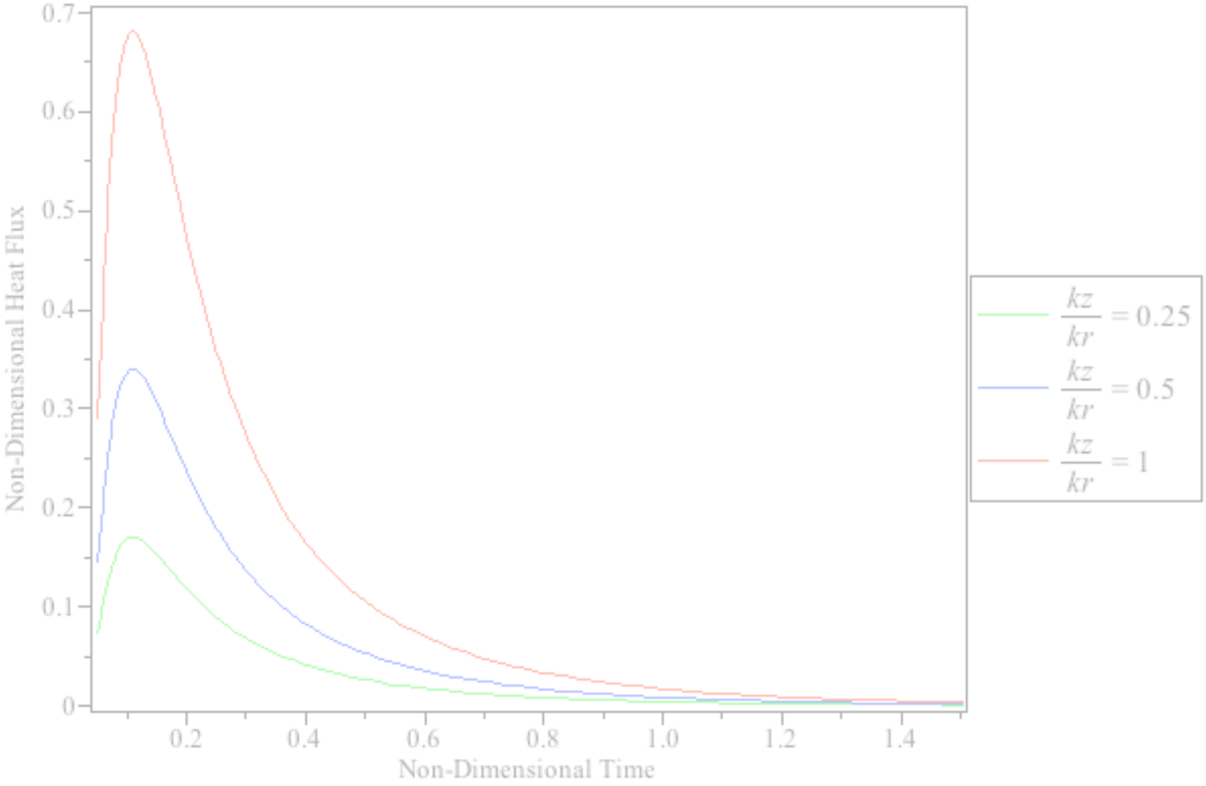

Figure 3-3: Non-dimensional heat flux as function of time for varying ratios of thermal conductivity, ρ=0 and ζ=1

Away from the source term, at an arbitrary non-dimensional radial position of ρ=2, the non-dimensional heat flux is shown in Figure 3.4 as a function of non-dimensional time. The magnitude of the non-dimensional heat flux is much less than it was at ρ=0, signifying that the majority of the heat transfer occurs within a very small area. The same amount of energy has been released and transferred over a larger area, essentially making the energy less concentrated. Although the magnitude is greater at larger radial locations, this effect is desirable at the cost of reducing the maximum magnitude of energy transfer at the center, directly under where the energy has been released. Another thing to note is that the thermal diffusivity of the material for the radial direction is decreased as well when using an orthotropic material with a radial thermal conductivity larger than the axial. This is indicated by the time shift of the maximum heat flux in Figure 3-4.

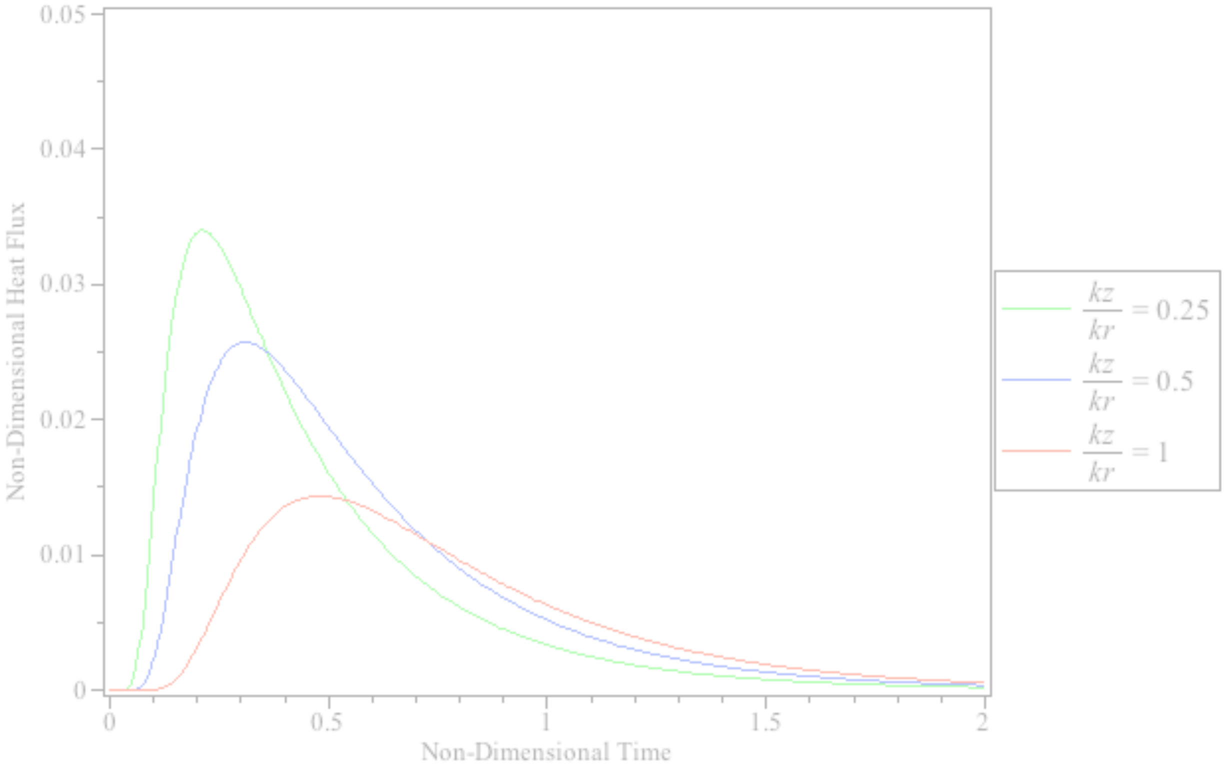

Figure 3-4: Non-dimensional heat flux as function of time for varying ratios of thermal conductivity, ρ=2 and ζ=1

As the information from the previous figures are useful in determining how the heat flux through the fabric varies with time, the information is incomplete to determine how the heat flux varies spatially. Figure 3.5 shows the non-dimensional heat flux at an arbitrary non-dimensional time of τ=0.01 as a function of the non-dimensional radial position. At this early time, the magnitude of the amount of energy transferred varies significantly as the radial thermal conductivity becomes greater than the axial thermal conductivity. Although the magnitude is decreased, the area in which the energy transfer occurs doesn't vary significantly, indicated by the non-dimensional heat flux diminishing to zero at a non-dimensional radial position at ρ=1 for the orthotropic cases as compared to the isotropic case diminishing to zero at around ρ=0.5.

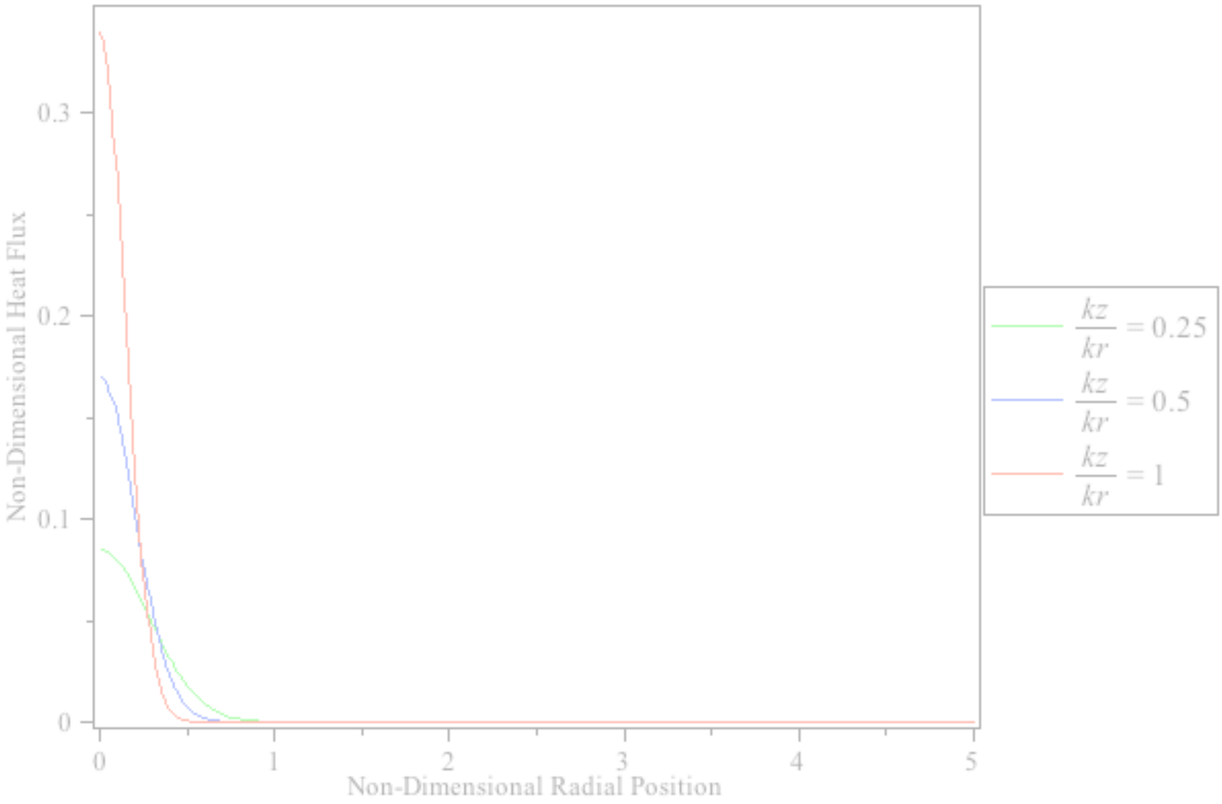

Figure 3-5: Non-dimensional heat flux as function of radial position for varying ratios of thermal conductivity, τ=0.01 and ζ=1

At a later arbitrary non-dimensional time of τ=0.1, the effect using an orthotropic material begins to become more apparent. The non-dimensional heat flux is shown as a function of non-dimensional radial position in Figure 3-6 for various ratios of thermal conductivities. Not only is the magnitude of the non-dimensional heat flux decreased through use of an orthotropic material, but energy transfer begins to occur over a larger area. At this time step, the heat flux diminishes to zero at around a non-dimensional radial position of about ρ=2.5 when the radial thermal conductivity is much greater than the axial as compared to the isotropic case where the heat flux diminishes to zero around ρ=2.5.

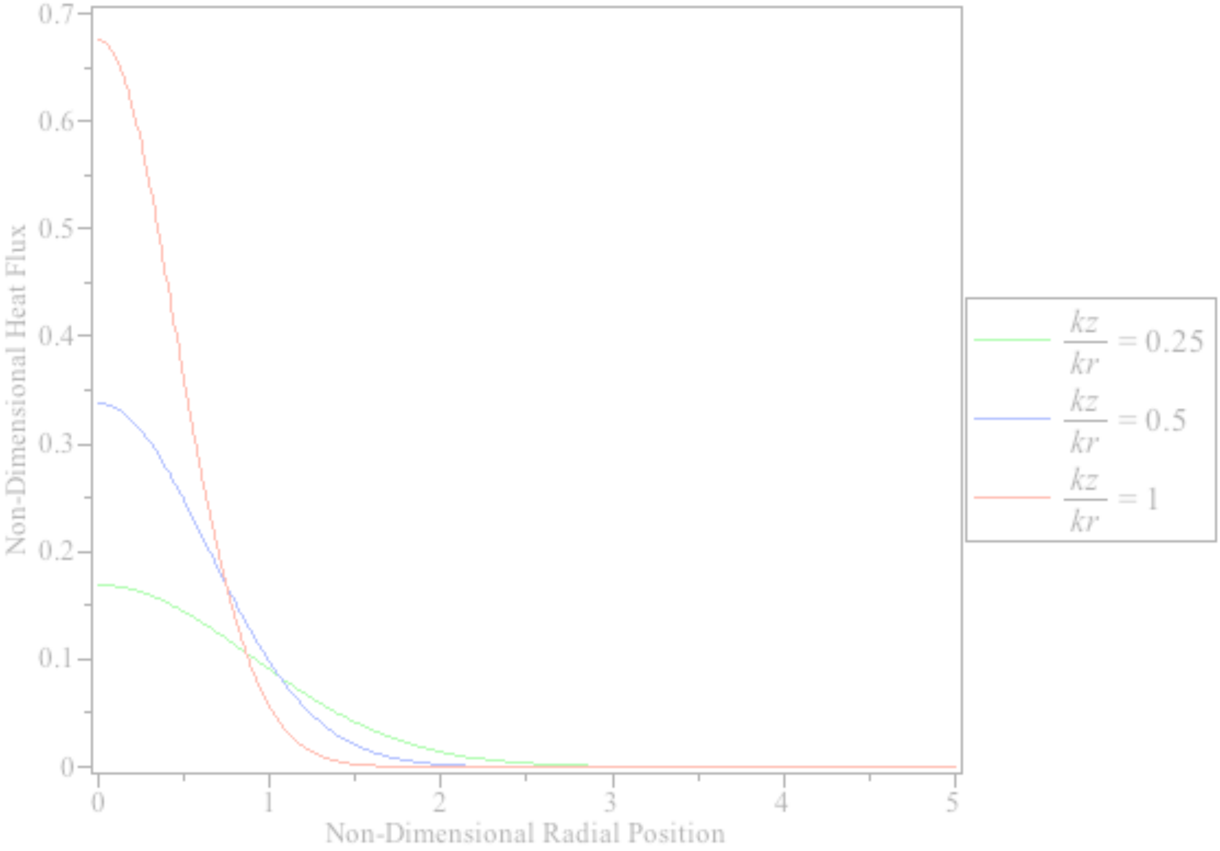

Figure 3-6: Non-dimensional heat flux as function of radial position for varying ratios of thermal conductivity, τ=0.1 and ζ=1

Figure 3.7 shows the non-dimensional heat flux as a function of non-dimensional radial position at an arbitrary non-dimensional time of τ=0.5. At this time there is still significant heat flux occurring when the radial thermal conductivity has a value equal to the axial thermal conductivity, but when the radial thermal conductivity becomes larger than the axial, the heat transfer has nearly diminished to zero. Heat transfer extends out radially much more at later times, and for this non-dimensional time, it doesn't diminish to zero until a non-dimensional radial position of about ρ=3 for the isotropic case to ρ=5 for cases when the radial thermal conductivity is much larger, in this case an order of 4 times greater, than the axial thermal conductivity.

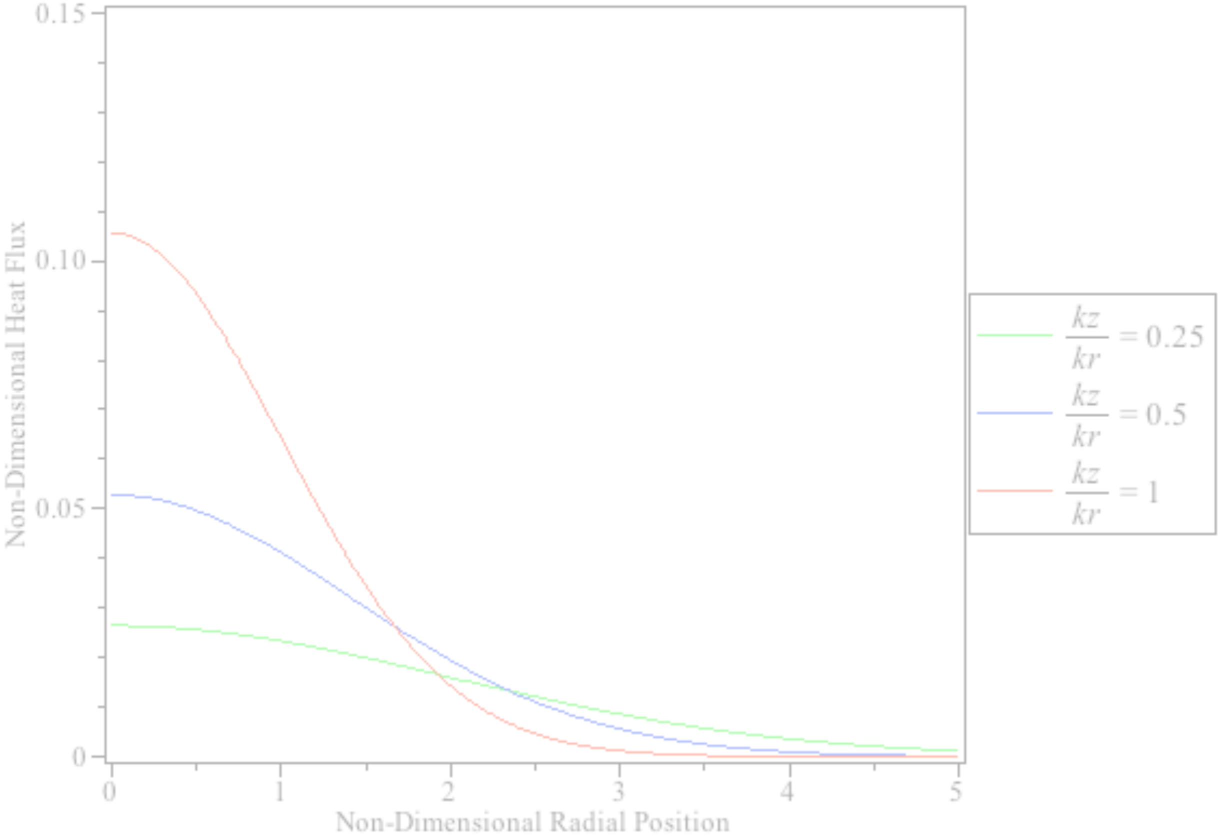

Figure 3-7: Non-dimensional heat flux as function of radial position for varying ratios of thermal conductivity, τ=0.5 and ζ=1

Figure 3.8 shows the non-dimensional heat flux as a function of non-dimensional position for a non-dimensional time of τ=1 when nearly all the energy has been transferred. Although there is still some energy transfer occurring at this time, the magnitude relative to the maximum is almost two orders of magnitude less. A thing that should be noted, for at least the specific case analyzed, is that the heat is only transferred out to a non-dimensional radial position of around ρ=5, and the magnitude of heat transfer is small at that location. Converting that back into an actual physical dimension using the definition of the non-dimensional radial position, this corresponds to a radial distance of 5 mm for a 1 mm fabric thickness, which is a small amount of area.

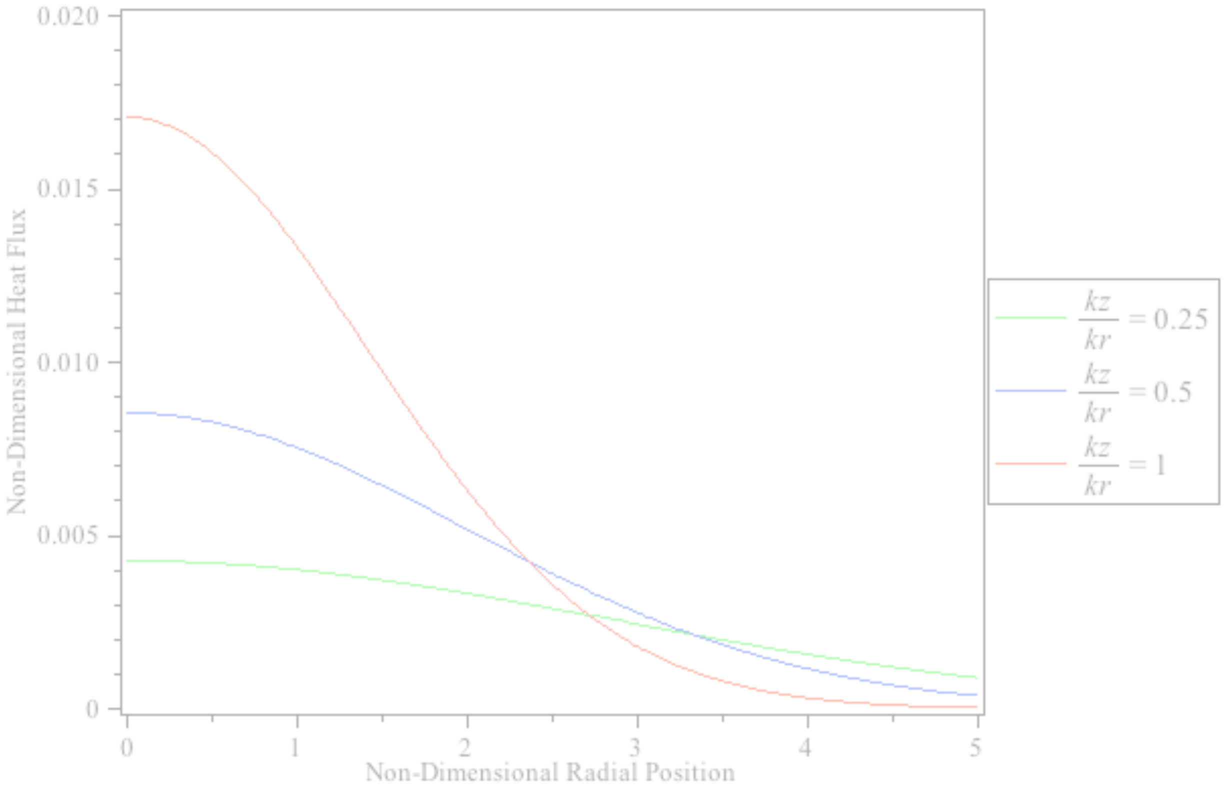

Figure 3-8: Non-dimensional heat flux as function of radial position for varying ratios of thermal conductivity, τ=1 and ζ=1

3.1.3 Finite Area and Time Solution and Results

The second scenario that will be considered is the more realistic case when the energy is transferred through a larger finite area and over a finite amount of time indicated by the source term shown in Eq. 3.18 below

$$\dot{q} = \frac{Q_0(H(r) - H(r - r_0))(H(t) - H(t - t_0)\delta(z)}{\pi {r_0}^2(t_0)}. \tag{3.18}$$

An amount of thermal energy indicated by Q_0 is released constantly over a length of time indicated by t_0, and uniformly over the cylindrical volume specified by the area of $\pi {r_0}^2$ and depth of $\delta(z)$. Heaviside functions are used to allow for uniform values within the indicated ranges of space and time, while use of the delta function for the depth ensures that heat generation occurs only at the surface. This model more closely resembles what would actually occur when a hot liquid splashes on the surface of a fabric. The splash has a finite area in which energy transfer occurs for a finite amount of time before it is shed from the surface of the fabric.

Transforming the source term of Eq. 3.18 into non-dimensional format yields the non-dimensional source term, given in Eq. 3.19 below

$$\dot{q} = \left(H(\rho) - H\left(\rho - \frac{r_0}{w}\right)\right)(H(\tau) - H\left(\tau - \frac{\alpha t_0}{w^2}\right)\delta(\zeta). \tag{3.19}$$

The solution is similar to that of the point source model in that it still depends on the parameters Bi_w, Bi_0, and ε. However, in this case there are two additional parameters that the solution is dependent upon, r_0/w and $\alpha t_0/w^2$, which correspond to the size of the splash and the duration of the splash, respectively.

The source term defined in Eq. 3.19 is substituted into Eq. 3.4 and evaluated to obtain the transformed source term. Substituting the transformed source term into Eq. 3.3 yields the final solution, and is given in Eq. 3.20 through 3.24 below. The derivation of the solution is given in Appendix A.

$$\theta(\rho,\zeta,\tau) = \int_0^\infty \sum_{n=1}^\infty \frac{\phi(\beta_n,\zeta)}{N(\beta_n)} \lambda J_0(\lambda \frac{r}{w}) e^{\left\{-\left(\frac{\lambda^2}{\epsilon^2}+\beta_n{}^2\right)\tau\right\}} \bar{\bar{Q}}\; d\lambda \qquad (3..20)$$

$$\bar{\bar{Q}} = \frac{1}{\frac{\lambda^2}{\epsilon^2}+\beta_n{}^2}\left(e^{\left\{\left(\frac{\lambda^2}{\epsilon^2}+\beta_n{}^2\right)\dot{\tau}\right\}} - 1\right)\left(\frac{\beta_n}{2}\right)\left(\frac{r_0}{\lambda w}J_1\left(\lambda \frac{r_0}{w}\right)\right)\; if\ \tau \le \frac{\alpha_2 t_0}{w^2} \qquad (3.21)$$

$$\bar{\bar{Q}} = \frac{1}{\frac{\lambda^2}{\epsilon^2}+\beta_n{}^2}\left(e^{\left\{\left(\frac{\lambda^2}{\epsilon^2}+\beta_n{}^2\right)\overset{\cdot}{\frac{\alpha_2 t_0}{w^2}}\right\}} - 1\right)\left(\frac{\beta_n}{2}\right)\left(\frac{r_0}{\lambda w}J_1\left(\lambda \frac{r_0}{w}\right)\right)\; if\ \tau \ge \frac{\alpha_2 t_0}{w^2}$$

$$\phi(\beta_n,\zeta) = \beta_n \cos(\beta_n \zeta) + Bi_0 \sin(\beta_n \zeta) \qquad (3.22)$$

$$N(\beta_n) = \frac{1}{2}((\beta_n{}^2 + Bi_0{}^2)(1 + \frac{Bi_w}{(\beta_n{}^2+Bi_0{}^2)} + Bi_0)) \qquad (3.23)$$

$$tan(\beta_n) = \frac{\beta_n(Bi_0+Bi_w)}{\beta_n{}^2 - Bi_0 Bi_w} \qquad (3.24)$$

The same values used for the point source will be used here for the boundary conditions to determine the non-dimensional boundary conditions; h=2 W/m^2*K, U=400 W/m^2*K, k_z=0.03 W/m*K, and w=1 mm. The values of $_{r0}$/w and αt$_0$/w^2 vary. Splashes can vary widely is size and duration depending on the liquid properties and the surface tension and adherence between the liquid and fabric surface. In this analysis, arbitrary typical values of r$_0$/w=5 and αt$_0$/w^2=0.8 will be used to determine how use of an orthotropic material affects energy transfer.

The non-dimensional heat flux is shown a function of non-dimensional time at the center in Figure 3.9. At this location of ρ=0, use of an orthotropic material has some effect on reducing the magnitude of the heat flux, but the reduction is minimal and only occurs at later times after the source term is over.

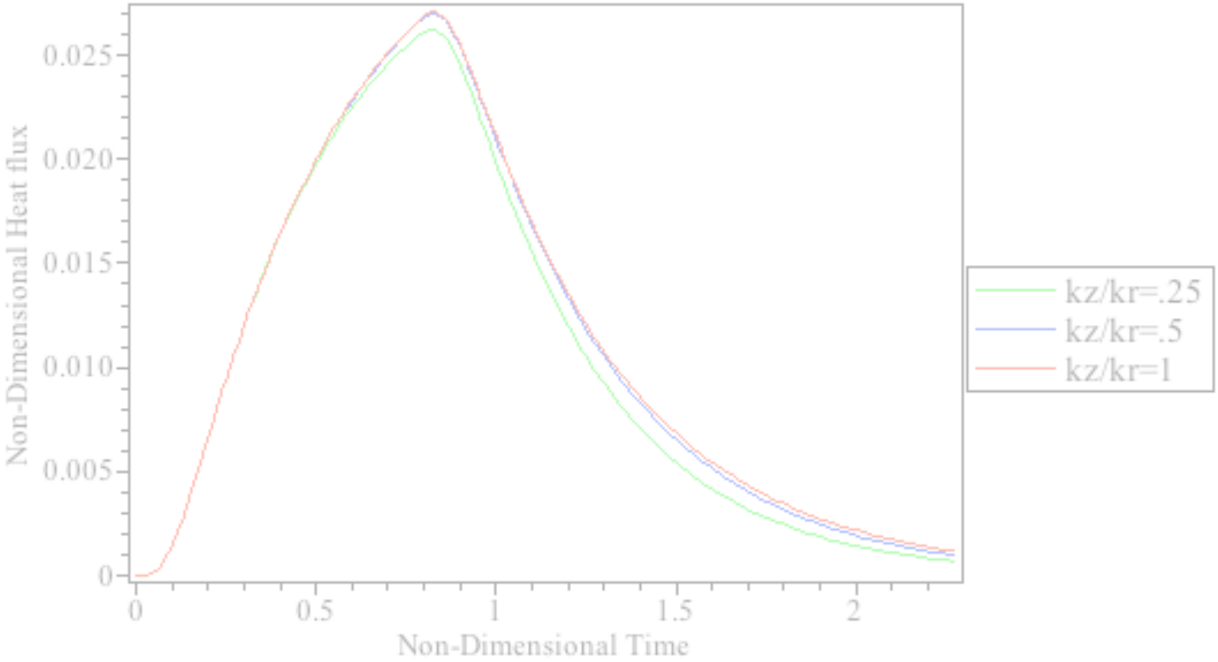

Figure 3-9: Non-dimensional heat flux as function of non-dimensional time for varying ratios of thermal conductivity, ρ=0 and ζ=1 ($r_0/w=5$, $\alpha t_0/w^2=0.8$)

Further out towards the edge of the source term, at a non-dimensional radial distance of ρ=5, the effect of an orthotropic material becomes more apparent. The non-dimensional heat flux plotted as a function of non-dimensional time at a non-dimensional radial position of ρ=5 is shown in Figure 3.10. Varying the thermal conductivity ratio has a larger affect in minimizing the magnitude of energy transfer near the edge of the source term than it does near the center, but any reduction is still small, less than 10 percent.

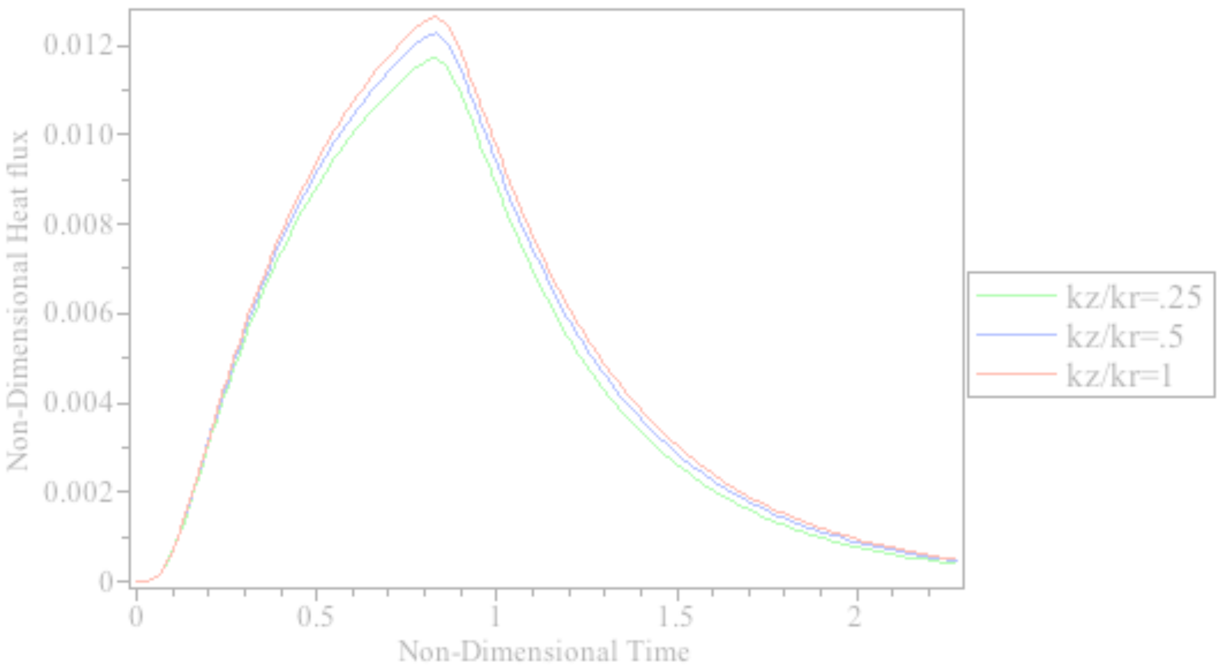

Figure 3-10: Non-dimensional heat flux as function of non-dimensional time for varying ratios of thermal conductivity, ρ=5 and ζ=1 ($r_0/w=5$, $\alpha t_0/w^2=0.8$)

The non-dimensional heat flux is shown in Figure 3.11 as a function of non-dimensional time at non-dimensional radial distance of ρ=7. Beyond the edge of the source term, the non-dimensional heat flux looks very much like it did for the point source model in that an orthotropic material decreases the magnitude of the heat transfer within the area in which energy is being released and increases the magnitude elsewhere. In addition, as a larger radial thermal conductivity results in a smaller radial thermal diffusivity, the time in which the maximum heat flux occurs outside the source area also is decreased.

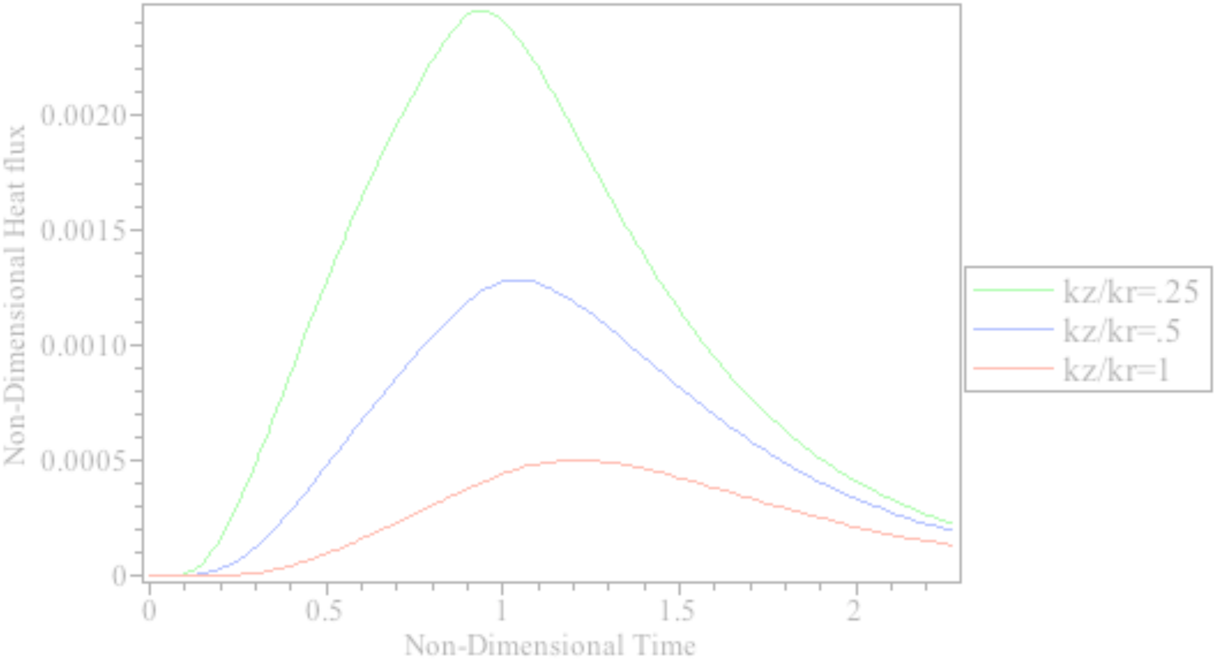

Figure 3-11: Non-dimensional heat flux as function of non-dimensional time for varying ratios of thermal conductivity, ρ=7 and ζ=1 (r_0/w=5, $\alpha t_0/w^2$=0.8)

The previous results in Figure 3-9 through Figure 3-11 show how the non-dimensional heat flux varies with non-dimensional time at a single point in each figure. The non-dimensional heat flux will now be examined as a function of non-dimensional radial position at fixed points in time so that more insight can be gained as to how an orthotropic material affects the spatial distribution of energy transfer.

Figure 3.12 shows the non-dimensional heat flux as a function of non-dimensional radial position at an arbitrarily selected non-dimensional time of τ=0.2. It should be noted that in this case, delta-dirac functions are not being used in time and the process happens slowly, so larger values will be used as at the same time steps in the previous case, nothing is really happening due to the gradual energy release. Varying the thermal conductivity has only a minor effect of reducing the magnitude of the heat flux, and only occurs near the edge of the source term. Near the center, there is no reduction of the amount of heat transferred until a radial position of approximately ρ=2-3, depending on the ratio of thermal conductivities.

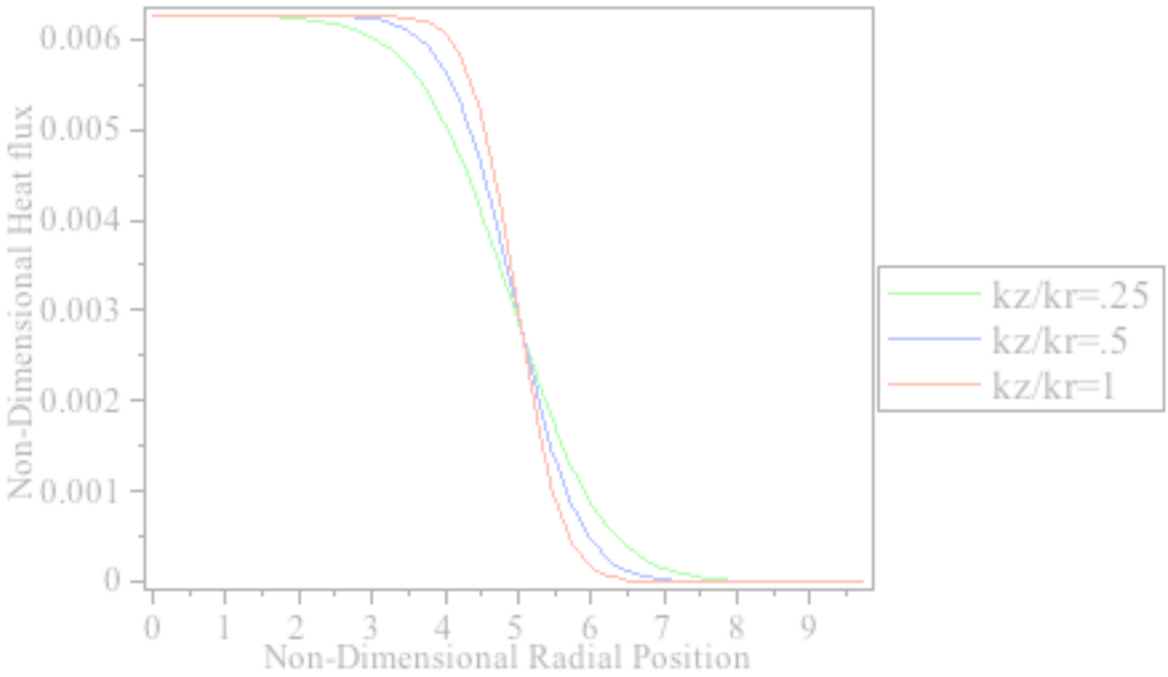

Figure 3-12: Non-dimensional heat flux as function of non-dimensional radial position for varying ratios of thermal conductivity, τ=0.2 and ζ=1 ($r_0/w=5$, $\alpha t_0/w^2=0.8$)

At a later non-dimensional time of τ=0.4, the non-dimensional heat flux is shown as a function of non-dimensional radial position in Figure 3.13. Use of an orthotropic material has more of an effect on reducing the magnitude of heat transfer than it did in the previous time step, but still is only apparent near the edge of the source term. Reduction in the magnitude of energy transfer doesn't begin to occur until a non-dimensional radial position of ρ=1-2, depending on the ratio of thermal conductivities.

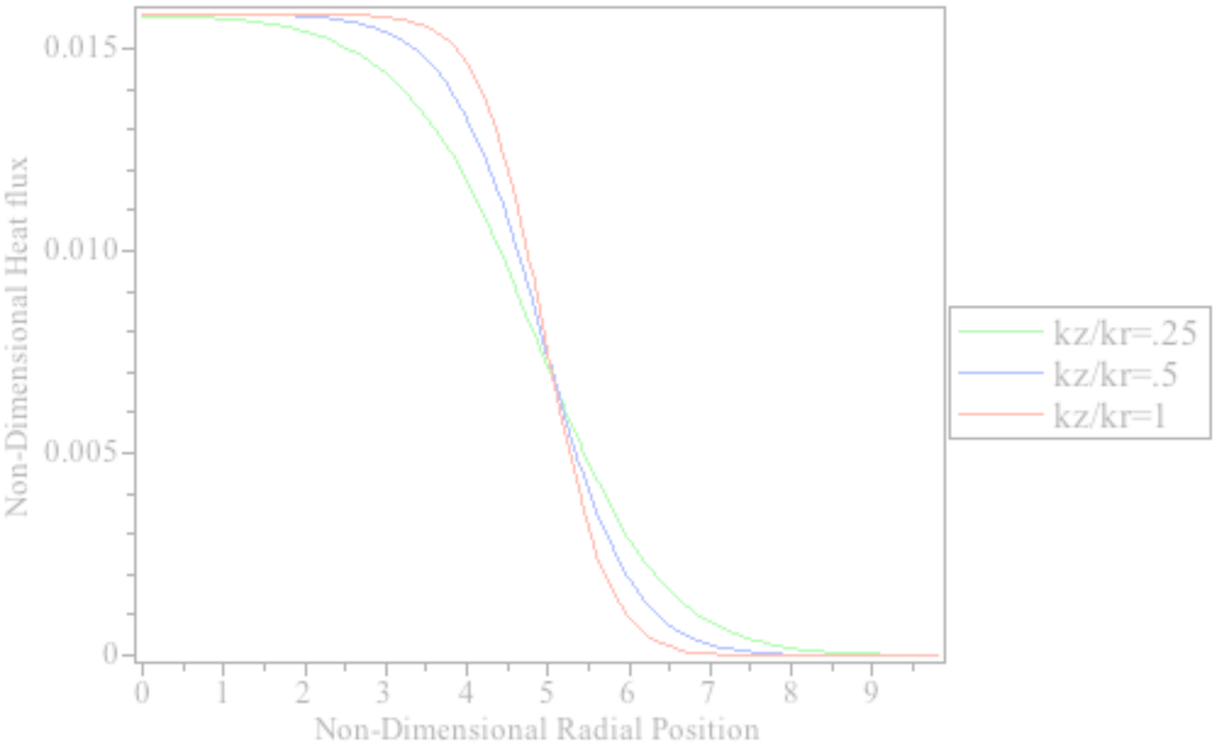

Figure 3-13: Non-dimensional heat flux as function of non-dimensional radial position for varying ratios of thermal conductivity, τ=0.4 and ζ=1 (r_0/w=5, $\alpha t_0/w^2$=0.8)

At larger non-dimensional times, the effect of varying the thermal conductivity ratio continues to have more of an impact over the entire area where the source term is releasing energy. Figure 3.14 shows the non-dimensional heat flux as a function of a non-dimensional radial position at a non-dimensional time of τ=0.6. There is a reduction in the energy transfer throughout the area under the source term when the radial thermal conductivity is much larger than the axial thermal conductivity, but for values when the ratio of thermal conductivities is moderate, reduction in the magnitude of energy transfer doesn't begin until around ρ=1-2.

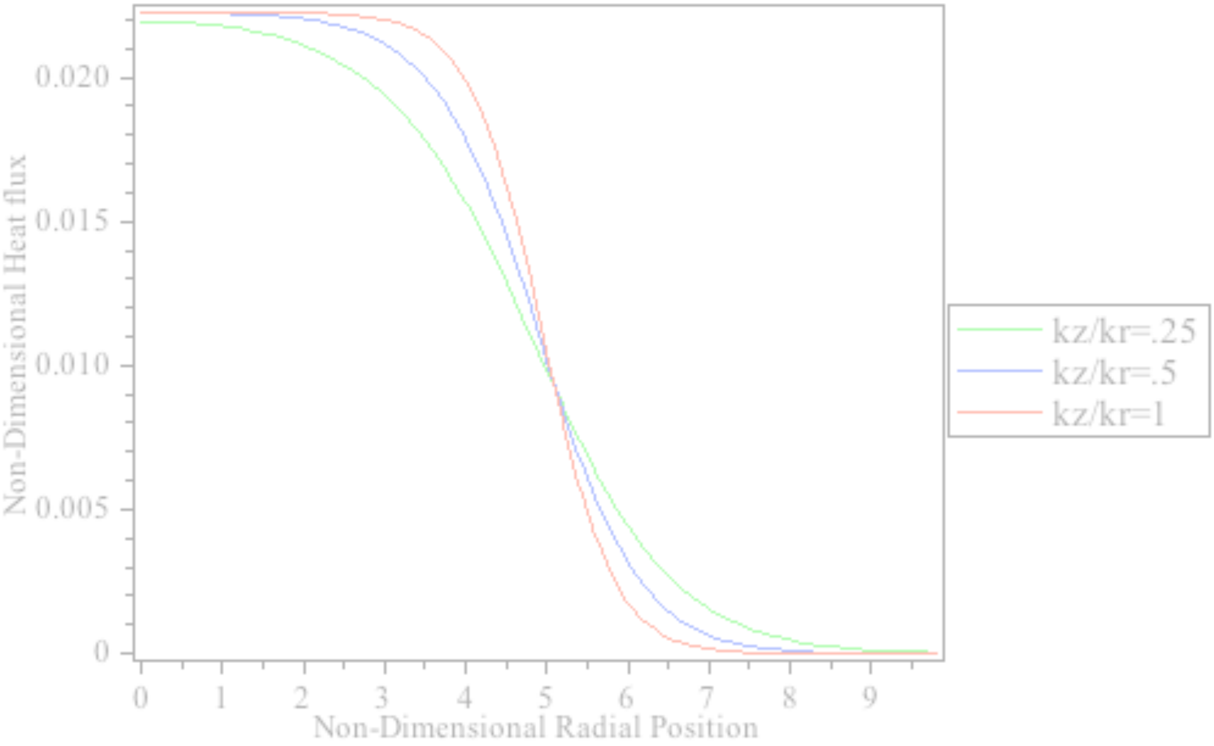

Figure 3-14: Non-dimensional heat flux as function of non-dimensional radial position for varying ratios of thermal conductivity, τ=0.6 and ζ=1 ($r_0/w=5$, $\alpha t_0/w^2=0.8$)

Figure 3.15 shows the non-dimensional heat flux as a function of non-dimensional radial position at τ=0.8, and this time marks the end of the time that the source term is releasing energy for this case that was analyzed. The results are very similar to the previous time step. There is a reduction in the magnitude of heat transfer throughout the area where energy is being released when the radial thermal conductivity is much larger than the axial thermal conductivity. However, there is no reduction in the magnitude of energy transfer until approximately ρ=1 for moderate values of the ratio of thermal conductivities.

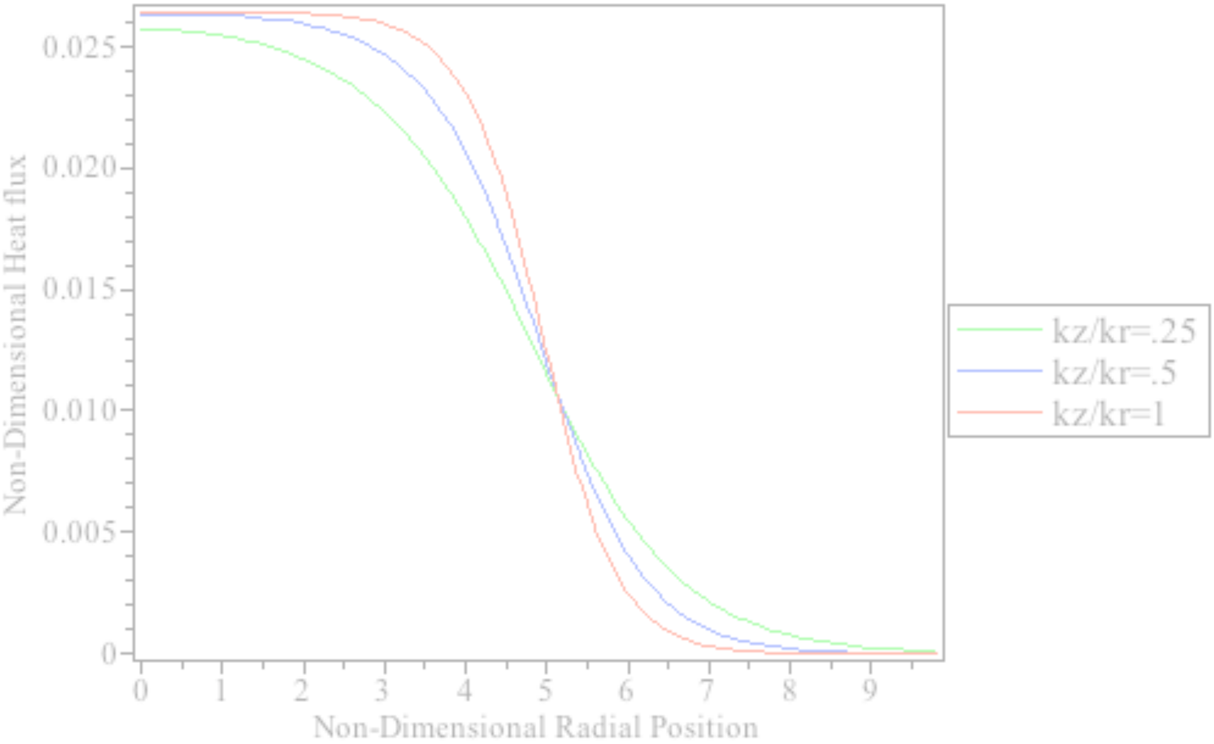

Figure 3-15: Non-dimensional heat flux as function of non-dimensional radial position for varying ratios of thermal conductivity, τ=0.8 and ζ=1 ($r_0/w=5$, $\alpha t_0/w^2=0.8$)

At later times, after all the energy has been released by the source term, is when the use of an orthotropic material has the largest impact on reducing the magnitude of energy transfer. The non-dimensional heat flux as a function of non-dimensional radial position is shown in Figure 3-16 for a non-dimensional time of τ=1.2, and in Figure 3-17 for a non-dimensional time of τ=1.6. In both figures, there is a reduction in the magnitude of heat transfer throughout the area where the source term was releasing energy. At later times, the difference between the radial thermal conductivity being much larger than the axial thermal conductivity becomes much more pronounced and significant as compared to when the radial thermal conductivity is only moderately larger.

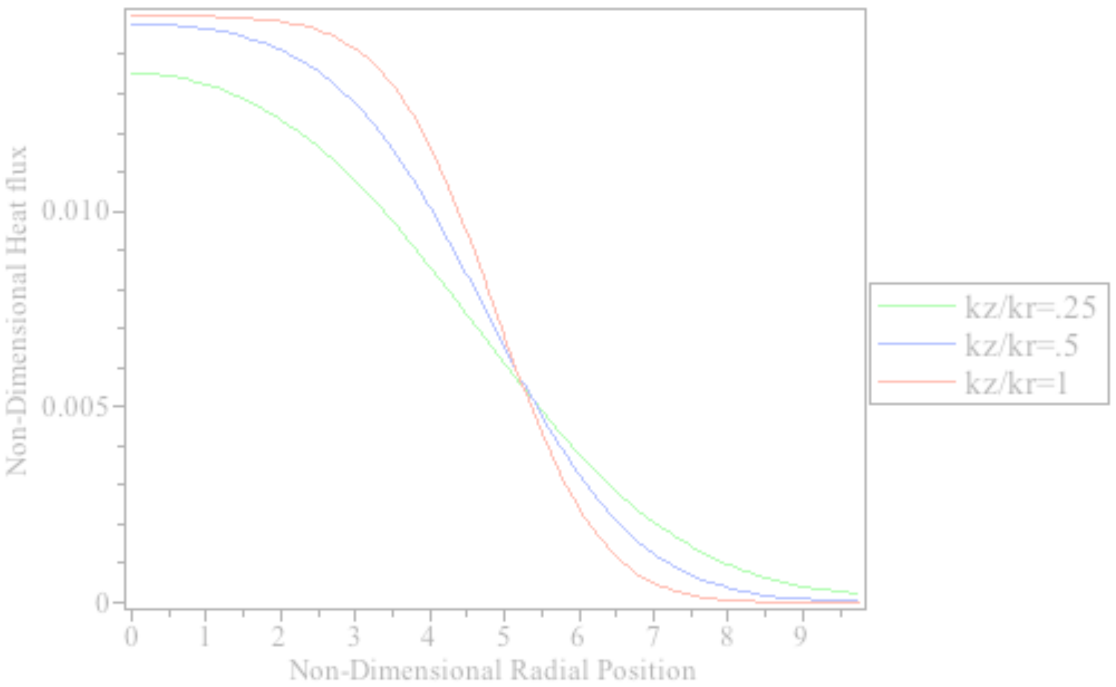

Figure 3-16: Non-dimensional heat flux as function of non-dimensional radial position for varying ratios of thermal conductivity, τ=1.1 and ζ=1 (r_0/w=5, αt_0/w^2=0.8)

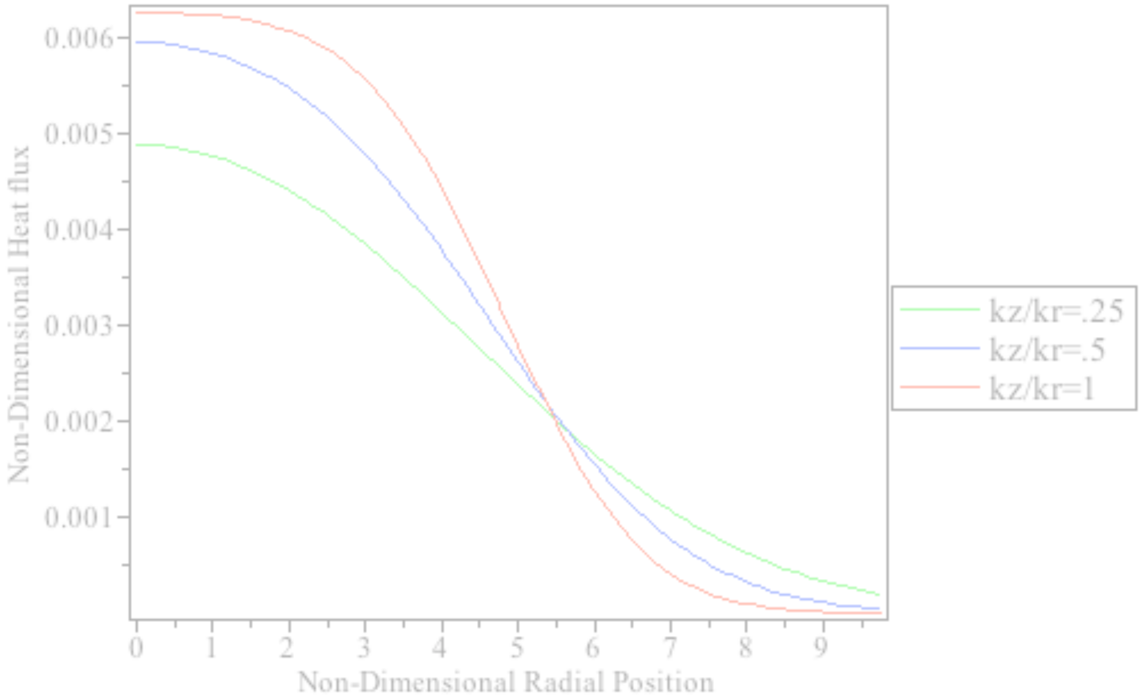

Figure 3-17: Non-dimensional heat flux as function of non-dimensional radial position for varying ratios of thermal conductivity, τ=1.5 and ζ=1 (r_0/w=5, αt_0/w^2=0.8)

In the previous results shown in Figures 3-9 to Figures 3-17, a relatively small value of r_0/w was used. That value would correspond to a splash radius of 5 mm based on the value of the parameters used in the model, such as material thickness. A larger area will now be examined in which $r_0/w=10$, while maintaining the same non-dimensional time duration of $\alpha t_0/w^2=0.8$.

Figure 3.18 shows the non-dimensional heat flux as a function of non-dimensional time at a non-dimensional radial position of $\rho=0$. There is no reduction in the magnitude of heat flux, regardless if the material is orthotropic or isotropic. In essence, the material cannot sense that there are any temperature gradients in the radial direction because the source term is large, so increasing the radial thermal conductivity has no effect on the magnitude of the heat flux.

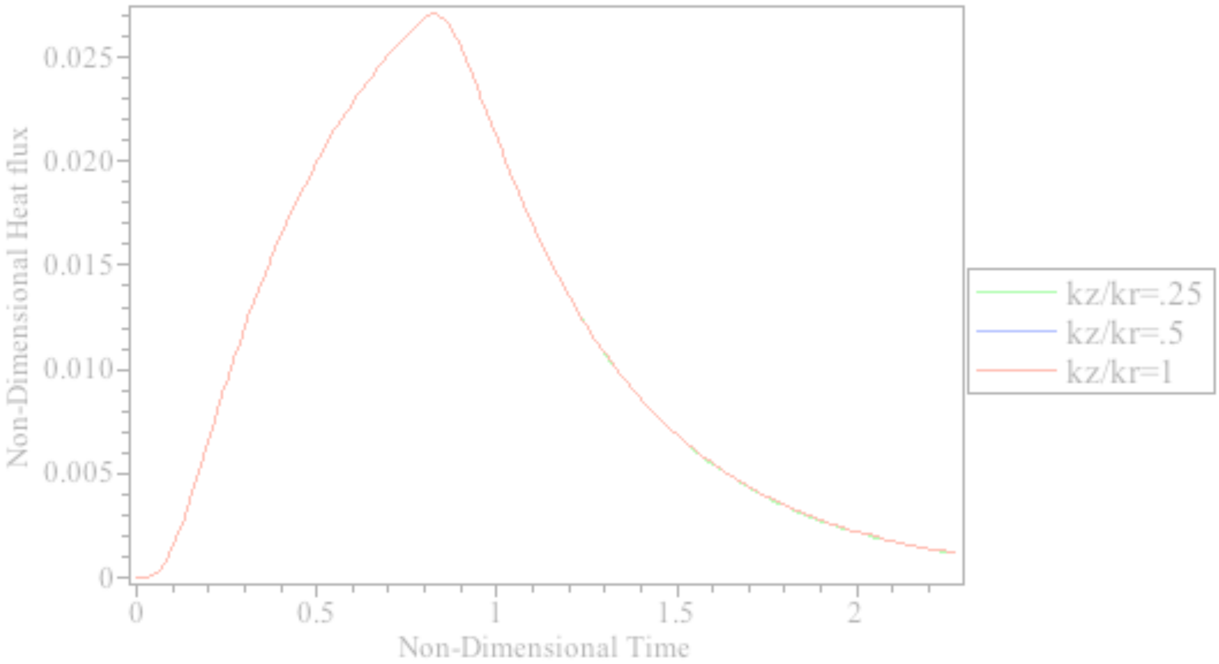

Figure 3-18: Non-dimensional heat flux as function of non-dimensional time for varying ratios of thermal conductivity, $\rho=0$ and $\zeta=1$ ($r_0/w=10$, $\alpha t_0/w^2=0.8$)

Near the edge of the source term, at a non-dimensional radial position of ρ=10, there is a slight reduction in the magnitude of the non-dimensional heat flux. The non-dimensional heat flux is shown as a function of non-dimensional time in Figure 3.19. Although there is some reduction, it is much less than it was at the edge of the source term in the other case when the area of the source term was designated by $r_0/w=5$. It can be inferred that as the area in which the source term acts becomes larger, the ratio of thermal conductivities becomes less significant. As the parameter r_0/w becomes larger and larger, the process becomes essentially more one-dimensional, rather than two-dimensional.

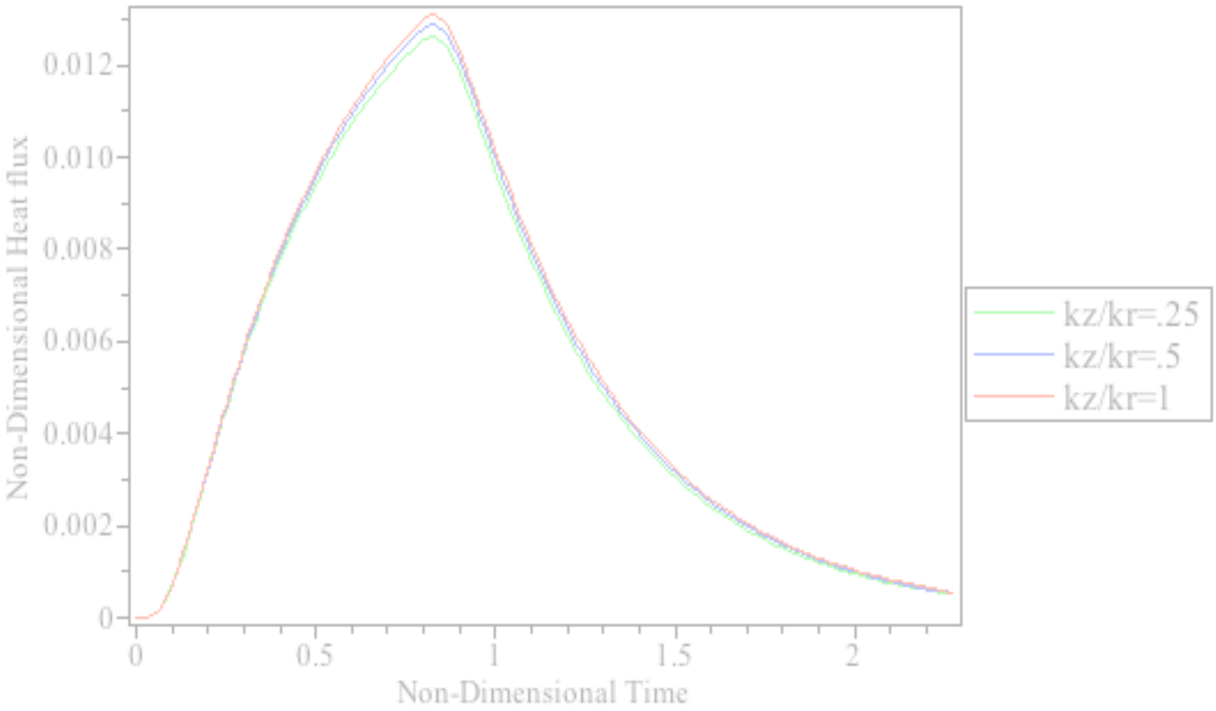

Figure 3-19: Non-dimensional heat flux as function of non-dimensional time for varying ratios of thermal conductivity, ρ=10 and ζ=1 (r0/w=10, $\alpha t_0/w^2$=0.8)

The non-dimensional heat flux as a function of non-dimensional radial position is shown for a non-dimensional time step of τ=0.8, which is the end of the non-dimensional time duration in which the source term is releasing energy and is shown in Figure 3-20. In this situation, where $r_0/w=10$, the reduction in the magnitude of heat transfer is limited to a local reduction near the edges of the source term. For this case, for the ranges from ρ=0-4, there is no reduction regardless of the ratio of thermal conductivities. Because this is the time that the source term has finished releasing energy, this would correspond to the time in which the maximum magnitude of heat transfer would occur. Use of an orthotropic material will certainly reduce the local magnitude of heat transfer in parts of the fabric, but will have little effect in other locations.

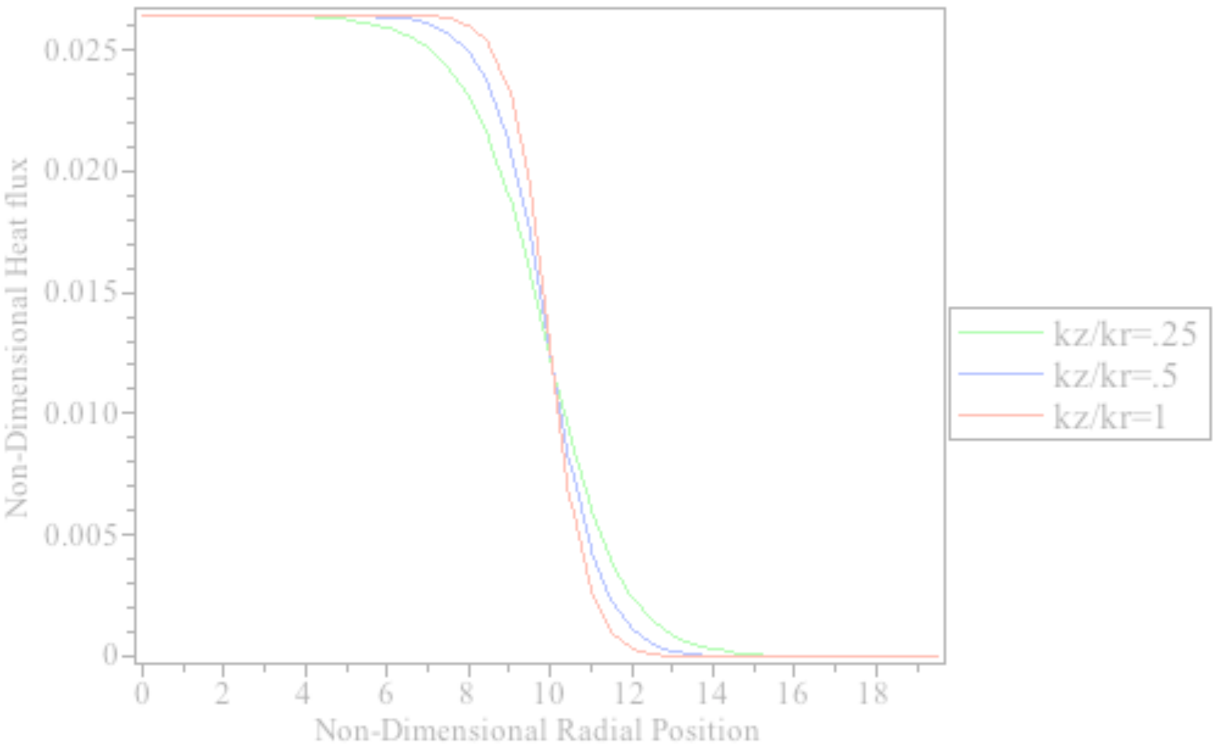

Figure 3-20: Non-dimensional heat flux as function of non-dimensional radial position for varying ratios of thermal conductivity, τ=0.8 and ζ=1 ($r_0/w=10$, $\alpha t_0/w^2=0.8$)

At a non-dimensional time of τ=1.5, as shown in Figure 3-21, the magnitude of the heat flux has nearly diminished. At this later time step when the radial thermal conductivity is much larger than the axial thermal conductivity, there is a reduction in the magnitude of energy transfer, but as this reduction occurs at a time where the magnitude has nearly diminished, the effects of the reduction in energy transfer may not be significant. Because the reduction in energy transfer was limited locally within the material, the total heat absorbed may not be reduced enough so that a burn could have been prevented using an orthotropic material.

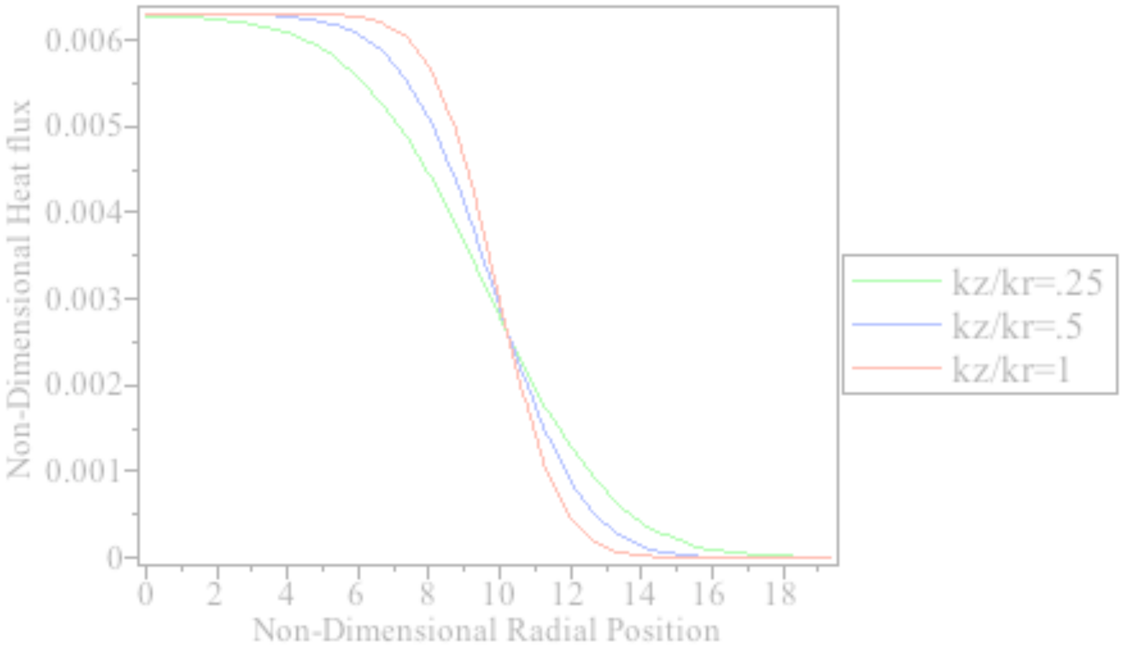

Figure 3-21: Non-dimensional heat flux as function of non-dimensional radial position for varying ratios of thermal conductivity, τ=1.5 and ζ=1 (r_0/w=10, $\alpha t_0/w^2$=0.8)

More graphs of specific individual cases could be presented to examine more of the individual effects, but the information presented thus far is sufficient to draw some basic conclusions. Firstly, that regardless of the size or duration of what a splash might be, using an orthotropic material with a higher radial thermal conductivity will reduce the magnitude of heat transfer to some extent. The reduction in the magnitude of heat transfer is significant in situations where splashes may be small and of short duration, whereas for situations that involve larger splashes over longer durations, the heat reduction is minimal except in areas near the edge.

4 NUMERICAL VERIFICATION

4.1 **Numerical Verification Overview**

To verify that the analytical model was solved correctly, numerical verification studies were performed. Fluent was used to compare the numerical results to the analytical results. The setup of the model will be discussed, and the results presented.

4.2 **Setup**

The numerical verification studies were performed using Fluent. A mesh was created in Gambit, and is shown in Figure 4.1. The upper surface, indicated as surface 1, was set a wall boundary condition with a convection coefficient of h=2 W/m^2*K and free stream temperature of T_∞ =298 K. The lower surface, indicated as surface 2, was set as a wall boundary condition as well with a heat transfer coefficient of U=400 W/m^2*K. At the centerline, or surface 3, the boundary was set to be an axis indicating that the mesh is axisymmetric about this surface. The outer surface, indicated by surface 4, boundary condition was set to be adiabatic, simulating a semi-infinite medium. The model was initialized with a uniform temperature of T_∞=298 K.

Figure 4-1: Mesh used for numerical verification for point source term

For material properties, the estimated properties of cotton were used, as they are readily available and typical values of other similar types of fabrics used in PPE. The density was set at d=300 kg/m^3, the heat capacity at c_p=900 J/kg*K, and value of k_z=.05 W/m*K for the axial thermal conductivity, and values of k_r=0.05-.020 W/m*K for the radial thermal conductivity, which corresponds to the ratio of k_z/k_r ranging from 0.25-1.0.

The model was solved using a two-dimensional axisymmetric transient problem. A first-order upwinding scheme was used to solve the energy equation. The solution was obtained using values of several different times step, and a time step size of Δt=0.01 seconds was used.

4.3 **Results**

The results for the point source heat generation case are presented first. To simulate a point source, a user-defined function was created to control the spatial and temporal bounds of the source term. A small volume specified by .0001 m x .0009 m was specified for a volumetric heat generation rate of $4.5*10^6$ W/m^3 for a time duration of t_0=0.05 seconds. The user-defined function used is shown in Appendix E.

Figure 4.2 shows the comparison of the FEM model results to the analytical model results of the heat flux through the fabric as a function of position for various times for the isotropic case when $k_z/k_r=1$. Figure 4.3 shows the FEM results compared to the analytical results for the heat flux for the case wen $k_z/k_r=0.5$. Figure 4.4 shows the FEM results compared to the analytical results for the case when $k_z/k_r=0.25$. There is good agreement, on the order of 1-5% between the FEM results and the predicted analytical results. From these results, it can be assumed that the point source solution has been verified using the Fluent FEM results.

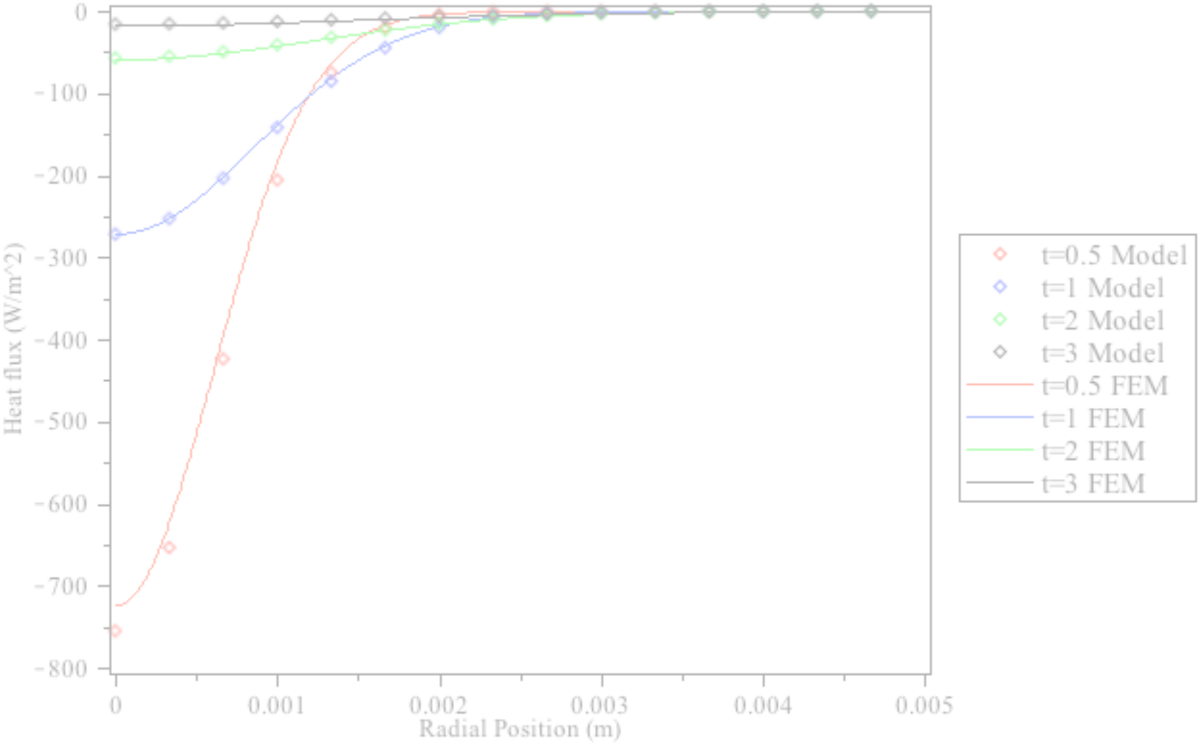

Figure 4-2: Comparison of FEM and analytical point source model ($k_z/k_r=1$)

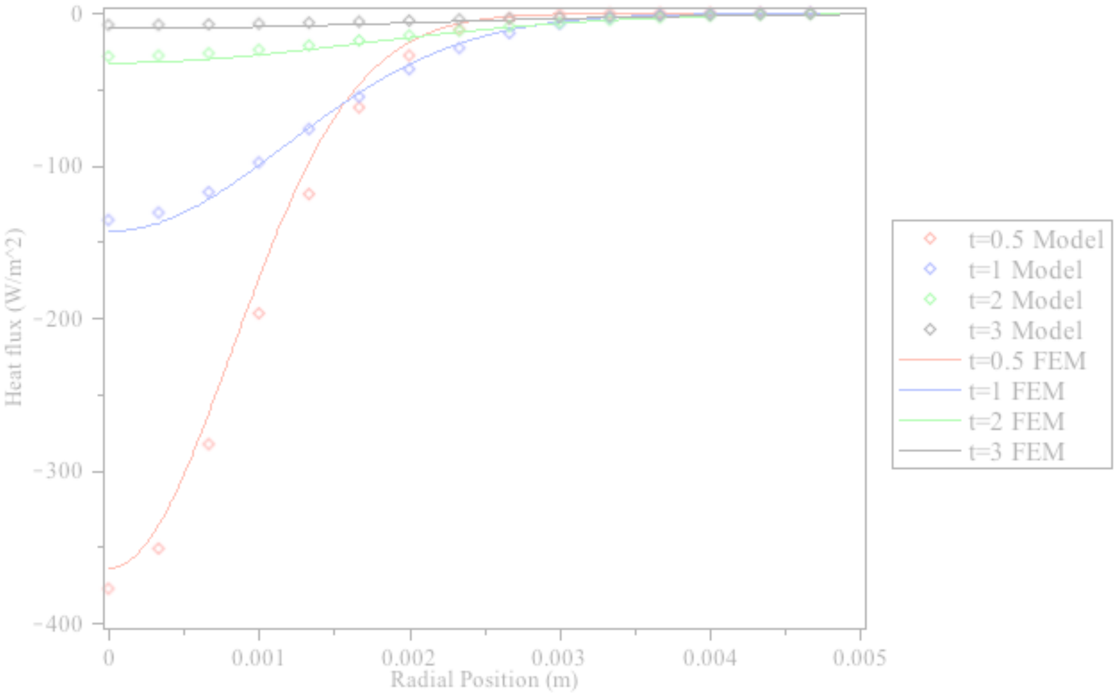

Figure 4-3: Comparison of FEM and analytical point source (k_z/k_r=0.5)

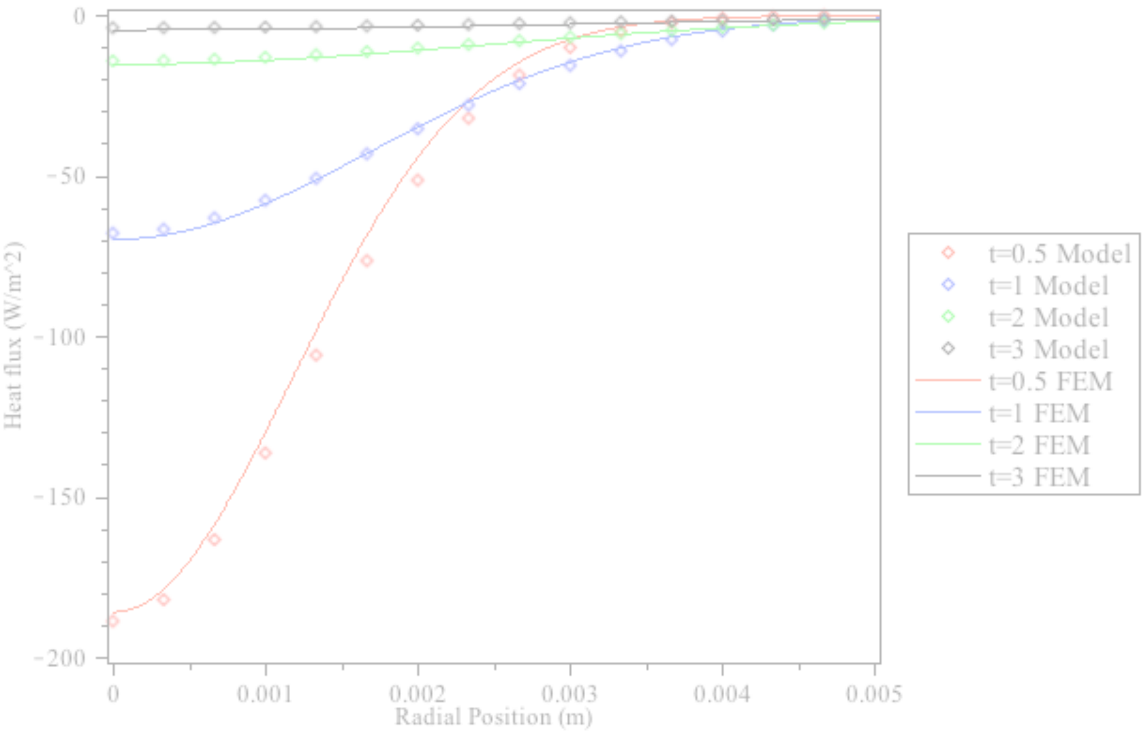

Figure 4-4: Comparison of FEM and analytical point source (k_z/k_r=0.25)

The results for the finite area and time source term will now be examined. To simulate a point source, a user-defined function will be used again to create the spatial and temporal bounds of the source term in Appendix F. A finite volume specified by .0001 m x .005 m was specified for a volumetric heat generation rate of $4.5*10^6$ W/m^3 for a temporal duration of 2 seconds.

Figure 4.5 shows the spatial profile for the FEM and analytical results for the isotropic case when the radial and axial thermal conductivity are the same for various times. Figure 4.6 shows the spatial profile as a function of radial position for the FEM and analytical results of heat flux for various times when $k_z/k_r=0.5$. Figure 4.7 shows the spatial profile as of the FEM and analytical results of the heat flux as a function of radial position for various times when $k_z/k_r=0.25$. The analytical results and FEM results are in good agreement, within 1%, and it can be assumed that the solution finite time and area source term is being solved correctly as verified by the Fluent FEM results.

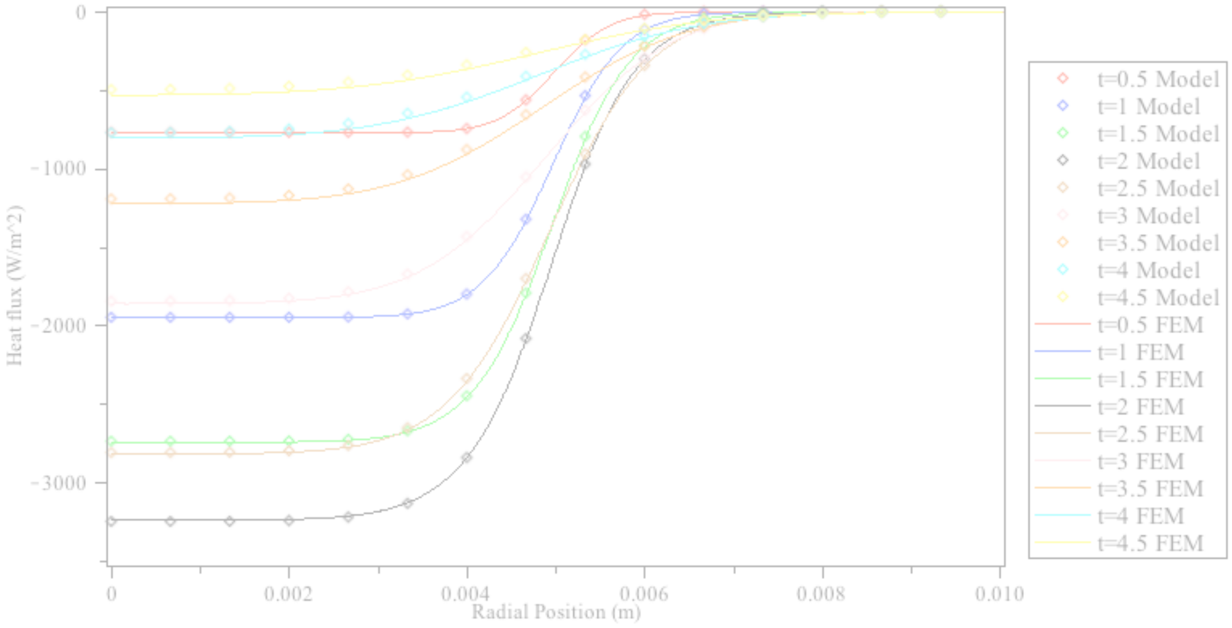

Figure 4-5: Comparison of FEM and analytical profile (k_z/k_r =1, t_0=2, r_0=0.005)

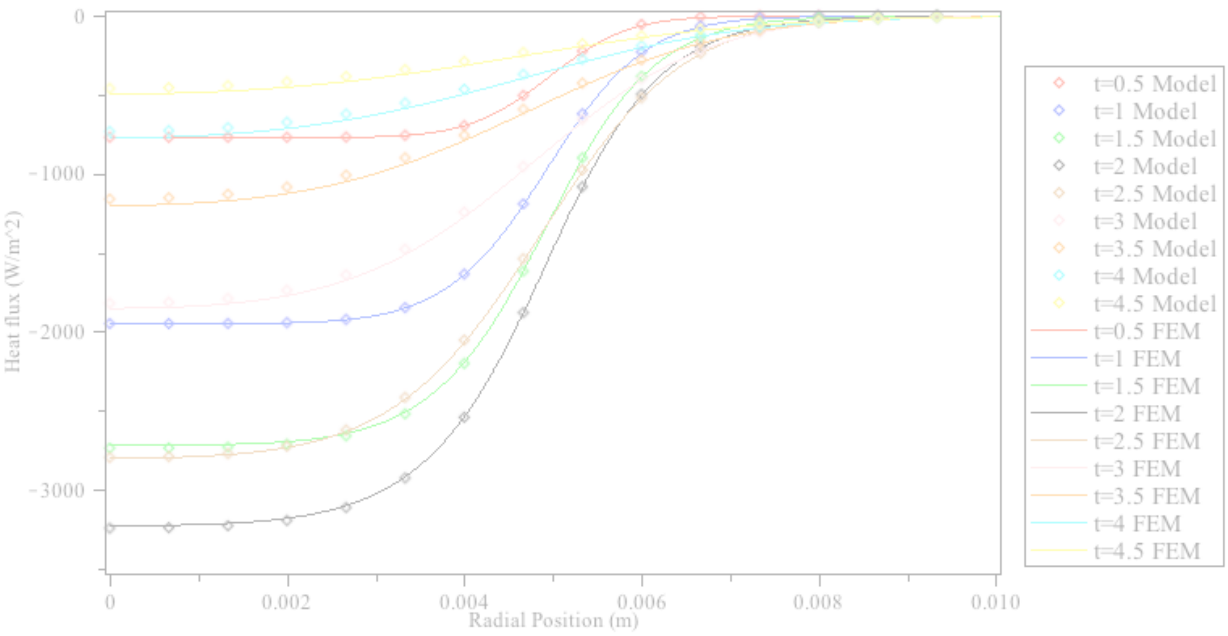

Figure 4-6: Comparison of FEM and analytical profile (k_z/k_r=0.5, t_0=2, r_0=0.005)

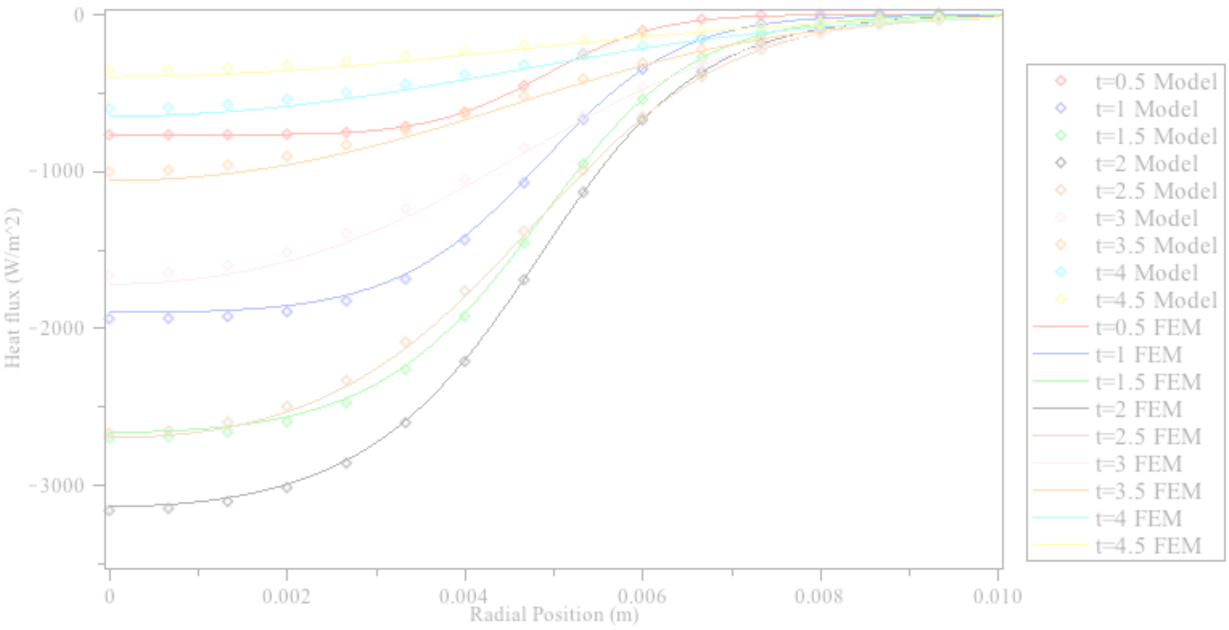

Figure 4-7: Comparison of FEM and analytical profile (k_z/k_r=0.25, t_0=2, r_0=0.005)

4.4 Verification of Overall Heat Transfer Coefficient

Most of the material properties and system parameters needed in the model can be calculated or estimated with a reasonable level of certainty in the calculations. However, in the analytical model, the overall heat transfer coefficient at the lower surface is used to simulate heat transfer from a solid to another semi-infinite solid. This is effectively using the inverse of a contact resistance at that interface to model the heat transfer in a convection-like manner. As mentioned previous, related literature estimates the inverse of the contact resistance to be around U=200-400 W/m*K under laboratory conditions for the experimentation that was done with the specific materials and conditions used. In this research, the contact resistance is unknown, and an overall heat transfer coefficient is used instead to allow a simplified analytical solution. To be able to determine if the values that were used in the analytical model for that overall heat transfer coefficient were reasonable values, an equivalent heat transfer coefficient at the lower surface was determined using an FEM model to simulate conditions of perfect contact between what would be a solid fabric and a semi-infinite media being the tissue. As the analytical model requires an overall heat transfer coefficient at that boundary condition, to have the most realistic results a time dependent overall heat transfer coefficient would be needed. This would make the model too complex and an approximation is being made, so the equivalent heat transfer coefficient will be plotted at that interface as a function of time using the FEM results. If the time dependent FEM overall heat transfer coefficient results at were averaged over time, then that average value will be compared to the value used to verify that the FEM model has similar conditions as the analytical model.

A similar method that was used previously for model verification was used again, but in this case the lower surface was in contact with a solid that has the thermal properties of tissue.

This would model a fabric being in perfect contact with an individual, while a point source is used again to simulate a splash of a hot liquid. The upper surface, or the left most surface in Figure 4-8, is still maintained as a wall with a convection coefficient of 2 W/m^2*K and a free stream temperature of 298 K. The lower surface, or the right most surface of the first solid area in Figure 4-8, has been set in contact with another solid so within Fluent a shadow wall is created that couples the heat transfer between the two materials. The meshed area on the left was defined as a solid with the thermal properties of the density being d=300 kg/m^3, the heat capacity at c_p=900 J/kg*k, and an isotropic material with thermal conductivity of k=0.05 W/m*K. The meshed area of the right was defined as a solid with properties representative of tissue with the density being d=1000 kg/m^3, the heat capacity at c_p=3000 J/kg*K, and a thermal conductivity of k=0.4 W/m*K.

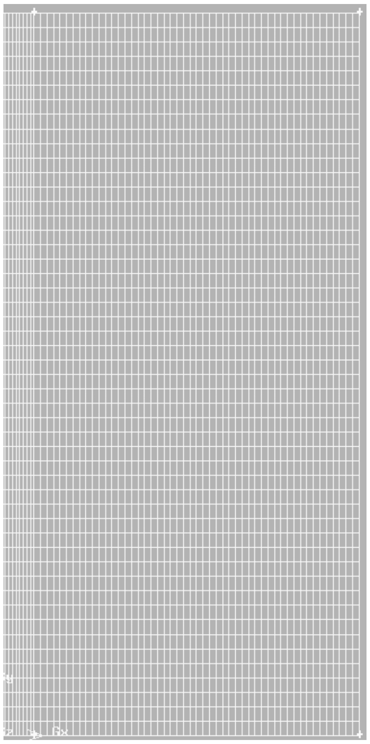

Figure 4-8: Mesh used for numerical verification for finite size source term

A first order upwinding scheme was used to solve the two-dimensional axisymmetric model of the energy equation. A time step size of Δt=0.01 seconds was used.

The surface heat transfer coefficient at the lower surface was then plotted as a function of position at various time steps, as shown in Figure 4-9. The local surface heat transfer coefficient varies with time, and ranges from around U=2000 W/m^2*K at early times to just under U=400 W/m^2*K. In the FEM solution, no contact resistance is included in this model. To compare these values with what was estimated previously, the surface heat transfer coefficient would have to be averaged over time and space to determine an average heat transfer coefficient from the local and instantaneous surface heat transfer coefficient. This would result in a surface heat transfer coefficient much higher than what was used in the model, but accounts for no contact resistance. The contact resistance between a fabric and tissue, or between fabric and another fabric would likely be large as most fabrics are worn rather loosely. With the addition of contact resistance at the interface, the average surface heat transfer coefficient value could easily be on the same order as U=200-400 W/m*K.

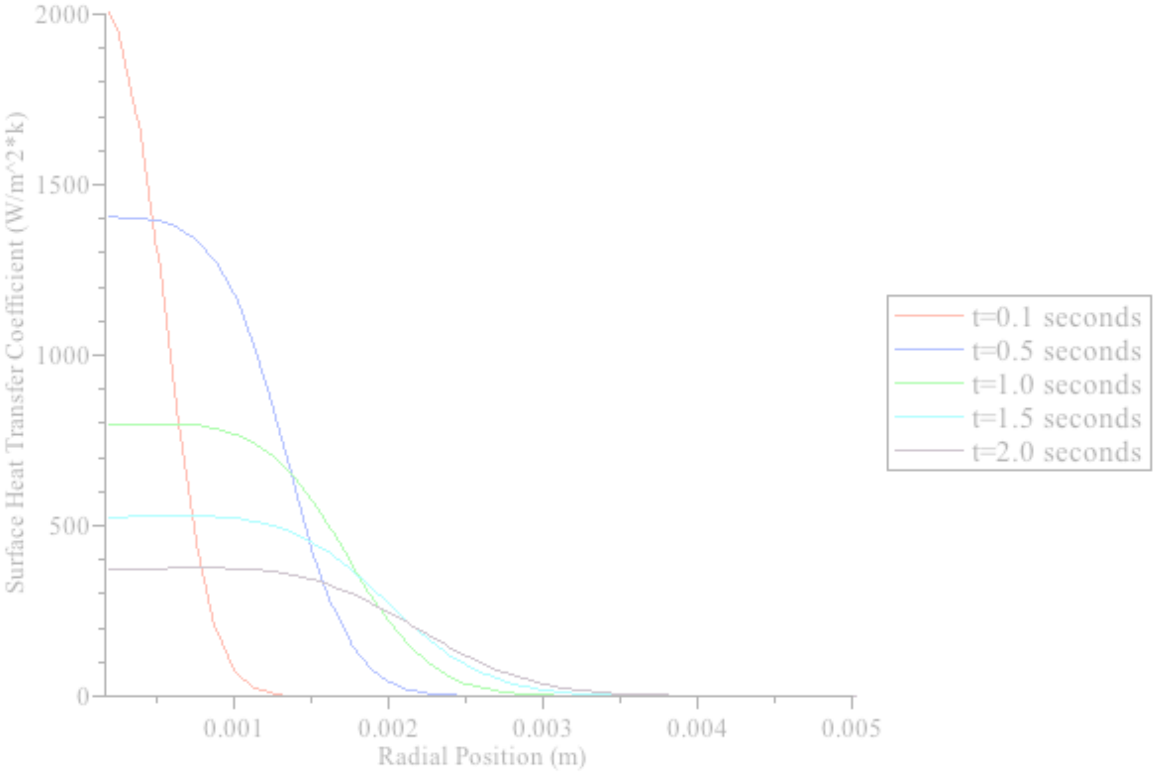

Figure 4-9: FEM solution for effective overall heat transfer coefficient at lower surface (no contact resistance)

5 SIMULATED EXPERIMENTS

5.1 Overview

As shown in previous chapters through analytical and numerical analysis, an orthotropic material can be beneficial in maximizing the amount of protection provided by a fabric. Possibly the biggest challenge associated with orthotropic materials is being able to determine the material properties and to know to what extent a fabric may be orthotropic. There are currently no standard tests available that could be used to determine the radial thermal conductivity. The theory for a method that could be used will be described here, as well as the analytical results as compared to a set of simulated experiments as a preliminary validation of this method of being able to extract information about determining the radial thermal conductivity.

This serves a double purpose as well and allows for the model used in Chapter 3 to be validated. Verification done in Chapter 4 is used a numerical model to solve the same conditions on the analytical model to essentially verify that the solution to the model is correct. There are inherent approximations made in the model to allow for an analytical solution, and the validity and limitations of those approximations can be determined using the analysis method that will be described in this chapter.

5.2 Theory Development

A semi-empirical method in which simulated experimental data obtained using a commercial CFD package is matched with analytical results. These results will be used to show how information pertaining to the radial thermal conductivity may be obtained. Although the experimentation used is in this research is numerical in nature, the method will be described generally so that it could be applied to physical experimentation as well. The methodology is based on flash radial diffusivity [18], which has been described in other applications involving orthotropic materials. The methodology entails taking temperature measurements at two locations simultaneously using a sinusoidal source to drive the temperature response, and effectively measuring the amplitude and phase shift between the two locations by normalizing the analytical results to one another and then matching them to the experimental results by iteratively changing the unknown parameter. Only one parameter can be unknown, which in this application will be the radial thermal conductivity. The approach described here requires precise knowledge of all the other material properties and parameters.

A mathematical model similar to what has been presented in earlier chapters is used again in this case. With a few minor modifications, the same non-dimensional model that was derived and used in Chapter 3 is applicable. The first is that a lower boundary condition will no longer be an overall heat transfer coefficient to model a contact with a surface, but will be a true convective boundary where the surface is in contact with the ambient air. This doesn't change the model at all as the boundary condition is mathematically the same, but should be noted that it represents a true convective boundary condition now. Although the boundary condition is of the same mathematical form, instead of using an overall heat transfer coefficient to simulate contact with another surface, the value used is the average convective heat transfer coefficient. The other distinction is that the source term will be a sinusoidal term located at a point. The rationale for using a sinusoidal source term is that to use the analytical model described in previous chapters and to compare its results to temperatures requires knowledge of the magnitude of the heat source term, as that parameter is part of the non-dimensional parameters. As the source term is used as an approximation to merely simulate a temperature spike, it is not a true parameter that is involved in the physics of a hot liquid splash. To eliminate the dependency on terms such as the magnitude of the source term, a source term that varies sinusoidally with respect to time, with controllable mean and oscillating components is used. This idea has been used in other applications for determining material properties [19-20]. The only information needed is the relative amplitude of the alternating and mean components of the sinusoidal term, as the non-dimensional solution can still be obtained with just that information. Ideally, the source term would act just at a point, but due to the nature of Dirac delta functions, the solution in mathematical terms is not as easily solved. Heaviside functions to control the size of the source term can be used instead with a small radius, thereby effectively simulating a small point source as the parameter r$_0$ is kept small. The source term described above is defined below in Eq. 5.1.

$$\dot{q} = \frac{\left(H(r)-H(r-r_0)\right)\delta(z)(\mathrm{A}+\mathrm{B}\sin(2\pi f t))}{\pi {r_0}^2}. \tag{5.1}$$

In Eq. 5.3.1, the source term that has a mean value of A and alternating component of B, acts over a small volume with an oscillation frequency of *f.* A and B signify the energy rate the mean and alternating components of energy released, respectively, in units of W/s. The source term is defined by the radius of r$_0$ through the use of Heaviside functions with respect to the radius and is limited to the upper surface of the fabric through use of the Dirac delta function, *δ(z)*.

Applying non-dimensional parameters used previously yields the non-dimensional source term given in Eq. 5.2, which will then be used in the solution.

$$\dot{q} = \left(H(\rho) - H\left(\rho - \frac{r_0}{w}\right)\right)\delta(\zeta)(\mathrm{A} + \mathrm{B}\sin(\omega\tau)) \tag{5.2}$$

Applying the Hankel and Finite Fourier Transform to the source term yields the transformed source term, which is then applied in to Eq. 3.4. The solution is summarized below in Eq. 5.3.3 through Eq. 5.7, while the transformed source term is shown in Eq. 5.3.4

$$\theta(\rho,\zeta,\tau) = \int_0^\infty \sum_{n=1}^\infty \frac{\phi(\beta_n,\zeta)}{N(\beta_n)} \lambda J_0(\lambda\rho) e^{\left\{-\left(\frac{\lambda^2}{\epsilon^2}+\beta_n{}^2\right)\tau\right\}} \bar{\bar{Q}}\, d\lambda \tag{5.3}$$

$$\bar{\bar{Q}} = \frac{\beta_n}{2}\frac{r_0}{\lambda w} J_1\left(\lambda\frac{r_0}{w}\right) \frac{-Ac-\frac{A}{c}\omega^2+B\omega+Ace^{c\tau}+\frac{A}{c}\omega^2 e^{c\tau}-B\omega\cos(\omega\tau)e^{c\tau}+B\sin(\omega\tau)e^{c\tau}}{(c^2+\omega^2)} \tag{5.4}$$

$$c = \left(\frac{\lambda}{\varepsilon}\right)^2 + \beta_n^2$$

$$\omega = \frac{2\pi f w^2}{\alpha}$$

$$\phi(\beta_n,\zeta) = \beta_n\cos(\beta_n\zeta) + Bi_0\sin(\beta_n\zeta) \tag{5.5}$$

$$N(\beta_n) = \frac{1}{2}((\beta_n{}^2 + Bi_0{}^2)(1 + \frac{Bi_w}{(\beta_n{}^2+Bi_0{}^2)} + Bi_0)) \tag{5.6}$$

$$tan(\beta_n) = \frac{\beta_n(Bi_0+Bi_w)}{\beta_n{}^2-Bi_0 Bi_w} \tag{5.7}$$

As mentioned previously, the only unknown property or parameter is the radial thermal conductivity, and the solution to the model requires an initial guess to come up with a solution. All other model parameters and properties are either material properties (density, axial thermal conductivity, heat capacity) that would either need to be known or determined with other experimentation, readily measured physical properties of the setup (material thickness, nominal radius of heat source, frequency of source oscillation, mean and relative magnitudes of source term, ambient temperature, initial temperature), or highly accurate estimations (upper and lower surface heat transfer coefficient).

As previously noted, the analytical model is used to determine the non-dimensional temperature at two locations simultaneously as a function of time, which are then normalized to each as shown in Eq. 5.8.

$$\frac{\theta_1}{\theta_2} = \frac{\int_0^\infty \sum_{n=1}^\infty \frac{\phi(\beta_n,\zeta=1)}{N(\beta_n)} \lambda J_0(\lambda\rho_1) e^{\left\{-\left(\frac{\lambda^2}{\epsilon^2}+\beta_n{}^2\right)\tau_1\right\}} \overline{\overline{\overline{Q}}}\, d\lambda}{\int_0^\infty \sum_{n=1}^\infty \frac{\phi(\beta_n,\zeta=1)}{N(\beta_n)} \lambda J_0(\lambda\rho_2) e^{\left\{-\left(\frac{\lambda^2}{\epsilon^2}+\beta_n{}^2\right)\tau_1\right\}} \overline{\overline{Q}}\, d\lambda} \tag{5.8}$$

The results of the model need to be taken over a time frame that begins at a large enough time so that the response would be quasi-steady in nature, characterized by a steady amplitude and mean value in the non-dimensional temperature results.

In this research, since this method will be validated against a numerical experiment using CFD, which requires all the parameters being known, properties and parameters typical of an orthotropic thermal protective fabric in which the radial thermal conductivity is twenty times larger than the axial thermal conductivity was used to validate this method. The model was solved at non-dimensional locations equivalent to r=2 and r=3 mm at the lower surface. The analytical non-dimensional temperature response for one period of oscillation is shown in Figure 5-1.

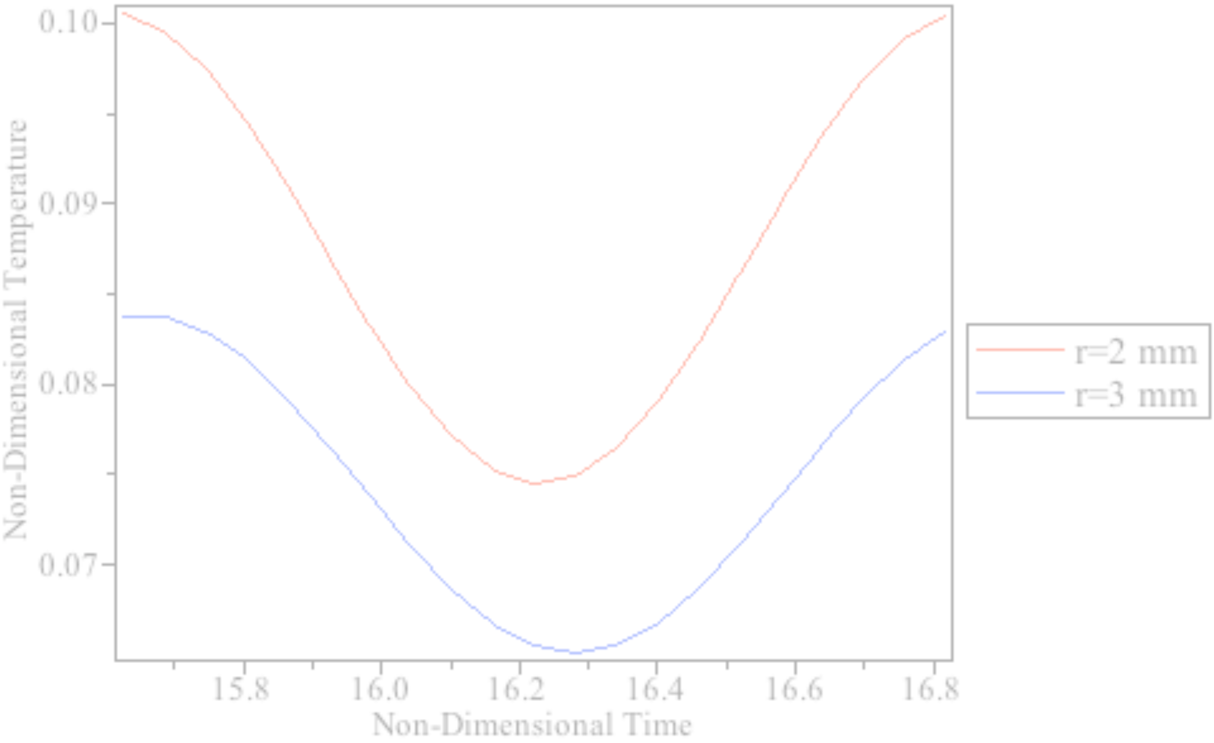

Figure 5-1: Analytical results of the non-dimensional temperature response at two different radial locations for duration of one period

It should be noted upon examination of Figure 5-1 that there is a shift in amplitude as well as a slight shift in phase between the results at the two different locations. This is all taken into account for when normalizing the results to each other, and yields responses curve such as shown in Figure 5-2.

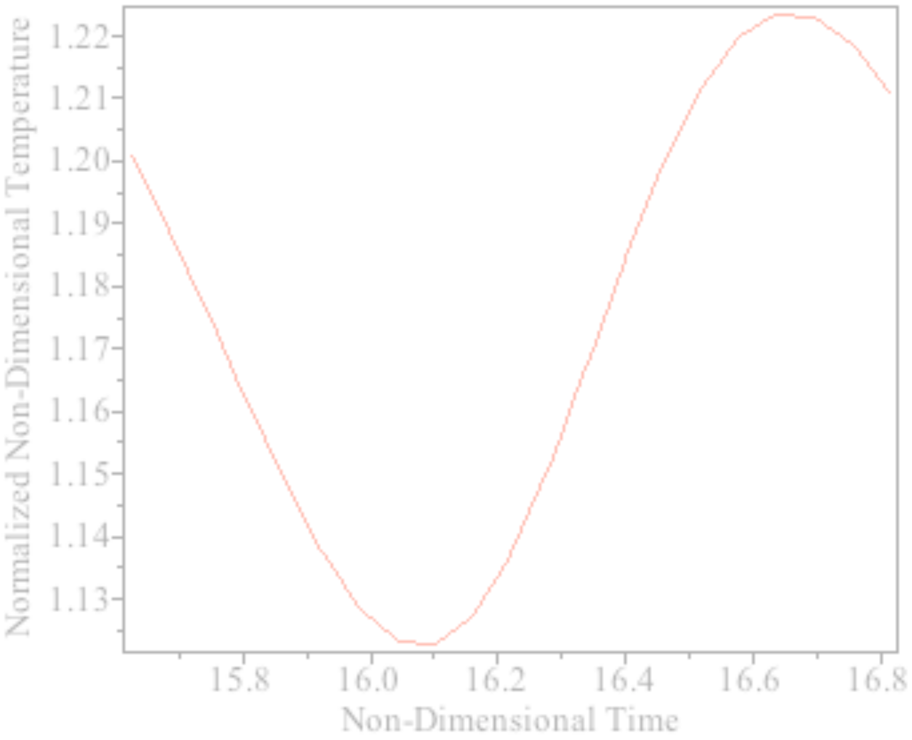

Figure 5-2: Normalized non-dimensional ratio of temperature of analytical results

Upon examination of Figure 5-2, it should be noted that the normalized non-dimensional temperature ratio has a sinusoidal response as well, and if the model has reached the point in time where the temperature results are quasi-steady, then the normalized non-dimensional temperature ratio results are quasi-steady in nature as well. This curve will be the basis for matching the analytical results to the experimental results so apples to apples comparisons can be made to experimental data.

The right hand side of the expression in Eq. 5.8 gives the analytical normalized non-dimensional temperatures ratio, which then needs to be equated to experimental results to be able to solve for an unknown parameter. As experimental results are in terms of a temperature that has units, the experimental results needs to be non-dimensionalized as well. This is done by using the definition of the non-dimensional parameter θ and replacing the analytical temperature response T(r$_1$,w,t) with the experimental results at the corresponding location as a function of time, and then normalizing the experimental results to each other to produce a single curve as was done similarly to the experimental results as shown in Eq. 5.9.

$$\frac{T_1(t)-T_\infty}{T_2(t)-T_\infty} = \frac{\int_0^\infty \sum_{n=1}^\infty \frac{\phi(\beta_n,\zeta=1)}{N(\beta_n)} \lambda J_0(\lambda\rho_1) e^{\left\{-\left(\frac{\lambda^2}{\epsilon^2}+\beta_n{}^2\right)\tau\right\}} \bar{\bar{Q}}\, d\lambda}{\int_0^\infty \sum_{n=1}^\infty \frac{\phi(\beta_n,\zeta=1)}{N(\beta_n)} \lambda J_0(\lambda\rho_2) e^{\left\{-\left(\frac{\lambda^2}{\epsilon^2}+\beta_n{}^2\right)\tau\right\}} \bar{\bar{Q}}\, d\lambda} \tag{5.9}$$

Experimental temperature measurements were obtained using CFD results. The setup of the CFD solution entailed using a thin solid layer 1 mm thick with properties typical of what might be expected for a thermal protective fabric. A conjugate solution of a stationary fluid modeled as air on the upper and lower surface was used, so the solution includes a more precises results that take into account solid-fluid interaction. A sinusoidal point source in which the temperature was modulated in the same manner as described in the analytical model was used. A screenshot image of the setup used is shown below in Figure 5-3.

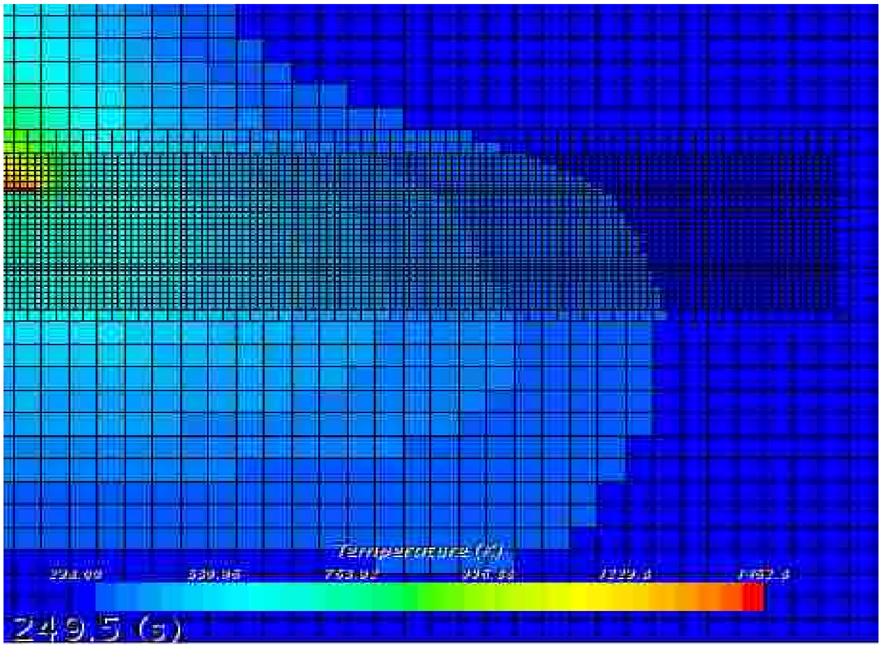

Figure 5-3: CFD setup grid and example results used to obtain simulated results

The temperature response for one period at locations of r=2 mm and r=3 mm is shown Figure 5-4/ Note that the time is not an absolute time of when the data was taken, but is relative to an arbitrary point in time after reaching it's quasi-steady state value. Also note that there is a difference in amplitude, as well as a slight phase shift.

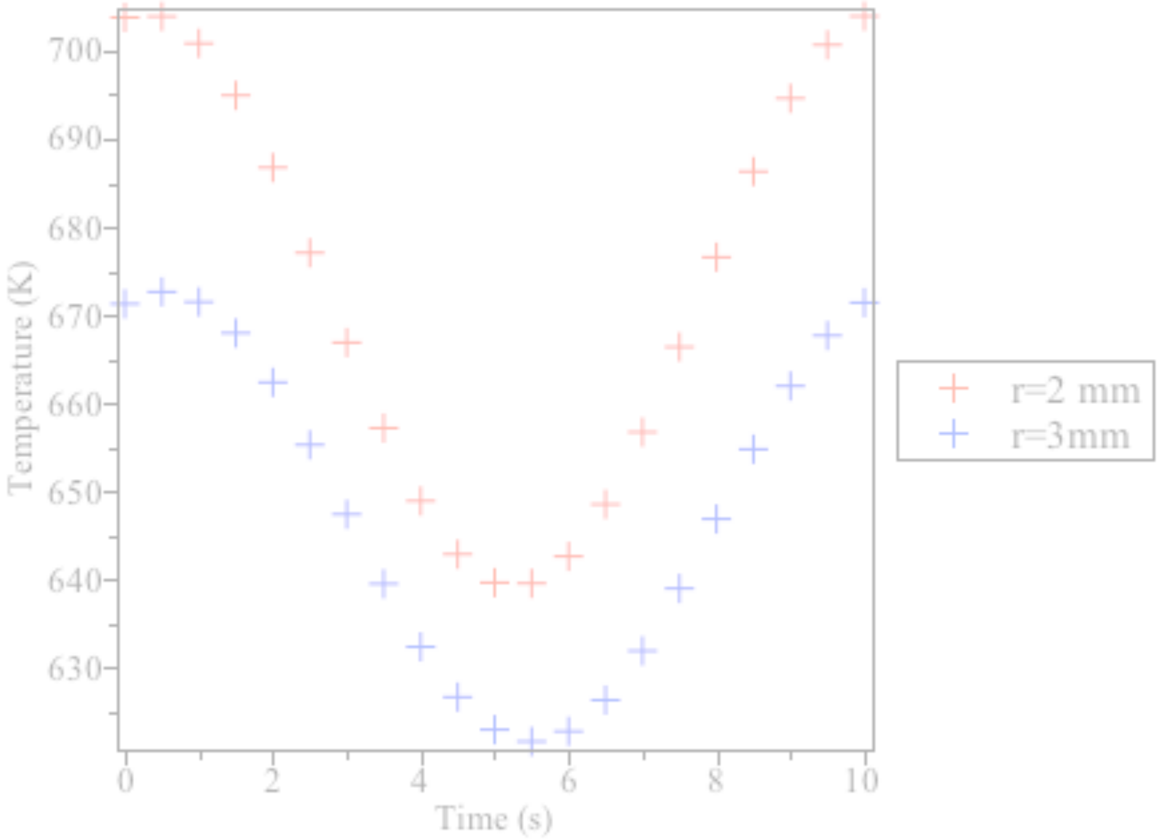

Figure 5-4: Simulated temperature raw data for temperature response at r=2 mm and r=3 mm

Normalizing the data in Figure 5-4 as shown on the left hand side of Eq. 5.9 yields the normalized non-dimensional temperature ratio for the experimental data, and is shown in Figure 5-5. It should be noted that any difference in amplitude or phase shift is taken into account in the normalization, and yields a similar quasi-steady sinusoidal response as that of the analytical normalized non-dimensional temperature ratio.

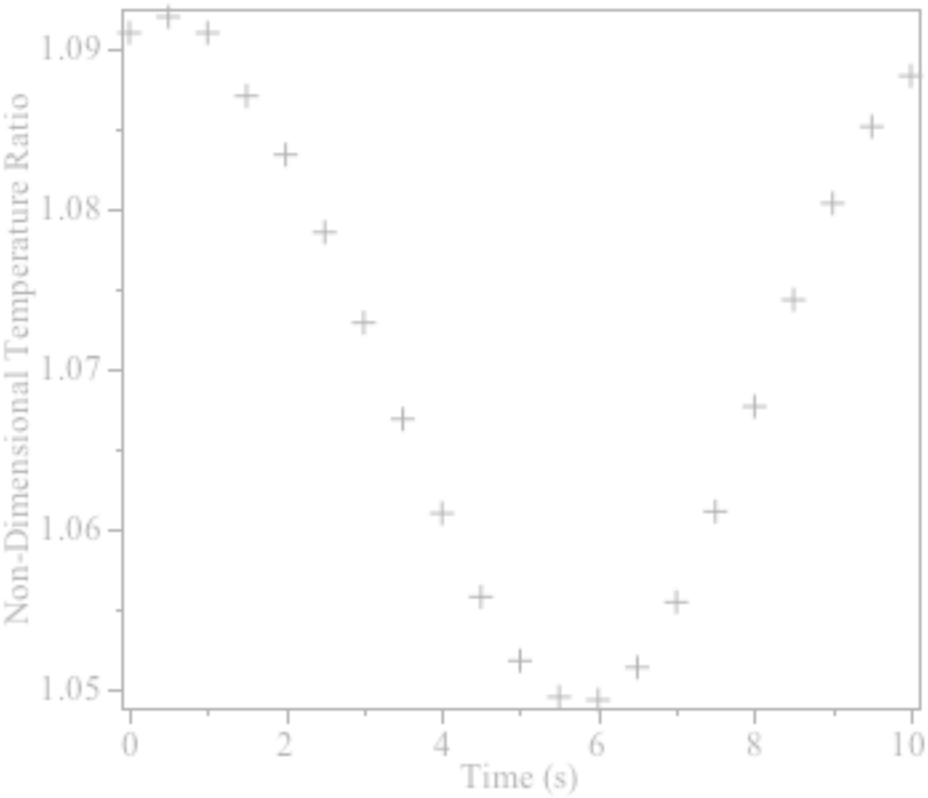

Figure 5-5: Normalized non-dimensional temperature ratio for simulated data

The analytical and experimental normalized non-dimensional temperature responses are shown on the same graph in Figure 5.6 for comparison. In this case, where the parameters such as the heat transfer coefficients have been estimated using reasonable values, the analytical results are not in good agreement with the experimental results.

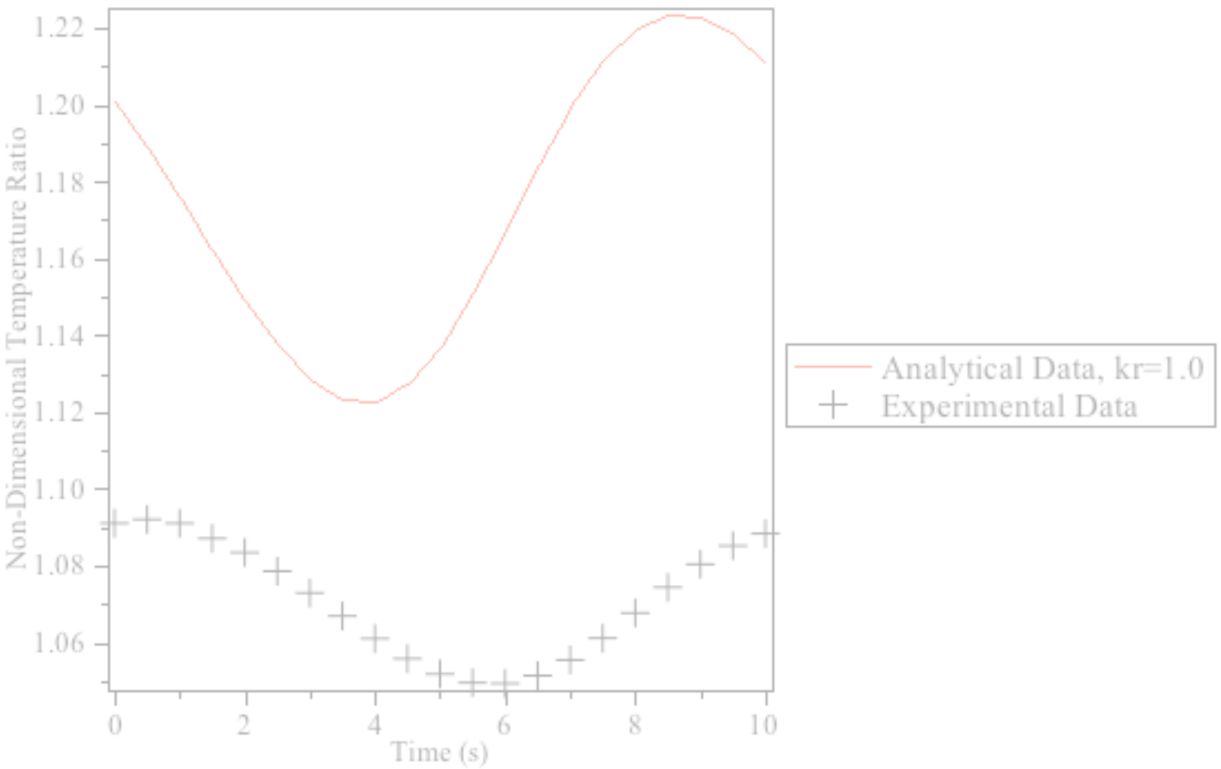

Figure 5-6: Analytical vs. simulated results for normalized non-dimensional temperature with estimated upper heat transfer coefficient

The discrepancy in the results is due to approximations in the model related to both the source term and the boundary condition on the upper surface. The biggest contributor to the discrepancy is the approximation of a uniform convection heat transfer coefficient. That is a poor approximation in this case, but is necessary to be able to come up with an analytical solution. Because the high temperature gradients over short distances, which the CFD solution is able to approximate, the heat transfer coefficient is not uniform and varies significantly with the large temperature gradients on the surface. In addition, with a hot spot on the surface, which creates a small plume centered over the hot spot, the air is not a uniform temperature either. The model results are fairly sensitive to changes in the upper and lower heat transfer coefficient. The model can be compensated by calibrating by adjusting the upper heat transfer coefficient so that the analytical normalized non-dimensional temperature profile ratio matches that of the experimental, but it does require knowing all model parameters to be able to calibrate the model. The calibration would only be valid for the two locations used and any other results at different locations would be invalid without calibrating to those specific locations. In this case, because a numerical experiment was set up where all parameters can be known either from the input values or the calculated outputs, that information can be used to compare then calibrate the model for the heat transfer coefficients. However, in an experiment with an actual sample of fabric in which the radial thermal conductivity is the information that is needed, all the parameters wouldn't be known. It might be possible to calibrate using a similar but separate material in which all properties are known, then use the calibration information for the heat transfer coefficients in the model to then extract the radial thermal conductivity for the material of interest. Although that might be a possibility, the specifics of feasibility of that is beyond the scope of this research and it will simply be stated that it is important to note that the necessity on having a model that can be calibrated with a high degree of certainty is a potential large source of error.

By only adjusting the upper heat transfer coefficient, the data is within 1% of the experimental results as shown in Figure 5-7. This is at the cost of using average heat transfer coefficient value that is very small to compensate. The reason for using a low heat transfer coefficient makes sense when considered in context of the physics occurring at the upper surface with a heat generation term used as the source and the boundary condition being model as uniform convection. The numerical experimental results have a set temperature at the surface for a small area, such as would occur if a wire were to contact the fabric. There would be no convection at that location, and because of the very high temperature gradients on the surface of the fabric, the upper heat transfer coefficient would not be uniform. In addition, as energy is transferred the localized air temperature is also not uniform, and with a very hot spot on the surface, can cause a significant thermal plume. The combined effect of that is less energy will be transferred near the source term and more of it will dissipate outward radially. A lower upper heat transfer coefficient in the model can compensate for that effect. Again, it is important to note that by calibrating the model, the resulting normalized non-dimensional temperature ratio can be made to be in good agreement, but that calibration applies on to the locations used.

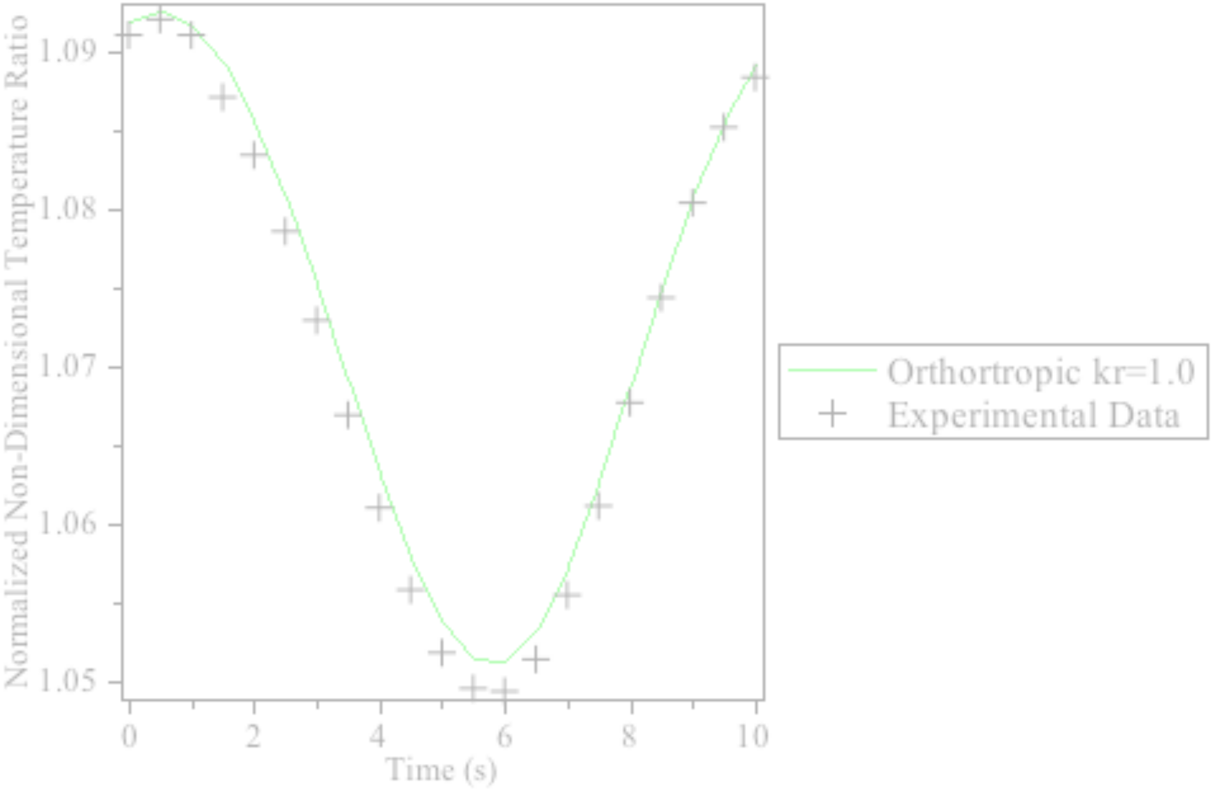

Figure 5-7: Analytical vs. simulated results for normalized non-dimensional temperature with calibrated upper heat transfer coefficient

Based on the calibrated model, the analytical results will now be compared for three different values for the radial thermal conductivity; the isotropic case (kr=0.05 W/m*K), the simulated case of a value in which the radial thermal conductivity is 20 times greater than the axial (kr=1.0 W/m*K) , and an intermediate case in which the radial thermal conductivity is 5 times greater than the axial thermal conductivity (kr=.25 W/m*K). All other properties and parameters are kept the same in all three cases.

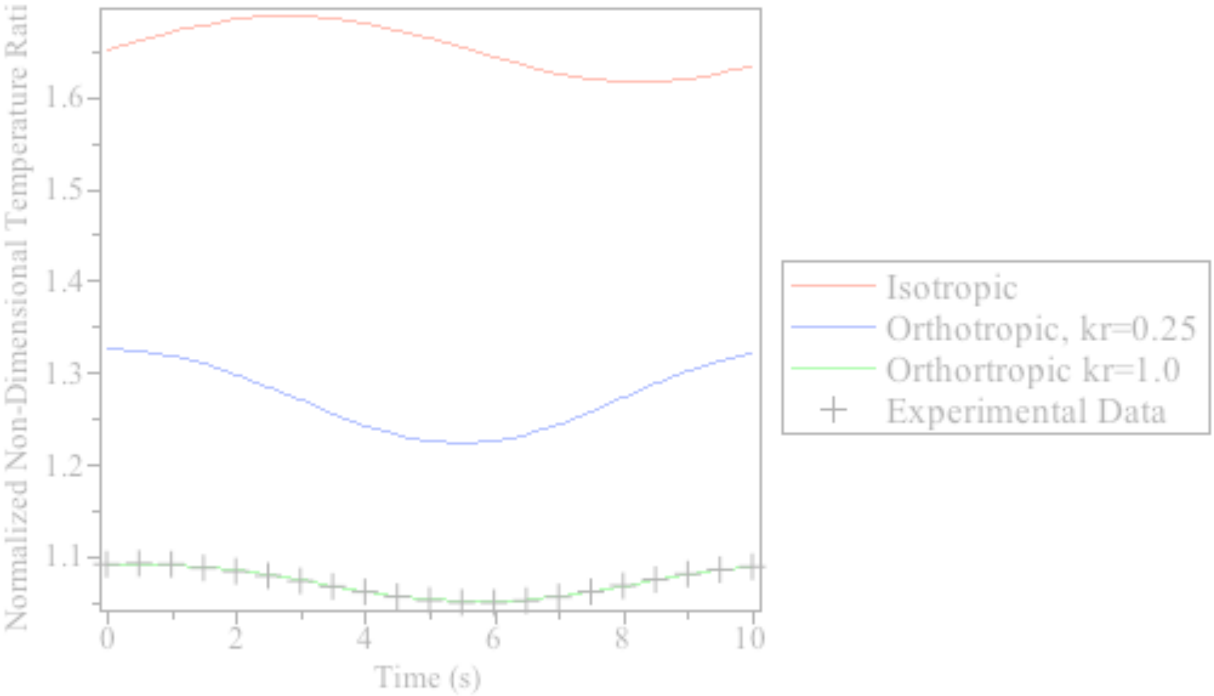

Figure 5-8: Analytical vs. experimental results for normalized non-dimensional temperature with calibrated upper heat transfer coefficient for various radial thermal conductivities

As shown in Figure 5-8, the analytical results for the normalized non-dimensional temperature ratio are distinct for different values of the radial thermal conductivity. As mentioned previously, if the model can be calibrated so that all other parameters and properties are known, then with a calibrated model there is the potential of getting good results. If the radial thermal conductivity were unknown and all other parameters known, the value in the analytical model can be iteratively changed until the results match, and thereby give an indication of what the radial thermal conductivity is. However, this is a very tedious process and requires doing the iterations and checking manually. Automation using computer results could potentially streamline the process, but as the analytical solution is very complicated, is beyond the scope and resources of this research.

The fundamental idea of extracting information about the radial thermal conductivity using an experiment in which a sinusoidal source term is used and then using the change in amplitude and phase shift seems promising. But based on these preliminary results however, use of this analytical model realistically has limited usefulness due to inherent poor approximations in the model of uniform convection and a source term simulating the temperature spike. For at materials with properties typical of what could be expected of most thermal protective fabrics, calibrating the analytical model to a real world physical setup that would allow for accurate results would be difficult at best. Tight experimental controls would be required to make certain that each parameter and property is known with a high degree of certainty. Any uncertainty in any one parameter will propagate into the results, and can even be compounded and augmented by the combination of uncertainty of other parameters/properties when multiple properties are combined into non-dimensional numbers.

Another thing to note is that better results might be obtained through use of a numerical rather than an analytical model. Through use of a numerical model, variation in the heat transfer coefficients can be accounted for and give much better results. This would require some sort of knowledge of how they might vary though, and may require experimentation or use of CFD solution to predict that with greater accuracy.

6 SUMMARY AND CONCLUSIONS

6.1 Conclusion

Thermal protective fabrics are commonly used to protect individuals against the hazards of hot liquid splashes. There is still potential for improvement amongst these types of fabrics so they can be made more comfortable to wear so individuals will be more willing to wear them. Although there are several ways to increase the amount of protection a fabric can provide, one way to do this is through use of materials that are orthotropic in nature in regards to the thermal conductivity.

The use of orthotropic materials with a radial thermal conductivity larger than the axial thermal conductivity is potential way that fabrics can be optimized to perform better to protect an individual against hot liquid splashes. In a situation where an individual would receive a burn based on the Stoll curve criteria from using an isotropic material, using an orthotropic material with a higher radial thermal conductivity may provide enough additional protection to prevent a burn based on the same criteria. This is especially true in situations where the splash sizes are small in size and short in time duration. However, in situations where the potential for large splash sizes and the duration of the splash becomes long, then the benefits of using an orthotropic material becomes minimal. Under conditions of large splashes and longtime durations, even though a second-degree burn may not be preventable using an orthotropic material, at the very least the fabric might be able to minimize the size and severity of any burns.

As real world use of protective fabrics requires protection against splashes that could be of any size, realistically fabrics can't be designed solely for small splashes. For situations for protecting people that are at very low risk, orthotropic fabrics may be an option to provide lighter and thinner fabrics. However, for most situations where splashes could potentially be large, using an orthotropic fabric only provides a small improvement in amount of protection a fabric provides, mainly near the edges of where a splash would occur. The benefit may only be minimal and fabrics still may need to be just as thick and bulky to protect for the large splash situations.

6.2 **Recommendations for Further Research**

Through analytical analysis, it has been shown that an orthotropic fabric can improve the performance of thermal protective fabrics. Only analytical and numerical work has been performed in this research. Physical experimentation to determine what the real world benefit is the recommended next step related to this research in two different areas.

The first area for further research would be to apply physical experimentation to the method presented in Chapter 5. Although the method appears to have potential for getting good results if a calibrated model can be achieved, it remains to be seen how well it can be applied in real life fabric. Using a physical experiment presents its own set of additional challenges beyond those encountered here, and a tightly controlled experiment in which parameters and properties that are known with high level of certainty would be required to get meaningful results.

The second area of research would be to actually apply an orthotropic fabric to a test, such as the ASTM 955 to validate that an orthotropic fabric has any real life benefit. As shown in Chapter 3, as a splash gets larger, the benefit of an orthotropic fabric is minimized to the point where some areas affected by a hot liquid splash may not see any reduction in the heat transfer through the fabric. If tests could be performed on an isotropic fabric, and then an orthotropic fabric that has all the other same properties, the true benefit of an orthotropic fabric could be determined beyond laboratory conditions to real life conditions.

REFERENCES

[1] Summary Report on Molten Metal Incidents. The Aluminum Association. January 2011.

[2] "Burn Incidence and Treatment in the United States: 2011 Fact Sheet." *American Burn Association*. American Burn Association. Web. 17 May 2013. <http://www.ameriburn.org/resources_factsheet.php>

[3] P. Lester. *The Morning Call*, 9 4 2011. Web. 17 Mar 2014. < http://articles.mcall.com/2011-04-09/news/mc-lower-macungie-victaulic-investiga20110409_1_molten-iron-victaulic-workers-molten-metal

[4] A. Stoll and M. Chianta, 1971 "Method and rating system for the evaluation of Thermal Protection." *Aerospace Medicine*. **40**. pp.1232-1237.

[5] ASTM F955-07. Standard Test Method for Evaluating Heat Transfer through Materials for Protective Clothing Upon Contact With Molten Substances.

[6] ASTM F2701 – 08. Standard Test Method for Evaluating Heat Transfer through Materials for Protective Clothing Upon Contact with a Hot Liquid Splash.

[7] J. Gersak and M. Marcic. 2007. "Development of a Mathematical Model for the Heat Transfer of the System Man-Clothing-Environment." *International Journal of Clothing Science and Technology*. 19. 234-241.

[8] D. Ding ,T. Tang, G. Song, and A. McDonald. 2010 "Characterizing the performance of a single-layer fabric system through a heat and mass transfer model - Part I: Heat and mass transfer model." *Textile Research Journal*. **81**, pp. 398.

[9] Z. Fanglong, M. Suqin, and Z. Weiyuan, 2008. "Study of Skin Model and Geometry Effects on Thermal Performance of Thermal Protective Fabrics." *Heat and Mass Transfer*. **45**, pp. 99-105.

[10] H. Morse, et al. 1973. "Analysis of the Thermal Response of Protective Fabrics." Trans. Array *Aerotherm Division/Acurex Corporation*.

[11] I. Holver, 2006. "Protective Clothing in Hot Environments." *Industrial Health*. **44, pp.** 404-413.

[12] W. Mell and R. Lawson, 1999. United States. National Institute of Standards and Technology. *Heat Transfer Model for Fire Fighter's Protective Clothing*. Gaithersburg, MD:

[13] G. Song, R. Barker, A. Kuznetsov, P. Chitrphiromsri, R. Grimes. 2004. "Modeling the Thermal Protective Performance of Heat Resistant Garments in Flash Fire Exposures." *Textile Research Journal*. **74**, pp. 1033.

[14] Z. Fanglong and C. Xiao, 2005. "Estimation of Thermal Performance of Flame Resistant Clothing Fabrics Sheathing a Cylinder with New Skin Model." *Textile Research Journal*. **79,** pp. 205.

[15] G. Song, and S. Paskaluk. 2011. "Thermal protective performance of protective clothing used for low radiant heat protection." *Textile Research Journal*. **81**, pp. 311.

[16] N. Ozisik. *Heat Conduction*. 2nd. John Wiley and Sons Inc., 1993.

[17] B.D. Gangon, May 2000, "Evaluation of New Test Methods for Fire Fighting Clothing". Master's Thesis, Worcester Polytechnic Institute.

[18] S. Graham, D. McDowell, R. Dinwiddie. 1999. "Multidimensional Flash Diffusivity Measurements of Orthotropic Materials." *International Journal of Thermophysics*. **20**(2), pp. 691.

[19] P. Gaal, M. Thermitus, and D. Stroe. "Thermal Conductivity Measurements using the Flash Method". Journal of Thermal Analysis and Calorimetry". 78. (2004): 185-189.

[20] ASTM E2716-09. "Standard Test Method for Determining Specific Heat Capacity by Sinusoidal Modulated Temperature Differential Scanning Calorimetry".

APPENDIX A. MATHEMATICAL DEVELOPMENT OF MODEL

A detailed step-by-step mathematical development of the analytical model is presented here.

A.1 Governing Equation

$$k_r \frac{1}{r}\frac{\partial}{\partial r}\left(r\frac{\partial T(r,z,t)}{\partial r}\right) + k_z \frac{\partial^2 T(r,z,t)}{\partial z^2} + k_\phi \frac{1}{r^2}\frac{\partial^2 T(r,z,t)}{\partial \phi^2} + \dot{q} = dc_p \frac{\partial T(r,z,t)}{\partial t}$$

$$k_r \frac{1}{r}\frac{\partial}{\partial r}\left(r\frac{\partial T(r,z,t)}{\partial r}\right) + k_z \frac{\partial^2 T(r,z,t)}{\partial z^2} + \dot{q} = dc_p \frac{\partial T(r,z,t)}{\partial t}$$

$$\frac{k_r}{k_2}\frac{1}{r}\frac{\partial}{\partial r}\left(r\frac{\partial T(r,z,t)}{\partial r}\right) + \frac{\partial^2 T(r,z,t)}{\partial z^2} + \frac{\dot{q}}{k_z} = \frac{dc_p}{k_z}\frac{\partial T(r,z,t)}{\partial t}$$

$$\frac{1}{\epsilon^2}\frac{1}{r}\frac{\partial}{\partial r}\left(r\frac{\partial T(r,z,t)}{\partial r}\right) + \frac{\partial^2 T(r,z,t)}{\partial z^2} + \frac{\dot{q}}{k_z} = \frac{1}{\alpha}\frac{\partial T(r,z,t)}{\partial t}$$

A.2 Boundary and Initial Conditions

$$k_z \left.\frac{\partial T}{\partial z}\right|_{z=0} = h(T(r,0,t) - T_\infty)$$

$$k_z \left.\frac{\partial T}{\partial z}\right|_{z=w} = -U(T(r,w,t) - T_\infty)$$

$$\left.\frac{\partial T}{\partial r}\right|_{r=0} = 0$$

$$T(r \to \infty, z, t) = T_\infty$$

$$T(r, z, 0) = T_\infty$$

A.3 Non-Dimensional Parameters

$$\theta = \frac{T - T_\infty}{T_{ref}}$$

$$\rho = \frac{r}{w}$$

$$\rho = \frac{\zeta}{w}$$

$$\tau = \frac{\alpha t}{w^2}$$

A.4 Non-Dimensional Governing Solution

$$\frac{1}{\epsilon^2}\frac{1}{\rho}\frac{\partial}{\partial \rho}\left(\rho \frac{\partial \theta(\rho,\zeta,\tau)}{\partial \rho}\right) + \frac{\partial^2 \theta(\rho,\zeta,\tau)}{\partial \zeta^2} + \frac{\dot{q} w^2}{k_z T_{ref}} = \frac{\partial \theta(\rho,\zeta,\tau)}{\partial \tau}$$

A.5 Non-Dimensional Boundary and Initial Conditions

$$\left.\frac{\partial \theta}{\partial \zeta}\right|_{\zeta=0} = \frac{hw}{k_z}\big(\theta(\rho,0,\tau)\big) = Bi_0 \theta(\rho,0,\tau)$$

$$\left.\frac{\partial \theta}{\partial \zeta}\right|_{\zeta=1} = \frac{Uw}{k_z}\big(\theta(\rho,1,\tau)\big) = -Bi_w \theta(\rho,1,\tau)$$

$$\left.\frac{\partial \theta}{\partial \rho}\right|_{\rho=0} = 0$$

$$\theta(\rho \to \infty, \zeta, \tau) = 0$$

$$\theta(\rho, \zeta, 0) = 0$$

A.6 Sturm-Louisville Problem

$$\frac{\delta^2 \phi}{\delta \zeta^2} + {\beta_n}^2 \phi = 0$$

$$\left.\frac{\partial \phi}{\partial \zeta}\right|_{\zeta=0} = Bi_0\phi(\beta_n, 0)$$

$$\left.\frac{\partial \phi}{\partial \zeta}\right|_{\zeta=1} = -Bi_w\phi(\beta_n, 1).$$

From Case 1, Table 2-2 of Ozisik 2nd edition (page 48)

$$\phi(\beta_n, \zeta) = \beta_n \cos(\beta_n \zeta) + Bi_0 \sin(\beta_n \zeta)$$

$$N(\beta_n) = \frac{1}{2}((\beta_n{}^2 + Bi_0{}^2)(1 + \frac{Bi_w}{(\beta_n{}^2 + Bi_0{}^2)} + Bi_0))$$

The eigenvalues are found from

$$tan(\beta_n) = \frac{\beta_n(Bi_0 + Bi_w)}{\beta_n{}^2 - Bi_0 Bi_w}$$

A.7 Fourier Transform

$$\bar{\theta}(\rho, \beta_n, \tau) = \int_0^1 \phi(\beta_n, \zeta)\theta(\rho, \zeta, \tau)\, d\zeta$$

$$\int_0^1 \phi(\beta_n, \zeta)\frac{1}{\epsilon^2}\frac{1}{\rho}\frac{\partial}{\partial \rho}\left(\rho\frac{\partial \theta(\rho, \zeta, \tau)}{\partial \rho}\right) + \int_0^1 \phi(\beta_n, \zeta)\frac{\theta(\rho, \zeta, \tau)}{\partial \zeta^2} + \int_0^1 \phi(\beta_n, \zeta)\frac{\dot{q}\alpha_2}{k_2 r_{ref} T_{ref}}$$

$$= \int_0^1 \phi(\beta_n, \zeta)\frac{\partial \theta(\rho, \zeta, \tau)}{\partial \tau}$$

$$\bar{Q} = \frac{\dot{q}w^2}{k_z T_{ref}}\int_0^1 \phi(\beta_n, \zeta)\dot{q}$$

$$\int_0^1 \phi(\beta_n, \zeta)\frac{1}{\epsilon^2}\frac{1}{\rho}\frac{\partial}{\partial \rho}\left(\rho\frac{\partial \theta(\rho, \zeta, \tau)}{\partial \rho}\right) = \frac{1}{\epsilon^2}\frac{1}{\rho}\frac{\partial}{\partial \rho}\left(\rho\frac{\partial \bar{\theta}}{\partial \rho}\right)$$

$$\int_0^1 \phi(\beta_n, \zeta)\frac{\partial \theta(\rho, \zeta, \tau)}{\partial \tau} = \frac{\partial \bar{\theta}(\rho, \beta_n, \tau)}{\partial \tau}$$

$$dv = \frac{\partial^2\theta}{\partial\zeta^2} \qquad u = \phi(\beta_n, \zeta)$$

$$v = \frac{\partial\theta}{\partial\zeta} \qquad du = \frac{\partial}{\partial\zeta}\phi(\beta_n, \zeta)$$

$$\int_0^1 \phi(\beta_n, \zeta)\frac{\partial^2\theta(\rho,\zeta,\tau)}{\partial\zeta^2} = \phi(\beta_n, \zeta)\frac{\partial\theta(\rho,\zeta,\tau)}{\partial\zeta}\bigg|_0^1 - \int_0^1 \frac{\partial\theta(\rho,\zeta,\tau)}{\partial\zeta}\frac{\partial\phi(\beta_n,\zeta)}{\partial\zeta}$$

$$dv = \frac{\partial\theta}{\partial\zeta} \qquad u = \frac{\partial\phi(\beta_n,\zeta)}{\partial\zeta}$$

$$v = \theta \qquad du = \frac{\partial^2\phi(\beta_n,\zeta)}{\partial\zeta^2}$$

$$\int_0^1 \phi(\beta_n, \zeta)\frac{\partial^2\theta(\rho,\zeta,\tau)}{\partial\zeta^2}$$

$$= \left[\phi(\beta_n, \zeta)\frac{\partial\theta(\rho,\zeta,\tau)}{\partial\zeta} - \frac{\partial\phi(\beta_n,\zeta)}{\partial\zeta}\phi(\beta_n,\zeta)\right]_0^1 - {\beta_n}^2\int_0^1 \phi(\beta_n,\zeta)\theta(\rho,\zeta,\tau)$$

$$= \left[\frac{\phi(\beta_n,1)}{Bi_w}[0-\theta(\rho,\zeta,\tau)] + \frac{\phi(\beta_n,1)\theta(\rho,\zeta,\tau)}{Bi_w} - \frac{\phi(\beta_n,0)}{Bi_0}[0-\theta(\rho,\zeta,\tau)]\right.$$

$$\left. - \frac{\phi(\beta_n,0)\theta(\rho,\zeta,\tau)}{Bi_0}\right]_0^1 - {\beta_n}^2\bar{\theta} = -{\beta_n}^2\bar{\theta}$$

$$\frac{1}{\epsilon^2}\frac{1}{\rho}\frac{\partial}{\partial\rho}\left(\rho\frac{\partial\bar{\theta}(\rho,\beta_n,\tau)}{\partial\rho}\right) - {\beta_n}^2\bar{\theta}(\rho,\beta_n,\tau) + \bar{Q} = \frac{\partial\bar{\theta}(\rho,\beta_n,\tau)}{\partial\tau}$$

A.8 Hankel Transform

$$\bar{\bar{\theta}}(\lambda,\beta_n,\tau) = \int_0^\infty \rho J_0(\lambda\rho)\,\bar{\theta}(\rho,\beta_n,\tau)d\rho$$

$$\int_0^\infty \rho J_0(\lambda\rho)\frac{1}{\epsilon^2}\frac{1}{\rho}\frac{\partial}{\partial\rho}\left(\rho\frac{\partial\bar{\theta}(\rho,\beta_n,\tau)}{\partial\rho}\right)d\rho - \int_0^\infty \rho J_0(\lambda\rho)\,{\beta_n}^2\bar{\theta}(\rho,\beta_n,\tau)d\rho + \int_0^\infty \rho J_0(\lambda\rho)\,\bar{Q}d\rho$$

$$= \int_0^\infty \rho J_0(\lambda\rho)\frac{\partial\bar{\theta}(\rho,\beta_n,\tau)}{\partial\tau}d\rho$$

$$\int_0^\infty \rho J_0(\lambda\rho)\,\beta_n{}^{2}\,\bar{\theta}(\rho,\beta_n,\tau)d\rho = \beta_n{}^{2}\bar{\bar{\theta}}(\lambda,\beta_n,\tau)$$

$$\int_0^\infty \rho J_0(\lambda\rho)\frac{\partial\bar{\theta}(\rho,\beta_n,\tau)}{\partial\tau}d\rho = \frac{\partial\bar{\bar{\theta}}(\lambda,\beta_n,\tau)}{\partial\tau}$$

$$\bar{\bar{Q}} = \int_0^\infty \rho J_0(\lambda\rho)\,\bar{Q}$$

$$dv = \frac{\partial}{\partial\rho}\left(\rho\frac{\partial\bar{\theta}}{\partial\rho}\right) \qquad u = J_0(\lambda\rho)$$

$$v = \rho\frac{\partial\bar{\theta}}{\partial\rho} \qquad du = -\lambda J_1(\lambda\rho)$$

$$\int_0^\infty \rho J_0(\lambda\rho)\frac{1}{\epsilon^2}\frac{1}{\rho}\frac{\partial}{\partial\rho}\left(\rho\frac{\partial\bar{\theta}}{\partial\rho}\right)d\rho = \frac{1}{\epsilon^2}\left(\left[J_0(\lambda\rho)\rho\frac{\partial\bar{\theta}}{\partial\rho}\right]_0^\infty + \int_0^\infty \rho\frac{\partial\bar{\theta}}{\partial\rho}\lambda J_1(\lambda\rho)\right)$$

$$dv = \frac{\partial\bar{\theta}}{\partial\rho} \qquad u = \lambda\rho J_1(\lambda\rho)$$

$$v = \bar{\theta} \qquad du = \lambda^2\rho J_0(\lambda\rho)$$

$$\int_0^\infty \rho J_0(\lambda\rho)\frac{1}{\epsilon^2}\frac{1}{\rho}\frac{\partial}{\partial\rho}\left(\rho\frac{\partial\bar{\theta}}{\partial\rho}\right)d\rho = \frac{1}{\epsilon^2}\left(\left[J_0(\lambda\rho)\rho\frac{\partial\bar{\theta}}{\partial\rho} + \lambda\rho J_1(\lambda\rho)\bar{\theta}\right]_0^\infty - \lambda^2\int_0^\infty \bar{\theta}\,\rho J_0(\lambda\rho)\right) = \frac{-\lambda^2}{\epsilon^2}$$

$$-\frac{1}{\epsilon^2}\lambda^2\bar{\bar{\theta}}(\lambda,\beta_n,\tau) - \beta_n{}^{2}\bar{\bar{\theta}}(\lambda,\beta_n,\tau) + \bar{\bar{Q}} = \frac{\partial\bar{\bar{\theta}}(\lambda,\beta_n,\tau)}{\partial\tau}$$

$$\bar{\bar{Q}} = \frac{\partial\bar{\bar{\theta}}(\lambda,\beta_n,\tau)}{\partial\tau} + \left(\frac{\lambda^2}{\epsilon^2} + \beta_n{}^{2}\right)\bar{\bar{\theta}}(\lambda,\beta_n,\tau)$$

A.9 Integrating Factor

$$e^{\left\{\left(\frac{\lambda^2}{\epsilon^2}+\beta_n{}^{2}\right)\tau\right\}}\bar{\bar{Q}} = e^{\left\{\left(\frac{\lambda^2}{\epsilon^2}+\beta_n{}^{2}\right)\tau\right\}}\frac{\partial\bar{\bar{\theta}}}{\partial\tau} + e^{\left\{\left(\frac{\lambda^2}{\epsilon^2}+\beta_n{}^{2}\right)\tau\right\}}\left(\frac{\lambda^2}{\epsilon^2} + \beta_n{}^{2}\right)\bar{\bar{\theta}}(\lambda,\beta_n,\tau)$$

$$e^{\left\{\left(\frac{\lambda^2}{\epsilon^2}+\beta_n{}^{2}\right)\tau\right\}}\bar{\bar{Q}} = \frac{\partial}{\partial\tau}\left(e^{\left\{\left(\frac{\lambda^2}{\epsilon^2}+\beta_n{}^{2}\right)\tau\right\}}\bar{\bar{\theta}}(\lambda,\beta_n,\tau)\right)$$

$$\int_0^{\tau} e^{\left\{\left(\frac{\lambda^2}{\epsilon^2}+{\beta_n}^2\right)\tau\right\}} \bar{\bar{Q}} d\tau = \int_0^{\tau} \frac{\partial}{\partial\tau}\left(e^{\left\{\left(\frac{\lambda^2}{\epsilon^2}+{\beta_n}^2\right)\tau\right\}} \bar{\bar{\theta}}\right) d\tau$$

$$\int_0^{\tau} \frac{\partial}{\partial\tau}\left(e^{\left\{\left(\frac{\lambda^2}{\epsilon^2}+{\beta_n}^2\right)\tau\right\}} \bar{\bar{\theta}}(\lambda,\beta_n,\tau)\right) d\tau = e^{\left\{\left(\frac{\lambda^2}{\epsilon^2}+{\beta_n}^2\right)\tau\right\}} \bar{\bar{\theta}}(\lambda,\beta_n,\tau) - e^{\left\{\left(\frac{\lambda^2}{\epsilon^2}+{\beta_n}^2\right)0\right\}} \bar{\bar{\theta}}(\lambda,\beta_n 0)$$

$$\int_0^{\tau} e^{\left\{\left(\frac{\lambda^2}{\epsilon^2}+{\beta_n}^2\right)\tau\right\}} \bar{\bar{Q}}\, d\tau = e^{\left\{\left(\frac{\lambda^2}{\epsilon^2}+{\beta_n}^2\right)\tau\right\}} \bar{\bar{\theta}}(\lambda,\beta_n,\tau)$$

$$\bar{\bar{\theta}}(\lambda,\beta_n,\tau) = e^{\left\{-\left(\frac{\lambda^2}{\epsilon^2}+{\beta_n}^2\right)\tau\right\}} \int_0^{\tau} e^{\left\{\left(\frac{\lambda^2}{\epsilon^2}+{\beta_n}^2\right)\tau\right\}} \bar{\bar{Q}} d\tau$$

A.10 Inverse Hankel Transform

$$\bar{\theta}(\rho,\beta_n,\tau) = \int_0^{\infty} \lambda J_0(\lambda\rho)\, \bar{\bar{\theta}}\, (\lambda,\beta_n,\tau) d\lambda$$

$$\int_0^{\infty} \lambda J_0(\lambda\rho)\, \bar{\bar{\theta}} d\lambda = \int_0^{\infty} \lambda J_0(\lambda\rho) e^{\left\{-\left(\frac{\lambda^2}{\epsilon^2}+{\beta_n}^2\right)\tau\right\}} \int_0^{\tau} e^{\left\{\left(\frac{\lambda^2}{\epsilon^2}+{\beta_n}^2\right)\tau\right\}} \bar{\bar{Q}} d\tau\ d\lambda$$

$$\bar{\theta}(\rho,\beta_n,\tau) = \int_0^{\infty} \lambda J_0(\lambda\rho) e^{\left\{-\left(\frac{\lambda^2}{\epsilon^2}+{\beta_n}^2\right)\tau\right\}} \int_0^{\tau} e^{\left\{\left(\frac{\lambda^2}{\epsilon^2}+{\beta_n}^2\right)\tau\right\}} \bar{\bar{Q}} d\tau\ d\lambda$$

A.11 Inverse Fourier Transform

$$\theta(\rho,\xi,\tau) = \sum_{n=1}^{\infty} \frac{\phi(\beta_n,\zeta)}{N(\beta_n)} \bar{\theta}(\rho,\beta_n,\tau)$$

$$\sum_{n=1}^{\infty} \frac{\phi(\beta_n,\zeta)}{N(\beta_n)} \bar{\theta} = \sum_{n=1}^{\infty} \frac{\phi(\beta_n,\zeta)}{N(\beta_n)} \int_0^{\infty} \lambda J_0(\lambda\rho) e^{\left\{-\left(\frac{\lambda^2}{\epsilon^2}+{\beta_n}^2\right)\tau\right\}} \int_0^{\tau} e^{\left\{\left(\frac{\lambda^2}{\epsilon^2}+{\beta_n}^2\right)\tau'\right\}} \bar{\bar{Q}} d\tau'\ d\lambda$$

$$\theta(\rho,\xi,\tau) = \sum_{n=1}^{\infty} \frac{\phi(\beta_n,\zeta)}{N(\beta_n)} \int_0^{\infty} \lambda J_0(\lambda\rho) e^{\left\{-\left(\frac{\lambda^2}{\epsilon^2}+{\beta_n}^2\right)\tau\right\}} \int_0^{\tau} e^{\left\{\left(\frac{\lambda^2}{\epsilon^2}+{\beta_n}^2\right)\tau'\right\}} \bar{\bar{Q}} d\tau'\ d\lambda$$

A.12 Solution for Point Source Heat Generation

$$\dot{q} = \frac{Q_0 \delta(r)\delta(t)\delta(z)}{2\pi r}$$

$$T_{ref} = \frac{Q_0}{2\pi w^3 k_z}$$

Applying the non-dimensional parameters yields the source term in non-dimensional format and then substituting into the transformed source term yields

$$\bar{\bar{Q}} = \delta(\tau) \int_0^\infty \rho J_0(\lambda\rho) \frac{\delta(\rho)}{\rho} d\rho \int_0^1 \phi(\beta_n, \zeta)\, \delta(\zeta) d\zeta$$

Solving for each integral individually yields

$$\int_0^\infty \rho J_0(\lambda\rho) \frac{\delta(\rho)}{\rho} d\rho = \frac{J_0(0)}{2} = \frac{1}{2}$$

$$\int_0^1 \phi(\beta_n, \zeta)\, \delta(\zeta) d\zeta = \int_0^1 \left(\beta_n \cos(\beta_n \zeta) + Bi_0 \sin(\beta_n \zeta)\right) \delta(\zeta) d\zeta$$

$$= \frac{\left(\beta_n \cos(\beta_n 0) + Bi_0 \sin(\beta_n 0)\right)}{2} = \frac{\beta_n}{2}$$

Substituting back into the transformed source term yields

$$\bar{\bar{Q}} = \delta(\tau) \frac{\beta_n}{4}$$

Substituting into the generalized form of the solution

$$\theta(\rho, \zeta, \tau) = \sum_{n=1}^{\infty} \int_0^\infty \frac{\phi(\beta_n, \zeta)}{N(\beta_n)} \lambda J_0(\lambda\rho) e^{\left\{-\left(\frac{\lambda^2}{\epsilon^2} + \beta_n{}^2\right)\tau\right\}} \int_0^\tau e^{\left\{\left(\frac{\lambda^2}{\epsilon^2} + \beta_n{}^2\right)\tau'\right\}} \delta(\tau') \frac{\beta_n}{4} d\tau'\ d\lambda$$

Evaluating the integral individually yields

$$\int_0^\tau e^{\left\{\left(\frac{\lambda^2}{\epsilon^2} + \beta_n{}^2\right)\tau'\right\}} \delta(\tau') \frac{\beta_n}{4} d\tau' = \frac{1}{2} \frac{\beta_n}{4} e^{\left\{\left(\frac{\lambda^2}{\epsilon^2} + \beta_n{}^2\right)0\right\}} = \frac{\beta_n}{8}$$

The final solution is therefore

$$\theta(\rho,\zeta,\tau) = \sum_{n=1}^{\infty} \int_0^{\infty} \frac{\phi(\beta_n,\zeta)}{N(\beta_n)} \lambda J_0(\lambda\rho) \frac{\beta_n}{8} e^{\left\{-\left(\frac{\lambda^2}{\epsilon^2}+\beta_n{}^2\right)\tau\right\}} \, d\lambda$$

A.13 Solution for Heaviside Function Heat Generation

$$\dot{q} = \frac{Q_0(H(r) - H(r - r_0))(H(t) - H(t - t_0)\delta(z)}{\pi r_0{}^2(t_0)}$$

$$T_{ref} = \frac{Q_0 w}{\pi r_0{}^2 t_0 k_z}$$

Applying the non-dimensional parameters yields the source term in non-dimensional format and then substituting into the transformed source term yields

$$\bar{\bar{Q}} = \left(H(\tau) - H\left(\tau - \frac{\alpha_2 t_0}{w^2}\right)\right) \int_0^{\infty} \rho J_0(\lambda\rho)\,(H(\rho) - H\left(\rho - \frac{r_0}{w}\right))d\rho \int_0^1 \phi(\beta_n,\zeta)\,\delta(\zeta)d\zeta$$

Solving for each integral individually yields

$$\int_0^1 \phi(\beta_n,\zeta)\,\delta(\zeta)d\zeta = \int_0^1 \big(\beta_n \cos(\beta_n\zeta) + Bi_0 \sin(\beta_n\zeta)\big)\,\delta(\zeta)d\zeta$$

$$= \frac{\big(\beta_n \cos(\beta_n 0) + Bi_0 \sin(\beta_n 0)\big)}{2} = \frac{\beta_n}{2}$$

$$\int_0^{\infty} \rho J_0(\lambda\rho)\left(H(\rho) - H\left(\rho - \frac{r_0}{w}\right)\right) d\rho = \frac{r_0}{\lambda w} J_1\left(\lambda \frac{r_0}{w}\right)$$

Substituting back into the transformed source term yields transformed source term

$$\bar{\bar{Q}} = \left(H(\tau) - H\left(\tau - \frac{\alpha_2 t_0}{w^2}\right)\right)\left(\frac{\beta_n}{2} \frac{r_0}{\lambda w} J_1\left(\lambda \frac{r_0}{w}\right)\right)$$

$$\theta(\rho,\zeta,\tau) = \sum_{n=1}^{\infty} \int_0^{\infty} \frac{\phi(\beta_n,\zeta)}{N(\beta_n)} \lambda J_0(\lambda\rho) \left[\int_0^{\tau} \bar{\bar{Q}}\, e^{\left\{\left(\frac{\lambda^2}{\epsilon^2}+\beta_n{}^2\right)\tau'\right\}} d\tau'\right] e^{\left\{-\left(\frac{\lambda^2}{\epsilon^2}+\beta_n{}^2\right)\tau\right\}} \, d\lambda$$

$$\int_0^{\tau} \bar{\bar{Q}}\, e^{\left\{\left(\frac{\lambda^2}{\epsilon^2}+{\beta_n}^2\right)\tau'\right\}} dt = \begin{matrix} \left(\frac{\beta_n}{2}\frac{r_0}{\lambda w} J_1\left(\lambda \frac{r_0}{w}\right)\right)\left(\frac{e^{\left\{\left(\frac{\lambda^2}{\epsilon^2}+{\beta_n}^2\right)\frac{\alpha t0}{w^2}\right\}}-1}{\frac{\lambda^2}{\epsilon^2}+{\beta_n}^2}\right) if\ \tau \geq \frac{\alpha t0}{w^2} \\ \left(\frac{\beta_n}{2}\frac{r_0}{\lambda w} J_1\left(\lambda \frac{r_0}{w}\right)\right)\left(\frac{e^{\left\{\left(\frac{\lambda^2}{\epsilon^2}+{\beta_n}^2\right)\tau\right\}}-1}{\frac{\lambda^2}{\epsilon^2}+{\beta_n}^2}\right) if\ \tau \leq \frac{\alpha t0}{w^2} \end{matrix}$$

Substituting back into the generalized form of the solution yields the specific solution

If $\tau \geq \frac{\alpha t0}{w^2}$, then

$$\theta(\rho, \zeta, \tau) = \sum_{n=1}^{\infty} \int_0^{\infty} \frac{\phi(\beta_n, \zeta)}{N(\beta_n)} \lambda J_0(\lambda\rho) \left(\frac{\beta_n}{2}\frac{r_0}{\lambda w} J_1\left(\lambda \frac{r_0}{w}\right)\right)\left(\frac{e^{\left\{\left(\frac{\lambda^2}{\epsilon^2}+{\beta_n}^2\right)\frac{\alpha t0}{w^2}\right\}}-1}{\frac{\lambda^2}{\epsilon^2}+{\beta_n}^2}\right) e^{\left\{-\left(\frac{\lambda^2}{\epsilon^2}+{\beta_n}^2\right)\tau\right\}}\, d\lambda$$

If $\tau \leq \frac{\alpha t0}{w^2}$, then

$$\theta(\rho, \zeta, \tau) = \sum_{n=1}^{\infty} \int_0^{\infty} \frac{\phi(\beta_n, \zeta)}{N(\beta_n)} \lambda J_0(\lambda\rho) \left(\frac{\beta_n}{2}\frac{r_0}{\lambda w} J_1\left(\lambda \frac{r_0}{w}\right)\right)\left(\frac{e^{\left\{\left(\frac{\lambda^2}{\epsilon^2}+{\beta_n}^2\right)\tau\right\}}-1}{\frac{\lambda^2}{\epsilon^2}+{\beta_n}^2}\right) e^{\left\{-\left(\frac{\lambda^2}{\epsilon^2}+{\beta_n}^2\right)\tau\right\}}\, d\lambda$$

APPENDIX B. MAPLE SUBROUTINE USED IN POINT SOURCE

```
> restart;
> with(plots);
> NULL;
> h := 2;
> NULL;
> U := 400;
> NULL;
> kr := 0.3e-1;
> NULL;
> kz := 0.3e-1;
> NULL;
> NULL;
> density := 300;
> NULL;
> T[infinity] := 25;
> NULL;
> cp := 1100;
> NULL;
> alpha := kz/(density*cp);
> NULL;
> w := 0.1e-2;
> Q0 := 2;
> Tref := Q0*alpha/(2*Pi*w^3*kz);
> Bio := h*w/kz;
> Biw := U*w/kz;
> m := 1;
> f := -tan(beta)+beta*(Bio+Biw)/(beta^2-Bio*Biw);
> for i to 250 do Alpha := fsolve(f = 0, beta = (i-.99)*2 .. 2*i); if type(Alpha, float) then beta[m]
:= Alpha; m := m+1 end if end do;
> m;
```

```
> M := (1/2)*(beta[n]^2+Bio^2)*(1+Biw/(beta[n]^2+Biw^2)+Bio);
> theta := sum(int((1/8)*(beta[n]*cos(beta[n]*Zeta)+Bio*sin(beta[n]*Zeta))*lambda*BesselJ(0,
lambda*rho)*beta[n]*exp(-((lambda/`&epsilon;`)^2+beta[n]^2)*tau)/M, lambda = 0 .. infinity),
n = 1 .. 100);

>Q1 := Biw*theta
>
> plot([eval(Q1, [`&epsilon;` = .5, rho = 0, Zeta = 1]), eval(Q1, [`&epsilon;` = .707, rho = 0,
Zeta = 1]), eval(Q1, [`&epsilon;` = 1, rho = 0, Zeta = 1])], tau = 0 .. 5, view = [0.25e-1 .. 2, 0 ..
.7], axes = boxed, legend = [kz/kr = .25, kz/kr = .5, kz/kr = 1], labeldirections = [horizontal,
vertical], labels = ["Non-Dimensional Time", "Non-Dimensional Heat Flux"], legendstyle =
[location = right], linestyle = [solid, solid, solid], color = [green, blue, red]);
```

APPENDIX C. MAPLE SUBROUTINE USED IN FINITE AREA/TIME SOURCE

```
> restart;
> with(plots);
> NULL;
> h := 2;
> NULL;
> U := 400;
> NULL;
> kr := 0.3e-1;
> NULL;
> kz := 0.3e-1;
> `&epsilon;` := (kz/kr)^.5;
> NULL;
> density := 300;
> NULL;
> T[infinity] := 25;
> NULL;
> cp := 260;
> NULL;
> alpha := kz/(density*cp);
> NULL;
> w := 0.1e-2;
> Q0 := 1.45;
> Tref := Q0*w/(Pi*r0^2*t0*kz);
> Bio := h*w/kz;
> Biw := U*w/kz;
> m := 1;
> f := -tan(beta)+beta*(Bio+Biw)/(beta^2-Bio*Biw);
> for i to 130 do Alpha := fsolve(f = 0, beta = (i-.99)*2 .. 2*i); if type(Alpha, float) then beta[m]
:= Alpha; m := m+1 end if end do;
> m;
> NULL;
```

```
> r0 := 0.5e-2;
> NULL;
> t0 := 2;
> r0/w;
> alpha*t0/w^2;
> NULL;
> numpoints := 15;
> NULL;
> rhomax := 10;
> for i to numpoints do rho[i] := rhomax*(i-1)/numpoints end do;
> NULL;
> zeta := 1;
> M := (1/2)*(beta[n]^2+Bio^2)*(1+Biw/(beta[n]^2+Biw^2)+Bio);
> NULL;
> t := 1.5;
> tau1 := alpha*t/w^2;
> tau0 := alpha*t/w^2;
> `&epsilon;` := 1;
>for i to numpoints do theta1[i] :=
evalf(Int(sum(((1/2)*(beta[n]*cos(beta[n]*zeta)+Bio*sin(beta[n]*zeta))*lambda*BesselJ(0,
lambda*rho[i])*beta[n]/M*(r0/(w*lambda)))*BesselJ(1,
lambda*r0/w)*(exp(((lambda/`&epsilon;`)^2+beta[n]^2)*tau0)-1)*exp(-
((lambda/`&epsilon;`)^2+beta[n]^2)*tau1)/((lambda/`&epsilon;`)^2+beta[n]^2), n = 1 .. 50),
lambda = 0 .. 30, digits = 8, method = _d01akc)) end do;
> `&epsilon;` := .707;
> for i to numpoints do theta2[i] :=
evalf(Int(sum(((1/2)*(beta[n]*cos(beta[n]*zeta)+Bio*sin(beta[n]*zeta))*lambda*BesselJ(0,
lambda*rho[i])*beta[n]/M*(r0/(w*lambda)))*BesselJ(1,
lambda*r0/w)*(exp(((lambda/`&epsilon;`)^2+beta[n]^2)*tau0)-1)*exp(-
((lambda/`&epsilon;`)^2+beta[n]^2)*tau1)/((lambda/`&epsilon;`)^2+beta[n]^2), n = 1 .. 50),
lambda = 0 .. 30, digits = 8, method = _d01akc)) end do;
> `&epsilon;` := .5;
> for i to numpoints do theta3[i] :=
evalf(Int(sum(((1/2)*(beta[n]*cos(beta[n]*zeta)+Bio*sin(beta[n]*zeta))*lambda*BesselJ(0,
lambda*rho[i])*beta[n]/M*(r0/(w*lambda)))*BesselJ(1,
lambda*r0/w)*(exp(((lambda/`&epsilon;`)^2+beta[n]^2)*tau0)-1)*exp(-
((lambda/`&epsilon;`)^2+beta[n]^2)*tau1)/((lambda/`&epsilon;`)^2+beta[n]^2), n = 1 .. 50),
lambda = 0 .. 30, digits = 8, method = _d01akc)) end do;
> X := convert(rho, list);
>
```

```
> Q1a := convert(theta1, list);
> P1 := plot(X, Q1a, color = red, legend = "kz/kr=1", labels = ["Radial Position (m)", "Heat flux (W/m^2)"], labeldirections = [horizontal, vertical]);
>
> Q2a := convert(theta2, list);
> P2 := plot(X, Q2a, color = blue, legend = "kz/kr=.5", labels = ["Radial Position (m)", "Heat flux (W/m^2)"], labeldirections = [horizontal, vertical]);
>
> Q3a := convert(theta3, list);
> P3 := plot(X, Q3a, color = green, legend = "kz/kr=.25", labels = ["Non-Dimensional Radial Position", "Non-Dimensional Heat flux "], labeldirections = [horizontal, vertical], axes = boxed, legendstyle = [location = right]);
> display(P3, P2, P1);
```

APPENDIX D. USER DEFINED FUNCTION FOR POINT SOURCE NUMERICAL VERIFICATION

```
/* **********************************************************************
   heatgen_exp.c
   UDF for specifying volumetric generation function in solid
*********************************************************************** */
#include "udf.h"

#define PI 3.1415926535897932384626433832795
#define Power 350000000.

DEFINE_SOURCE(energy_source, c, thread, dS, eqn)
{
  real source;
  real x[ND_ND];        /* this will hold the position vector */
  real t = CURRENT_TIME;
  real t_p = .05;
  real r;
  real z;
  real r_l = 0.0004;
  real z_l = 0.0002;

  C_CENTROID(x,c,thread);

  r = x[1];
  z = x[0];

    if (t <= t_p)
    {if (r <= r_l)
      {if (z <= z_l)
    {source = Power;
        dS[eqn] = 0;}
        else
    {source = 0.0;
      dS[eqn] = 0; }}
      else
```

```
    {source = 0.0;
  dS[eqn] = 0;}}

  else
  {source = 0.0;
    dS[eqn] = 0.0;}

return source;}
```

APPENDIX E. USER DEFINED FUNCTION FOR FINITE AREA/SOURCE NUMERICAL VERIFICATION

```
/* *********************************************************************
   heatgen_exp.c
   UDF for specifying volumetric generation function in solid
********************************************************************* */
#include "udf.h"

#define PI 3.1415926535897932384626433832795
#define Power 350000000.

DEFINE_SOURCE(energy_source, c, thread, dS, eqn)
{
  real source;
  real x[ND_ND];        /* this will hold the position vector */
  real t = CURRENT_TIME;
  real t_p = .05;
  real r;
  real z;
  real r_l = 0.005;
  real z_l = 0.0002;

  C_CENTROID(x,c,thread);

  r = x[1];
  z = x[0];

    if (t <= t_p)
    { if (r <= r_l)
      {if (z <= z_l)
    {source = Power;
        dS[eqn] = 0;}
        else
    {source = 0.0;
      dS[eqn] = 0;}}
      else
```

```
   {source = 0.0;
  dS[eqn] = 0;}  }

  else
  {source = 0.0;
    dS[eqn] = 0.0;}

return source;}
```